UNIVERSITY OF LEEDS

Dissecting muscle synergies in the task space

David O'Reilly

Submitted in accordance with the requirements for the degree of Phd.
Computational Neuroscience

The University of Leeds

School of Biomedical sciences

Faculty of Biological sciences

February 2024

Intellectual Property

The candidate confirms that the work submitted is his own and that appropriate credit has been given where reference has been made to the work of others.

This copy has been supplied on the understanding that it is copyright material and that no quotation from the thesis may be published without proper acknowledgement.

To Desi and Gloria, my new module....

Executive Summary

The research presented here concerns the notion of modularity and its role in the functional organisation of the human motor system. In *Chapter 1*, I introduce the concept of modularity and a popular computational approach to its investigation in the motor neurosciences known as muscle synergy analysis. I highlight open problems in this field, in particular the lack of a direct mapping of muscle synergies to task performance, and present the ways in which i will address these open problems both conceptually and analytically. In *Chapter 2*, I address current analytical limitations in the field by leveraging information- and network-theoretic tools to present a novel, generalisable approach to muscle synergy extraction under relaxed model assumptions. This approach builds on top of traditional methods and is referred to as the Network-Information Framework (NIF). In *Chapter 3*, I then employ the NIF to provide a new perspective on muscle synergies that is made implicit in this novel computational approach. This novel perspective integrates important findings from recent influential works showing how muscles not only *'work together'* towards common task-goals as previously conceived, but also complementary and task-irrelevant objectives concomitantly. By directly including task parameters into muscle synergy extraction, i effectively dissect the task-relevant information dynamics underlying coordinated movement, thus providing a principled way to access this complex functional architecture. In *Chapter 4*, I further develop the NIF to simultaneously quantify diverse types of muscle interactions across inter- and intra-muscular scales, including functionally similar (i.e. redundant), -complementary (i.e. synergistic) and -independent (i.e. unique) interactions. In doing so, I reveal novel insights into movement control in health and with pathology. I also align current muscle synergy analysis with the forefront in theoretical understanding on human movement modularity. To conclude this work, in *Chapter 5* I summarise these contributions, their implications for neurobiological mechanisms, and the novel research opportunities they present for the motor control field.

Contents

Chapter 1

General Introduction

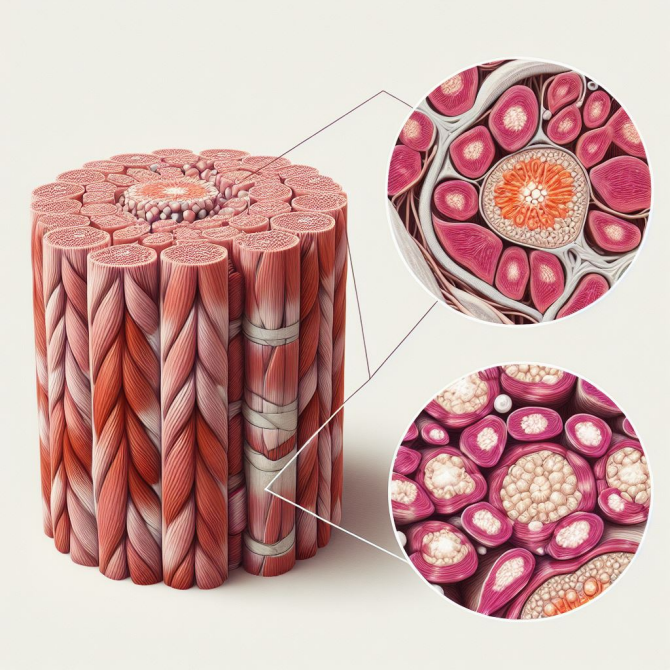

Figure 1: Muscle tissue at various scales illustrating the concept of multi-scale modularity.

The research presented here concerns the concept and analysis of modularity as an organisational principle underlying the function of the human motor control system. Modularity is a notoriously hard-to-pin down concept, with ongoing debate over its practical definition [1]. Nonetheless, it has been exceptionally useful in its various guises in the scientific domain. Generically speaking, this concept describes structures that display an encapsulation from their environment [2], with the elements encapsulated exhibiting a higher structural and/or functional association than their surrounding environment. It is a more significant phenomenon than local clustering, in that it represents the compartmentalisation of global system structure for the sake of functional specialisation [3]. An interesting facet of this concept is its dependence on the perspective of an ideal observer [4]. For example, when analysing human muscle tissue under a microscope (Fig.1), you can expect to see the cellular constituents that comprise it, namely myocytes. However, zooming in further reveals individual myocytes themselves consist of organelles, and conversely on a larger scale, entire muscles contribute as parts towards the neuromusculoskeletal system. Hence, no specific scale of observation is unique in comprising exclusively of modules. Rather, modularity is a scale-free attribute of complex living systems, exemplifying a general principle of biological organisation.

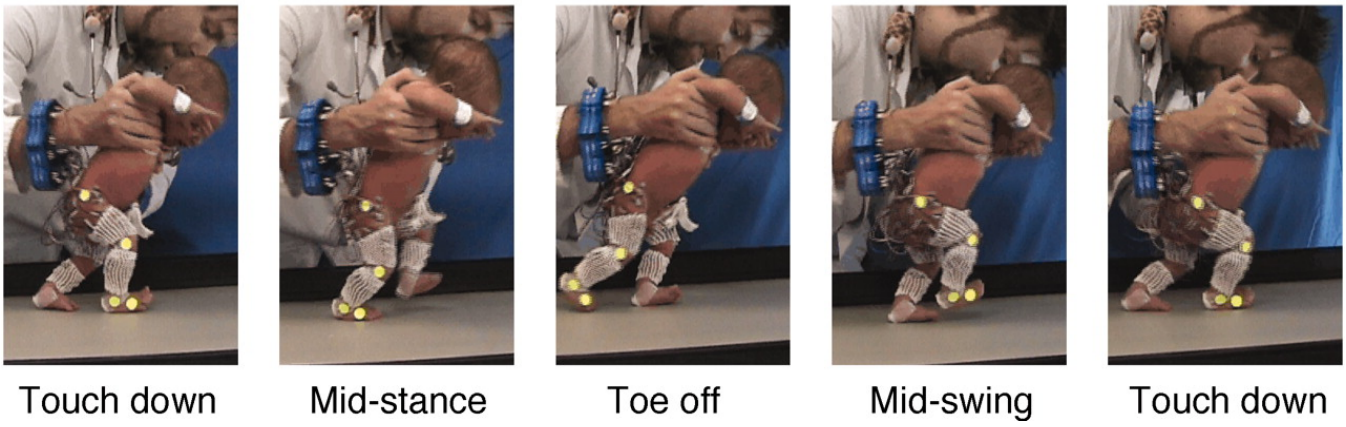

Figure 2: Proprioceptive stimulation of the feet on the ground is sufficient to activate reflex-like gait patterns in neonatal infants, each of which has a distinct functional role with respect to the whole movement. This observation suggests hard-wired motor modules are present at the spinal level from birth. These modules then undergo continual updating with maturation and experience to effectively address task demands. This figure has been adapted with permission directly from [5].

Appreciating Fig.1 further, clear structural boundaries can be observed around the muscle fibres that endow their contents with a conditional independence from their surrounding environment. This structural organisation can be considered a concrete manifestation of temporally persistent functional specialisation shaped by evolutionary pressures and life experience. However, the more temporary, dynamic, and transient functional interrelationships among muscles are not as obvious and require sophisticated statistical methods to accurately quantify. To elaborate, the functional roles of muscles arise from the scaling-up of basal operations by cellular networks (e.g. homeostasis) coupled with top-down constraints (e.g. neural circuitry dynamics) [6, 7], a complex process manifesting most directly to task performance as coordinated muscle activity patterns. These coordination patterns (commonly referred to as *muscle synergies*) are thought to emerge from a small set of motor primitives present at the spinal level from birth that are combined and sequenced in a task-specific way and undergo continual updating and refinement across the lifespan (e.g. Fig.2) [8, 5, 9, 10]. It is this direct relationship of muscle activation patterns to task performance that makes the reductionist view so attractive in motor control research, as found across the neurosciences more generally [11]. A view suggesting that muscle synergies representing the output of spinal neural circuitry dynamics are the fundamental scale of analysis concerning motor behaviour. In the current work, I will present an alternative perspective that gives credit to this direct relationship while capturing the fact that muscle synergies emerge from functionally dependent interactions across various scales.

Redundancy plays a key role in the success story of modularity as an organisational principle. Although the contractile state of neighbouring muscles may influence each other to a greater extent than distal muscles (facilitating the formation of submodules) [12], they all share a common functionality in aligning with the higher-order objectives of the system. Towards these higher-order objectives, different sets of muscles can carry out the same function (i.e. degeneracy) [13], promoting resilience and flexibility in the system within challenging environments. A caveat of this strategy is however the complexity cost incurred in coordinating the multitude of redundant degrees-of-freedom available to the human body [14]. An ensuing question then for researchers has been how exactly the human body does such a complex operation with great ease and generalisability under the constraint of limited computational resources [15, 16]. Substantial empirical evidence suggests that muscle synergies represent a key component in the answer to this question. They are considered to improve the computational efficiency of movement execution by providing a set of stereotypical motor patterns that can be flexibly combined in various ways by the nervous system to address task demands. Thus, instead of controlling the vast parameter space of everyday movements like reaching or gait (e.g. fig.2), the human motor system coarse-grains control into subcomponents that are executed in an automatic, reflexive way. Looking towards the future of this field, answers to this research problem have the potential to reveal important insight into evolutionarily tried-and-tested neural mechanisms governing coordinated movement both in health and with pathology [17]. Understandably, these insights are therefore highly sought after by health and engineering fields for designing clinical interventions, rehabilitation devices and robotics [18, 19].

The current-state-of-the-art in muscle synergy analysis applies unsupervised machine-learning to electromyographic (EMG) data with the aim of extracting low-dimensional, modular components of a given set of movements [20, 21]. The outputs of this approach can be combined and scaled in different ways to reconstruct any of the original movements, making them representative of the putative spinal modules. This approach, depending on the model employed, essentially quantifies global correlation patterns across muscle activations in spatial (i.e. between muscles across time) [22], temporal (i.e. between timepoints across

muscles) [5], or spatiotemporal (i.e. between muscles and timepoints across trials) domains [23, 24]. To exemplify the underlying motivation for this approach, by simply correlating the activity of a set of muscles (e.g. m_x and m_y in Fig.3(a)), researchers can ascertain whether they typically activate similarly, differently, or are independent in their activation patterns. During coordinated movements, these correlations provide clues as to which muscles respond similarly towards a motor task (i.e. are functionally redundant), albeit with some notable inferential work by the analyst. On this note, when assessing these correlations, it is important to consider that muscles are biomechanically constrained and so may present with inherent correlations irrespective of the task performed (i.e. task-irrelevant) [25]. Moreover, when assessing muscular correlations across tasks, commonalities in task constraints result in apparent functional dependencies between muscles, making the identification of genuine neural couplings difficult using current approaches [25, 26]. Taken together, the lack of a direct mapping between muscle interactions and their functional consequences results in the conflation of task-relevant (i.e. common muscle variability that is specific to a task (white shading of intersection in Fig.3(a)) and -irrelevant correlations (i.e. common muscle variability that is present across tasks (yellow shading of intersection in Fig.3(a)) [21]. Consequently, practical applications of muscle synergies without a direct task performance mapping have been shown to exhibit significant errors [27]. Some research groups have made efforts to address this limitation, including informing muscle synergy extraction and model-rank selection with relevant task parameters [28, 29, 19, 30]. Here, I will address this important limitation in current muscle synergy analysis, offering a direct approach to mapping muscular interactions to task performance (τ) and deciphering their specific task relevance (Fig.3(b)).

Although a key contributor to the versatility and resilience of the human body, redundancy constitutes only a part of this intricate systems' functional architecture. More specifically, the links that tie these modules together (e.g. the stereotyped movements in fig.2) into reciprocal combinations that form emergent patterns (e.g. gait) is a crucial aspect of motor behaviour. These cross-module interactions represent functional complementarities between muscles (i.e. muscles that work together towards different aspects of the same task) and promote functional integration across the system. Intuitively, the characteristic agonist-antagonist muscle pair (e.g. biceps vs triceps, hamstring vs quadriceps) exhibits a synergistic pattern, contributing towards flexion and extension of the arm and leg respectively. Only when synergistically combined can these distinct muscle activations generate complex movements such as reaching or gait for example. Yet, current conceptual and analytical perspective on muscle synergies only provide coverage to muscle groupings that *'work together'* towards functionally similar task-goals (Fig.3(a)) [31]. Hence, these complementary muscle interactions can only be indirectly inferred using current approaches by qualitatively comparing the co-occurrence of muscle weightings across the extracted modules. Consequently, the muscle interactions underlying coordinated movement are not comprehensively characterised by current approaches. In this work, I will present a novel perspective to the muscle synergy where muscles work together towards not only functionally similar (i.e. redundant (pink shading of pink-orange intersection) (Fig.3(b))) task-goals, but also functionally complementary objectives (i.e. synergistic (orange shading of pink-orange intersection) and secondary objectives irrelevant towards task performance (yellow intersection) (Fig.3(b)).

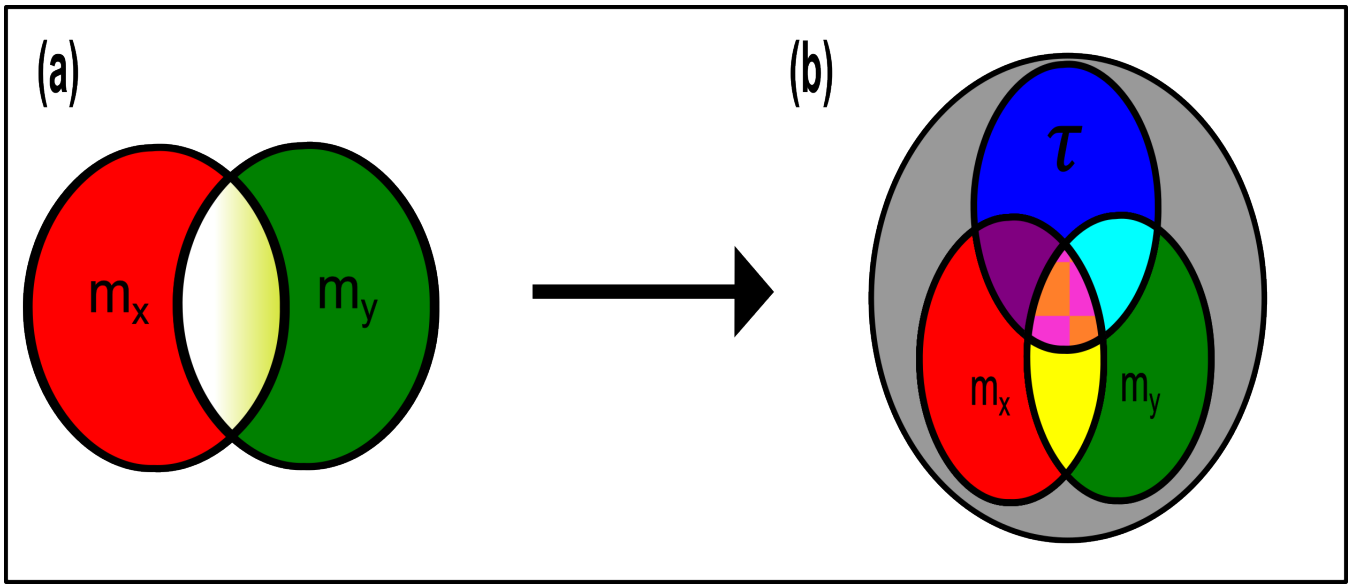

Figure 3: **(a)** A simple Venn diagram illustrating the underlying computation involved in current approaches to quantifying muscle synergies. The common variability (white-yellow intersection) between a set of muscle activities (e.g. m_x (red) and m_y (green)) is extracted using unsupervised machine-learning methods. These activation patterns are inferred to represent functional redundancies between muscles induced by neural couplings ('muscle synergies'). However, the lack of a direct mapping to task performance makes it difficult to parse task-specific neural couplings (white shading of intersection) from alternative sources of muscular correlations (e.g. biomechanical and task-level constraints) (yellow shading of intersection). **(b)** In this work, I will propose a novel approach that directly includes task parameters (τ (blue)) during muscle synergy extraction, distinguishing task-irrelevant information (yellow intersection) from task-relevant information (pink-orange intersection) and characterising their task relevance as either redundant (i.e. functionally similar (pink shading of pink-orange intersection)) or synergistic (i.e. functionally complementary (orange shading or pink-orange intersection)).

Modular control provides a strong mechanistic answer to the motor redundancy problem in that it explains how the human motor system efficiently allocates computational resources. Common neural inputs are mapped to behaviour via muscle synergy representations orchestrated by corticospinal interactions [32], thus reducing the degrees-of-freedom involved in controlling movement. It must be pointed out here however that the end-effectors of these common neural drives are individual muscles with their own unique anatomical attachments and consequently, their own unique contribution to task performance. Moreover, the receptors of each muscle provide unique feedback information that has been shown to shape whole motor patterns [7, 33]. Meanwhile feedforward mechanisms must incorporate information about the activation time-delays specific to each muscle to effectively coordinate movement and may directly control individual muscles where necessary to address task demands (e.g. early stages of motor learning, motor tasks requiring fine-grained control) [24, 34, 35]. This insight suggests that functional independence generated from both top-down and bottom-up sources likely manifests among muscular interactions, promoting the individual muscle as having a crucial role in movement construction. Although the independent control of muscles has been recognised in early studies [36], the muscle synergy approach currently does not provide conceptual or analytical coverage towards its functional role and only recently has it been formally embedded in theoretical frameworks on human movement modularity [37]. Building on traditional muscle synergy analysis and the work I will carry out in this project (Fig.4(a-b)), I will devise a computational approach that extracts diverse types of functional muscle interactions (i.e. functionally- similar (Redundant (pink intersection)), -complementary (Synergistic (orange shading)), and -independent (Unique (magenta and cyan intersections)) (Fig.4(c)). For an intuitive example of what each of these types of functional relationships between muscles represent, see Fig.5 for a toy simulation.

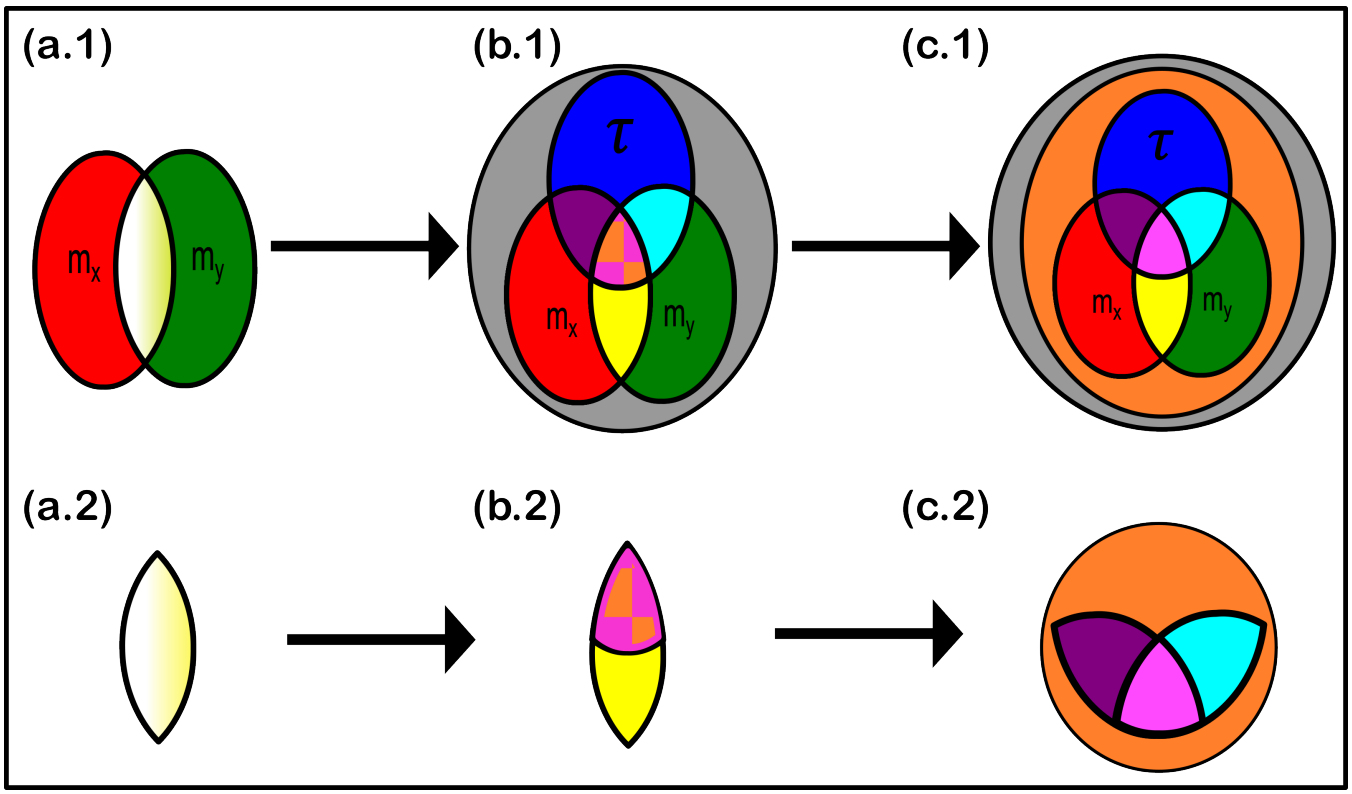

Figure 4: Building on traditional approaches to muscle synergy analysis **(a.1)** and the work I will carry out here in proposing a novel perspective to the muscle synergy **(b.1)**, I will develop a novel computational approach to muscle synergy analysis that quantifies diverse types of functional interactions simultaneously **(c.1)**. **(a.2)** Traditional approaches to muscle synergy analysis extract common variability between groups of muscles that conflates both task-relevant (white shading) and task-irrelevant (yellow shading) interactions between muscles. **b.2)** The novel perspective i will propose will separately distinguish the task-irrelevant information shared between muscles (yellow intersection) and characterise the task-relevant information as either redundant (pink shading) or synergistic (orange shading). **(c.2)** Building on this novel perspective, i will then develop a comprehensive analytical approach to separately characterising different types of task-relevant muscle interactions, including functionally similar (i.e. redundant (pink intersection)), and -complementary (i.e. synergistic (orange shading)) interactions along with the functionally independent (i.e. unique) contributions of individual muscles (magenta and cyan intersections)) to task performance.

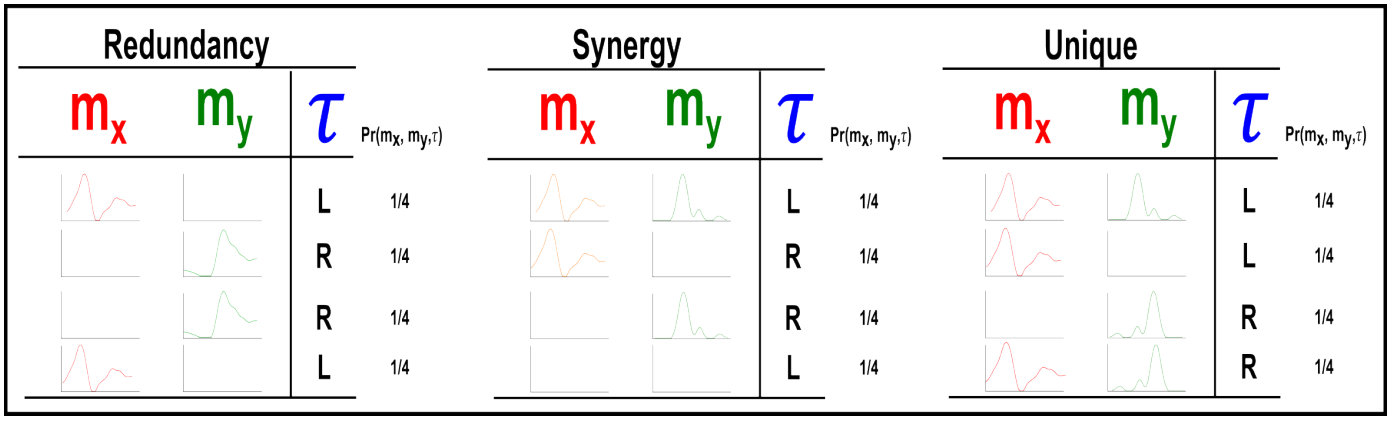

Figure 5: A toy example illustrating the three distinct interaction types I will quantify using the developed methodology. Four observations of a given muscle pair (m_x, m_y) and a corresponding binary task parameter (τ) representing left ('L') or right ('R') directions are depicted. Functionally similar muscle interactions (Redundancy) are quantified as the task information that can be provided equally by observing either m_x *or* m_y alone (i.e. when m_x is active or when m_y is inactive, it predicts L and vice versa for R). Functionally complementary interactions (Synergy) are quantified as the task information provided only when m_x *or* m_y are observed together (i.e. τ can only be successfully predicted here when observing the activation state of both muscles, when both are active or inactive τ=L, otherwise if only one muscle is active τ=R. Finally, functional independence between muscles (Unique) is quantified as the task information that can only be provided by either m_x *or* m_y. In other words, as illustrated here, when m_y is active in a particular way it predicts R irrespective of the activation state of m_x.

1.1 Summary of research objectives

- Address current limitations among analytical approaches to facilitate the direct inclusion of task parameters during muscle synergy extraction (Chapter 2).
- Propose a novel perspective to the muscle synergy concept that directly maps muscle interactions to task performance and characterises their specific task relevance (Chapter 3).
- Incorporate the extraction of diverse types of muscle interactions into muscle synergy analysis, including functionally similar, complementary, and independent muscle interactions (Chapter 4).

1.2 Key terms

Table 1.1: A list of definitions for key terms used in this work.

Term	Definition
Connectivity	dependencies between nodes in a network.
Degeneracy	structurally different components that perform the same function.
Dynamics	patterns of muscle activity that change or respond to behavioral states.
Emergence	system property arising from constituent interactions.
Hierarchy	system structure where units are composed of sub-units.
Information	surprise reduction when an event is observed.
Module	independent, functionally specialised component of a system
Multiplex network	a multidimensional network representing different types of relationships between nodes.
Mutual information	the variability in a random variable that can be predicted by the variability in another random variable.
Muscle coupling	statistical relationship between a pair of muscles such that they may behave as a unit.
Muscle interaction	mutually transformative exchange between muscles that doesn't necessarily result in functional grouping.
Muscle synergy	group of muscles that functionally cooperate during coordinated movements.
Network centrality	a measure of node importance in a network.
Network community	a more densely connected subset of nodes.
Redundancy	the duplication of functional roles.
Scale invariant	a pattern common across scales.
Synergistic information	information provided complementarily by two muscles.
Task-irrelevant	present across different tasks.
Task-relevant	predictive of specific task-specific attributes.
Task representation	muscle activation pattern correlated with a task.
Unique information	information provided exclusively by an individual muscle.

Chapter 2

A network information theoretic framework to characterise muscle synergies in space and time

David Ó' Reilly and Ioannis Delis 2022 J. Neural Eng. 19 016031

2.1 Abstract

Objective

Current approaches to muscle synergy extraction rely on linear dimensionality reduction algorithms that make specific assumptions on the underlying signals. However, to capture nonlinear time varying, large-scale but also muscle-specific interactions, a more generalised approach is required.

Approach

Here we developed a novel framework for muscle synergy extraction that relaxes model assumptions by using a combination of information- and network theory and dimensionality reduction. We first quantify informational dynamics between muscles, time-samples or muscle-time pairings using a novel mutual information formulation. We then model these pairwise interactions as multiplex networks and identify modules representing the network architecture. We employ this modularity criterion as the input parameter for dimensionality reduction, which verifiably extracts the identified modules, and also to characterise salient structures within each module.

Main results

This novel framework captures spatial, temporal and spatiotemporal interactions across two benchmark datasets of reaching movements, producing distinct spatial groupings and both tonic and phasic temporal patterns. Readily interpretable muscle synergies spanning multiple spatial and temporal scales were identified, demonstrating significant task dependence, ability to capture trial-to-trial fluctuations and concordance across participants. Furthermore, our framework identifies submodular structures that represent the distributed networks of co-occurring signal interactions across scales.

Significance

The capabilities of this framework are illustrated through the concomitant continuity with previous research and novelty of the insights gained. Several previous limitations are circumvented including the extraction of functionally meaningful and multiplexed pairwise muscle couplings under relaxed model assumptions. The extracted synergies provide a holistic view of the movement while important details of task performance are readily interpretable. The identified muscle groupings transcend biomechanical constraints and the temporal patterns reveal characteristics of fundamental motor control mechanisms. We conclude that this framework opens new opportunities for muscle synergy research and can constitute a bridge between existing models and recent network-theoretic endeavours.

2.2 Introduction

The question of whether the control of movement can be characterised by a simplified, low-dimensional strategy is a pertinent one in the motor control literature [21, 16, 15, 38, 39]. When one considers the numerous degrees-of-freedom available to the human body at the neural, musculoskeletal and dynamic level for a given movement, the task of selecting an adequate strategy from the set of redundant solutions becomes a computationally intensive operation [15]. Along with this, the capacity for the human body to adapt pre-existing movements and allow for the emergence of novel strategies calls into question, within the context of biomechanical constraints and environmental demands, the nature of the neural constraints on movement [8, 25]. It is thought that the central nervous system (CNS) activates movement building-blocks known as motor primitives and through their combination, complex motor patterns can be efficiently performed [15, 38]. This strategy allows for the efficient control of groups of neurons, motor-pools and consequently muscles rather than the more computationally intensive, individual control of each degree-of-freedom in the brain. Specifically at the muscle level, evidence for this phenomenon comes most conclusively from animal studies [40, 41], but a significant degree of indirect evidence is also accumulating in the human population, for example during development and with training experience [10].

The recent efforts in the motor control literature provide a foundation for furthering our understanding of the mechanisms underlying modularity in human motor control. Among those efforts, different research groups have formulated mathematical definitions to factorize EMG signals using unsupervised machine-learning in the spatial [42], temporal [5], and spatiotemporal domains [43] or their unification through the space-by-time model [23]. These investigations produced novel insights such as the presence of both task-specific and -shared synergies and the complexity of synergies being linearly related to neurological impairment [44, 45]. These muscle synergy models are typically implemented using non-negative matrix factorisation (NMF) but tensor decompositions have also recently been utilised with the particular advantage of concurrent extraction of both spatial and temporal synergies and their task-dependent modulations [23, 46]. Nonetheless, NMF and its higher-dimensional variants are constrained to extract linear representations of the EMG activity and so may not fully capture the nonlinear characteristics of the musculoskeletal system. Furthermore, the current muscle synergy models don't facilitate the incorporation of signals with such diverse properties and their extension to include task parameters often violates underlying model assumptions. An example of such an approach is the proposition of 'functional synergies' which incorporate task space variables in synergy extraction. Indeed, functional synergies have revealed interesting relationships between muscle activity and biomechanical function [47, 48, 49]. However, the muscle- and task spaces are not always expected to share the same mixing coefficients, as task space parameters are not necessarily non-negative and some of the extracted task components may not correspond to EMG data [19, 49]. As a consequence of the reliance of these approaches on dimensionality reduction, an emphasis is placed on muscle activations that account for the most variance at the expense of more subtle couplings and task relevancy [27]. Thus, a more generalised and non-parametric formulation of the current muscle synergy models is needed in order to overcome these limitations. Moreover, although current muscle synergy models support recent evidence for multi-functional group membership by individual muscles, [50, 51, 52], the dynamics of these functional groups at the level of pairwise couplings are not well elucidated and may hinder the outputs' inferentiality. Thus, a methodology that captures pairwise couplings and differential interactions between muscles with respect to a task at multiple spatial and temporal scales may provide more insight into these underlying mechanisms. A generalised approach will also be more amenable to future avenues of research on movement modularity discussed at length by [21], including the falsifiability of muscle synergy patterns by neural signals serving as model constraints. Thus, the development of an appropriate methodological approach that can meet these requirements is incentivised.

In the current study, we sought to develop a novel framework for the characterisation of muscle synergies using a combination of information- and network-theory and dimensionality reduction. Both information- and network theory have proven useful in the analysis of such muscle couplings with novel insights gained in both the temporal and frequency domains and by elucidating the shaping of these couplings by anatomical constraints for example [39, 53, 54, 12]. Our proposed framework extends existing muscle synergy models by exploiting the advantageous properties of a novel mutual information formulation for the efficient extraction of salient features across space, time, repetitions and experimental conditions. From the outset, we sought to stringently align the attributes of this framework with the unique characteristics of the synergy concept while positioning it as a useful tool for the progression of the motor control research field. A novel model selection procedure is introduced, where the extracted informational dynamics are modelled as a multiplex network and the predominant clusters are identified. The number of clusters then serves as the empirical input parameter for dimensionality reduction. Following the presentation of this framework, we apply it to two benchmark datasets of point-to-point reaching movements. We identify functionally and physiologically meaningful synergies that demonstrate a high level of consistency in structure, noise correlations and task dependence across participants. A submodular structure representing functional distinct connections is also highlighted across all synergies. This novel architecture of muscle activation signals transcends biomechanical constraints and reveals distributed networks of co-occurring interactions across spatial and temporal scales. Finally, we discuss the continuity of these models with previous research and novel insights gained along with potential directions for future research using this generalised approach. An open-source Matlab GUI (`https://github.com/DelisLab/GCMI-synergy-extraction`) is available for readers to

implement this novel computational framework on their own data as described here.

2.3 Materials and Methods

Informational dynamics in motor control

A muscle synergy consists of a set of muscles acting as a functional unit during the execution of a coordinated movement and has the identifiable characteristics of a sharing pattern, reciprocal compensation and task dependence [31]. In other words, muscles may share a consistent pattern of activation in space and time, their activations are interdependent and can be adjusted when deviations are experienced, and as elemental variables they can be re-organised for different objective functions. With such complex interdependencies between components, the accurate modelling of these emergent properties during naturalistic behaviour is challenging, requiring a high degree of computational sophistication. This analytical challenge is accompanied by the presence of noisy communication channels that innervate the numerous components of the human nervous system, requiring statistical tools that are robust to noise.

Mutual information (MI) is a statistical measure originally developed to determine the reliability of information transmission across noisy electrical circuits [55]. Recent applications of MI to neural circuitry have been fruitful, with dependence between cortical- and spinal-level activations and motor behaviours elucidated [56, 57, 58]. In the following, we briefly present the foundational concepts incorporated in the presented framework that allow for interactions between muscles in space and time to be quantified as informational dynamics in a computationally efficient and noise robust manner.

Mutual information

The MI between a pair of muscles M_x and M_y ($I(M_x; M_y)$) (or pair of time-samples T_x and T_y ($I(T_x; T_y)$)) can be thought of as the difference between the entropies of the individual variables ($H(M_x) + H(M_y)$) and their joint entropy ($H(M_x, M_y)$). The entropy of a random variable is the degree of uncertainty of getting a possible outcome from the given distribution and so MI quantifies the reduction of uncertainty in M_y due to M_x.

$$I(M_x; M_y) = H(M_x) + H(M_y) - H(M_x, M_y) \qquad \text{Equation 1.1}$$

In doing so, MI captures the non-linear dependence between M_x and M_y in the unit known as *bits*. This expression of MI will aid in the communication of the novel MI estimate in the next section. There are a number of equivalent expressions for MI in the literature, another is given in equation 1.2. Here, MI is quantified as the difference between the entropy of M_x and the conditional entropy of M_x given M_y, $H(M_x|M_y)$. Using this expression, it can be seen that when M_y completely determines M_x (and vice-versa), the MI is equal to $H(M_x)$.

$$I(M_x; M_y) = H(M_x) - H(M_x|M_y) \qquad \text{Equation 1.2}$$

Here we employ a parametric estimator for entropy and MI which enables a reliable estimation of information using limited samples and is computationally efficient [59]. Their formulations are presented in the closed-form in equations 1.3.1 and 1.3.2 respectively. Entropy is expressed as a function of the covariance matrix determinant ($|\sum|$) with dimensionality k. $\sum_{M_x}$ and $\sum_{M_y}$ are the covariance matrices of two Gaussian variables (EMG channels, time-sample vectors etc.) and $\sum_{M_{xy}}$ is the covariance matrix for the joint variable contrasted against these individual covariance's within the determinant. A bias-correction term was applied to these estimations as illustrated in [59].

$$(H(X) = \frac{1}{2ln2} \ln \left[(2\pi])^k |\sum| \right] \qquad \text{Equation 1.3.1}$$

$$I(X;Y) = \frac{1}{2ln2} \ln \left[\frac{|\sum_{M_x}| \; |\sum_{M_y}|}{|\sum_{M_{xy}}|} \right] \qquad \text{Equation 1.3.2}$$

Gaussian copula mutual information

Similarly to MI, a copula (c) is a statistical measure of non-linear dependence between a pair of random variables but in the case of c, this estimate has two advantageous properties described in Sklar's theorem and the invariance theorem [60, 61]. Briefly, a given multivariate cumulative distribution function (CDF) can be described by two components, the c linking the variables and their marginal CDFs in such a way that when the marginal CDFs are continuous, c is unique. c is a probability density over the unit square that is formulated through the rank normalization of individual variables and rescaling to a range between 0-1. In linking two random variables, c is therefore directly related to MI (Equation 2.1) [59, 62].

$$H\left(M_x, M_y\right) = H\left(M_x\right) + H\left(M_y\right) + H(c) \qquad \text{Equation 2.1}$$

As shown in equation 2.1, the joint entropy of M_x and M_y is equal to their individual entropies and the entropy of c. Plugging equation 2.1 into equation 1.1, we see that the marginal entropies will cancel out (Equation 2.2), meaning negative $H(c)$ is equal to the MI between the M_x and M_y variables referred to hereafter as the Gaussian copula mutual information (GCMI) [59, 62].

$$I\left(M_x; M_y\right) = -\,H(c) \qquad \text{Equation 2.2}$$

An attractive quality of this formulation is that the empirical copula can maintain this encapsulated relationship between variables following a monotonic transformation of their individual distributions [61]. Thus, it is appropriate to implement the computationally efficient parametric estimation in equation 1.3.1 following a marginal transformation of the individual random variables to a Gaussian distribution. Furthermore, a Gaussian distribution is desirable here as it has the maximum entropy of any distribution and therefore the resulting GCMI estimates serve as a conservative lower-bound on the true MI.

GCMI will form the cornerstone for the muscle synergy framework presented here, representing a robust, nonlinear statistical measure of dependence that can be applied to a broad range of calculations involving uni- and multi-variate samples and in permutation testing for example. An opensource toolbox containing the information-theoretic measures described here was utilised in Matlab software [59].

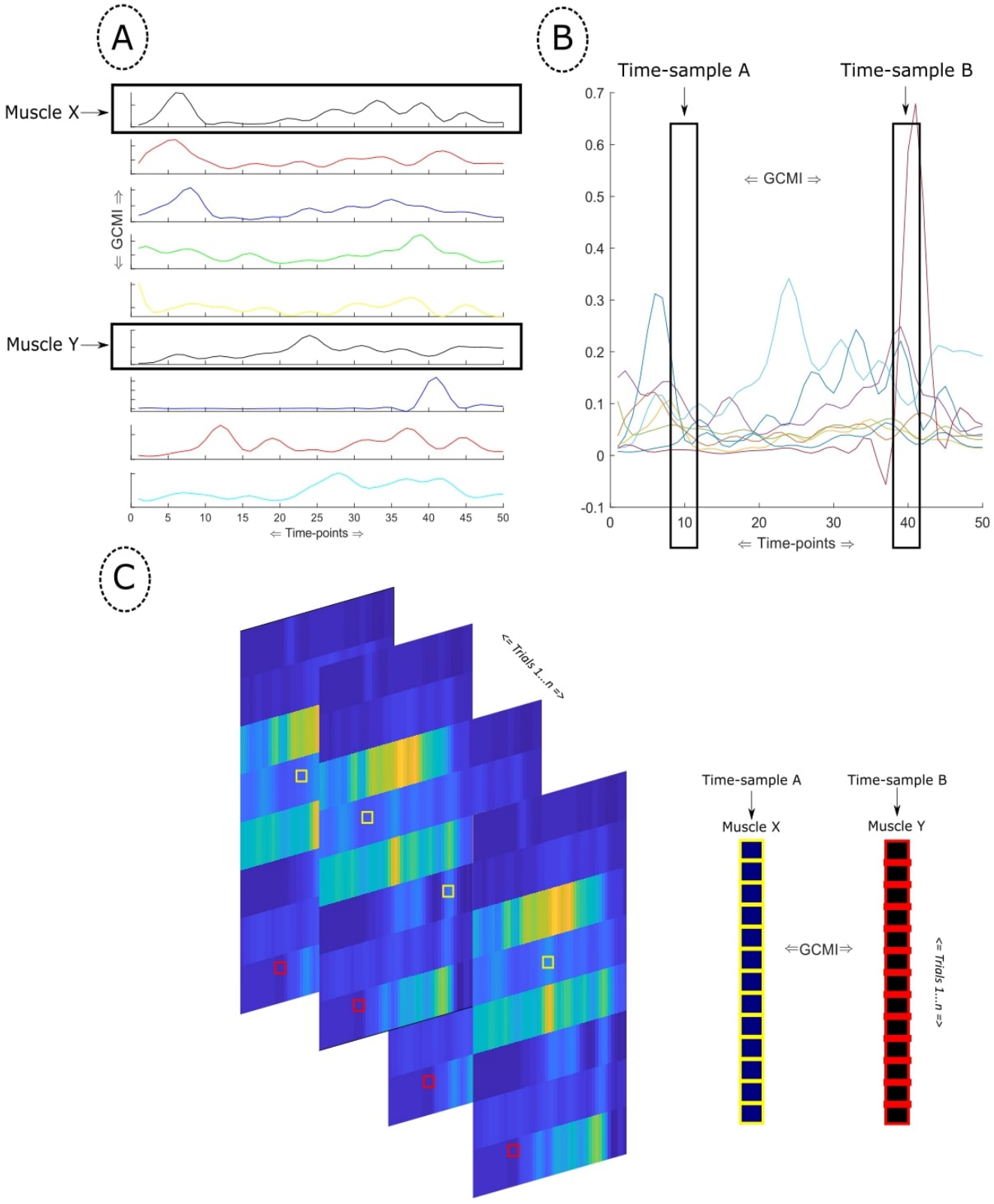

Fig.1: **(A)** An example of spatial information extraction with the GCMI computed from the EMG activity of two muscles across all time-samples in a single trial. **(B)** An example of temporal information extraction where the GCMI is computed between two time-vectors across all nine muscles in a single trial. **(C)** The space-time information extraction is illustrated where time-sample A for a single muscle across all trials is extracted, creating a vector that is used to compute the GCMI against a similar vector for another muscle at time-sample B.

Information extraction from EMG activity

To compute couplings between muscles m across time $t = 1, \ldots, T$ (i.e. synergies in the spatial domain), we took a pair of muscle activations M_x, M_y for a single trial *s* and determined the GCMI between them $I_s\,(M_x; M_y)$ (Fig.1 (A)). This procedure was iterated over each unique combination of muscles $k = 1, \ldots, K$ for all available trials $n = 1 \ldots N$, creating symmetric lower-triangular matrices equal in dimensions to the number of muscles (M) in the dataset (Fig.2(A)). These matrices for each trial were vectorised and concatenated (Fig.2 (B)), producing a N (No. of trials) x k= $M(M-1)/2$ (No. of muscle pairs) matrix ($I_{Space} = [I_{n^1} \ldots . I_{n^N}]$) (Fig.2(C)). This matrix served as input into a dimensionality reduction method known as projective non-negative matrix factorisation (PNMF), a variant of the frequently used NMF that has demonstrated a superior capacity for producing sparse representations of high dimensional data and identifying subspace clusters [63, 64]. This variant acts as a hybrid of NMF and Principal Component Analysis by using singular value decomposition (SVD) to extract linear, orthogonal features that are positively-constrained. In the current implementation, the SVD was initialised using non-negative Double SVD while the model-rank (i.e. number of extracted components) was determined using a novel procedure (Fig.2(E)) described in detail in the '*Model rank selection*' section that follows [65].

In the spatial domain, the factorisation of the input matrix, a matrix consisting of K unique muscle pairings across the set of trials $n = 1 \ldots N$ is described below in vector sum and matrix notation (Equation 3.1). Here the set of synergy weights (V) consists of column vectors ($\mathbf{v}$) representing clusters of muscle couplings across time in the jth module. The set of activation coefficients (A) consists of row vectors, $a_j^{n^N}$, are module- and trial-specific scalar values, inferred to be the neural commands driving the synergy patterns.

$$I_{Space} \approx AV \qquad \text{Equation 3.1}$$

$$\begin{pmatrix} (m^1)^{n^1} & \cdots & (m^1)^{n^N} \\ \vdots & \ddots & \vdots \\ (m^K)^{n^1} & \cdots & (m^K)^{n^N} \end{pmatrix} \approx \begin{pmatrix} a_j^{n^1} & \ldots & a_j^{n^N} \end{pmatrix} \bullet \begin{pmatrix} \mathbf{v}_j^{m^1} \\ \vdots \\ \mathbf{v}_j^{m^K} \end{pmatrix} + residuals$$

To determine the temporal dependencies across muscles, we computed GCMI between all unique pairs of time-sample vectors of length m ($L = T(T-1)/2$), creating an L x n matrix (I_{Time}) (Fig.1(B)). We then implemented the procedure described in Fig.2(A-E), resulting in a factorised output of temporal synergy weights (W) and activation coefficients (A). The factorised output in the temporal domain is described in equation 3.2 where the set of temporal synergy weights consists of row vectors ($\mathbf{w}$) representing clusters of temporal coupling across muscles for the ith module.

$$I_{Time} \approx WA \qquad \text{Equation 3.2}$$

$$\begin{pmatrix} (t^1)^{n^1} & \cdots & (t^1)^{n^N} \\ \vdots & \ddots & \vdots \\ (t^L)^{n^1} & \cdots & (t^L)^{n^N} \end{pmatrix} \approx \begin{pmatrix} \mathbf{w}_i^{t^1} & \ldots & \mathbf{w}_i^{t^L} \end{pmatrix} \bullet \begin{pmatrix} a_i^{n^1} \\ \vdots \\ a_i^{n^N} \end{pmatrix} + residuals$$

The spatial and temporal models previously described here capture these unique physical dynamics in isolation. To comprehensively capture spatiotemporal dynamics, we developed an extension of the above muscle synergy models and in continuation of previous work [23], spatial and temporal modules were concurrently extracted in a unifying space-time model through the following computation (Fig.1(C)). We extracted the EMG activity of a particular muscle M_x at a particular time-sample T_x across all trials and computed GCMI between this vector and that of a similar vector for muscle M_y at time-sample T_y. Once again we iterated this computation over all unique combinations of these vectors and then implemented the synergy extraction procedure described in Fig.2(A-E), i.e. we vectorised the GCMI values computed between these trial-to-trial vectors and concatenated them into a K (No. of muscle pairs) x L (No. of time-sample pairs) input matrix ($I_{Space-Time}$). This enabled us to determine trial-to-trial dependencies that are consistent across spatial (V) and temporal (W) dimensions. The factorised output for the space-time model is described below (Equation 3.3), with $\mathbf{v}$ and $\mathbf{w}$ being the spatial and temporal synergy weights for the jth module representing clusters of couplings between muscles in space and time across trials respectively.

$$I_{Space-Time} \approx WV \qquad \text{Equation 3.3}$$

$$\begin{pmatrix} (m^1 t^1) & \cdots & (m^1 t^L) \\ \vdots & \ddots & \vdots \\ (m^K t^1) & \cdots & (m^K t^L) \end{pmatrix} \approx \begin{pmatrix} \mathbf{w}_j^{t^1} & \cdots & \mathbf{w}_j^{t^L} \end{pmatrix} \bullet \begin{pmatrix} \mathbf{v}_j^{m^1} \\ \vdots \\ \mathbf{v}_j^{m^K} \end{pmatrix} + \textit{residuals}$$

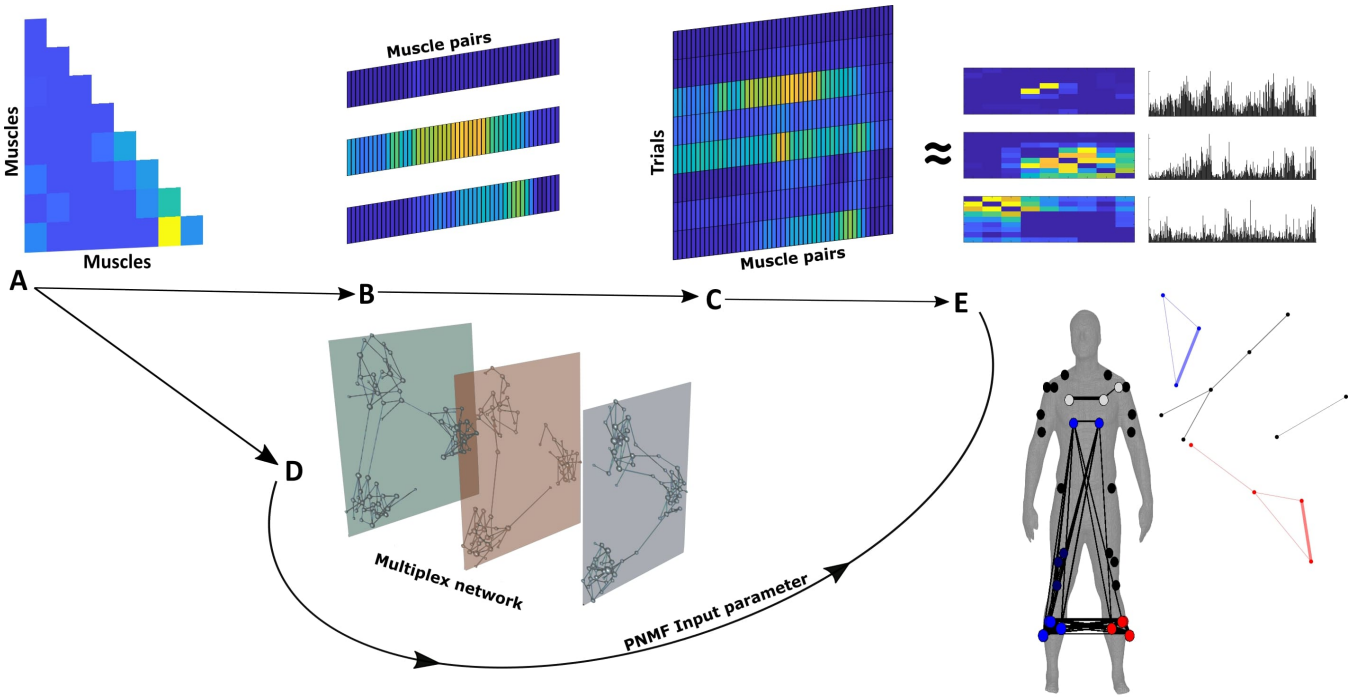

Fig.2:(A) The GCMI is computed between each unique pair of muscles (spatial) or time-sample vectors (temporal) or trial-to-trial (space-time) vectors, creating a lower-triangular matrix. **(B)** The lower-triangular matrices are reshaped into single vectors and concatenated, creating the input matrix as shown in **(C). (D)** The matrices depicted in (A) are concatenated into a multiplex network and input into a generalised Louvain algorithm to identify the optimal community structure (See 'Model rank specification' section). **(E)** These input matrices shown in (C) are then factorized into lower-dimensional representations of (D) using the optimal community structure as an input parameter to projective non-negative matrix factorisation (PNMF)**.** As an example, we illustrate the spatial synergy output here. The unique structure of the output for each of the synergy models is described in equations 3.1-3.3. A secondary community detection was then conducted to identify submodular structures in the extracted synergies.

Spurious dependencies typically associated with noise may be found in the above computations and so it was necessary to apply a threshold to identify only the significant associations. A methodology derived from statistical physics, namely a modified percolation analysis [66], was chosen for this framework. This form of percolation analysis was developed to reconcile two opposing characteristics of biological networks, modularity (i.e. the extent of sparsity between groups of densely connected nodes) and 'small-world' properties (i.e. the integration of all nodes in a network towards the shortest average path length) [66, 67]. The percolation analysis was shown to be effective in identifying functional modular structures while maintaining a sensitivity to the long-range connections that act as the bridges between modules which are often weaker in biological networks [68]. Moreover, this methodology is particularly suited to community detection procedures discussed in the '*Model-rank selection'* section that follows [69]. By iteratively removing the weakest dependencies until the *'giant component'* in the network starts to become affected, the network sparsification threshold can then be defined as this critical stopping point, providing a data-driven method to reduce the effect of noise that can be applied to specific networks.

Model rank specification

To represent muscle activations adequately, it is necessary to select an optimal number of components to extract. On the other hand, it is also necessary to maintain a model rank that produces physiologically and functionally meaningful synergies while also identifying a low-dimensional space, a challenging task within the literature [70]. To accommodate the unique characteristics of the GCMI matrices generated here, we developed a novel model rank selection criterion by defining a muscle synergy, a group of muscles acting cohesively as a functional unit, in network-theoretic terms. More specifically for the identification of these functional units in our data, we defined a synergy as a densely connected set of nodes otherwise known

as a community [71]. Hereafter, the term node refers to either a muscle, time-sample or muscle - time-sample pairing depending on the model in question. Prior to dimensionality reduction using PNMF, the row for each trial of an input matrix was converted to an adjacency matrix and became a layer in a multiplex network with all other trials. In the case of space-time computations, the temporal pattern across each spatial vector constituted the multiplex network. We implemented the percolation analysis described previously on each individual layer of the supra-adjacency matrix before the following computation.

Modularity in a monoplex network can be determined by the difference between the sum of all vertices that fall between all possible pairs of vertices in the network and that which would be expected by random chance [67]. This quantity is known as the Q-statistic which acts as an objective function to be optimised in community detection algorithms, ranging from 0-1 with 1 indicating maximal modularity [67, 72]. The multiplex modularity, a generalisation of the Q-statistic to multi-layered networks, was implemented here using the generalized Louvain algorithm where the community structure of intra-layer edges between all nodes and all inter-layer edges between nodes representing the same muscle/time-sample could be considered [71]. The resolution parameter γ was set to the default value of 1 for classical modularity [71]. The number of communities identified served as the input parameter for PNMF (Fig.3(E)). To verify the communities identified a priori were in fact extracted using PNMF, the maximum value in each row across synergy weight vectors ($\mathbf{w}$) served as an indicator for hard-cluster assignment [63]. By visually inspecting the cluster assignments produced by PNMF and those found through community detection, the output was found consistent (see supplementary materials (Fig.1.) for an example of this procedure).

Trial-to-trial network configuration and task dependence of extracted muscle synergies

Following the extraction of muscle synergies using the GCMI framework, we then investigated whether the identified sharing patterns also aligned with the other attributes of the synergy concept, i.e. reciprocal compensation/flexibility and task dependence [31]. As mentioned in the previous section, biological networks are generally characterised by two competing properties, fractal modularity and small-worldedness [66, 68]. The scale invariance of network architectures allows for greater robustness to injury and adaptability while the efficient transfer of information is crucial for within- and across-network communication and cohesion [73, 74]. It is therefore unsurprising to find modularity has been related to the motor learning process and small-worldedness to important integrative mechanisms such as working memory performance [75, 76]. In the context of the synergies extracted here and their reorganisation, fluctuations in these network properties from trial-to-trial may provide interesting insight into the neural control of movement. This is supported by experimental findings where increased integration in the muscle space and the reorganisation of modular structure from trial-to-trial were observed with additional motor noise and adaptations to task constraints respectively [77, 78].

Thus, we sought to determine if the GCMI framework could capture the dynamic balance between modularity and small-worldedness from trial-to-trial in the extracted activation coefficients. We firstly determined the global efficiency (GE) and Q-statistic for modularity (Q) for individual layers of the thresholded multiplex network depicted in Fig.3(D). GE quantifies the small-worldedness of a network through the ratio of present to possible edges [79]. Q was determined for individual network layers using the conventional Louvain algorithm [79, 72]. Analogous to previous work [80], this created two vectors in the spatial and temporal domains that were demeaned with respect to the task along with their corresponding activation coefficients. The correlations between single trial synergy activations and the network property measures defined above (GE, Q) for a fixed task (noise correlations) were then computed using Pearson's correlation [80]. The strength and direction of these correlations therefore provide insight into the sensitivity of the extracted synergies to this network level trade-off. To further exemplify the fractal modularity of the synergies produced by this framework, a secondary community detection procedure was carried out on the synergy weights using the traditional Louvain algorithm[72, 79]. The cluster assignment of these submodules were then represented on a human body model by the colour of nodes on the network [81].

To determine if the information encoded in the extracted muscle synergies can discriminate between the different experimental conditions/tasks, we computed the GCMI between individual spatial or temporal activation coefficient vectors and the reaching task variable. To assess whether the task-discriminative information presented in each component was significant, activation coefficients were also randomly shuffled and the GCMI with respect to the task was calculated. This procedure was repeated 100 times and the 95^{th} percentile of these collective values acted as an empirical threshold for significance. The specific task attributes for each dataset analysed in this study are detailed in the '*Experimental design and setup'* section.

Structural similarity of the muscle synergies across participants

It is crucial to the utility of this framework that the muscle synergies extracted are consistent across a set of participants who have conducted the same motor tasks. The same extraction procedures were therefore conducted across the remaining participants in each dataset and the following analysis was conducted to determine the structural similarity. Muscle synergies were first visually inspected and compared across participants and those with a similar functional interpretation were paired together. Following their vectorisation, the Pearson's correlation was then found between each pairing. This produced a set of coefficients that were transformed into Fisher's Z values, the average and standard deviation of which was taken and reverted to correlation coefficients. This value served as a global index of similarity across participants. To extract the average

muscle synergy from each model, the synergies across participants in each dataset were vectorized and the mean network was then found. To eliminate individual differences from the average synergies, the percolation analysis sparsification procedure described above was conducted.

Experimental design and data collection

Dataset 1

A dataset of EMG activity recordings was generated across seven healthy, right-handed adults (Age: 27±2 years, Height: 1.77±0.03m) who provided informed consent to participate in the experiment that conformed to the declaration of Helsinki (approved by the local ethical committee ASL-3 ("Azienda Sanitaria Locale," local health unit), Genoa) [23]. Participants were instructed to perform center-out (forward, denoted by *fwd*) and out-center (backward, denoted by *bwd*) one-shot point-to-point movements between a central location (P0) and 4 peripheral locations (P1-P2-P3-P4) evenly spaced along a circle of radius 40 cm at a fast pace (370-560 m/s duration on average across participants) (Fig.3(A)). 40 repetitions per target were captured per participant using the dominant hand. Movement onset and offset phases were defined at the points in which the velocity profile (captured via the kinematic data of a passive marker (Vicon, (Oxford, UK)) placed on the finger-tip that was numerically differentiated) fell above/below 5% of its maximum. The targets to which the participants reached were circles of radius 2 cm which they had to touch. No restraints or supports were provided while the order of the tasks were randomized.

Simultaneously, the activity of nine upper-body and arm muscles was recorded as presented in Fig.3(A) (Aurion (Milan, Italy)). The EMG setup was implemented in line with SENIAM guidelines. EMG signals were digitized, amplified (20-Hz high-pass and 450-Hz low-pass filters), and sampled at 1,000 Hz (synchronized with kinematic sampling). Subsequently, to extract the signal envelopes, the EMG signals were processed offline using a standard approach [43]: the EMGs for each sample were digitally full-wave rectified, low-pass filtered (Butterworth filter; 20-Hz cut-off; zero-phase distortion), normalized to 1,000 time-samples and then the signals were integrated over 20 time-step intervals yielding a waveform of 50 time-steps. Finally, the EMG signal of each muscle was normalized in amplitude by dividing each single-trial muscle signal by its maximal value attained throughout the experiment. For dataset 1 participants, the task dependence of individual spatial and temporal $\mathbf{a}$ was determined against discrete variables representing all point-to-point movements (P1-P8), all center-out (forward) movements (P1-P4), all out-center (backward) movements (P5-P8) and the movement direction (fwd vs. bwd).

Dataset 2

The EMG activity of 30 muscles from four healthy, right-handed adults (Age=25±3 years, height=1.72±0.08 meters, weight=70±7kg) was recorded (Aurion system, (Milan, Italy), SENIAM guidelines) while participants performed whole-body point-to-point movements in various directions and at differing heights. The muscles recorded included: tibialis anterior, soleus, peroneus, gastrocnemius, vastus lateralis, rectus femoris, biceps femoris, gluteus maximus, erector spinae, pectoralis major, trapezius, anterior deltoid, posterior deltoid, biceps and triceps brachii on both sides. The experimental setup (Fig.3(B)) was approved by the Dijon Regional Ethics Committee and conformed to the Declaration of Helsinki. Written informed consent was obtained by the participants following guidelines set by the Université de Bourgogne. This setup is described in detail elsewhere and will therefore be outlined briefly here [82]. Participants were asked to perform whole-body pointing movements between pairs of targets (9 targets at three different heights = 72 different movement tasks). Over the course of two separate sessions, participants performed 15 repetitions of each movement (30 repetitions in total), resulting in 72 x 30 = 2160 trials per participant. The processing of EMG recordings followed the same standardized protocol conducted on Dataset 1 while onset and end times for individual trials were determined in a similar manner using the kinematics of the pointing index finger at a frequency of 100 Hz. The left arm of participants was unconstrained and at rest throughout each trial while the order of movements was randomised. The resulting data was pooled, creating (50 time-sample x 2160 trials) x 30 muscle matrices. For dataset 2 participants, the task dependence of individual spatial $\mathbf{a}$ was determined against discrete variables representing the spatial movement features, i.e. start- and end-point bar and height (see fig.3(B)), up-down and left-right reaching directions. For individual temporal $\mathbf{a}$, the task dependence was determined with respect to temporal movement features representing the evolution of movement in time determined with respect to temporal movement features representing the evolution of movement in time, i.e. start-point, reaching direction and end-point target.

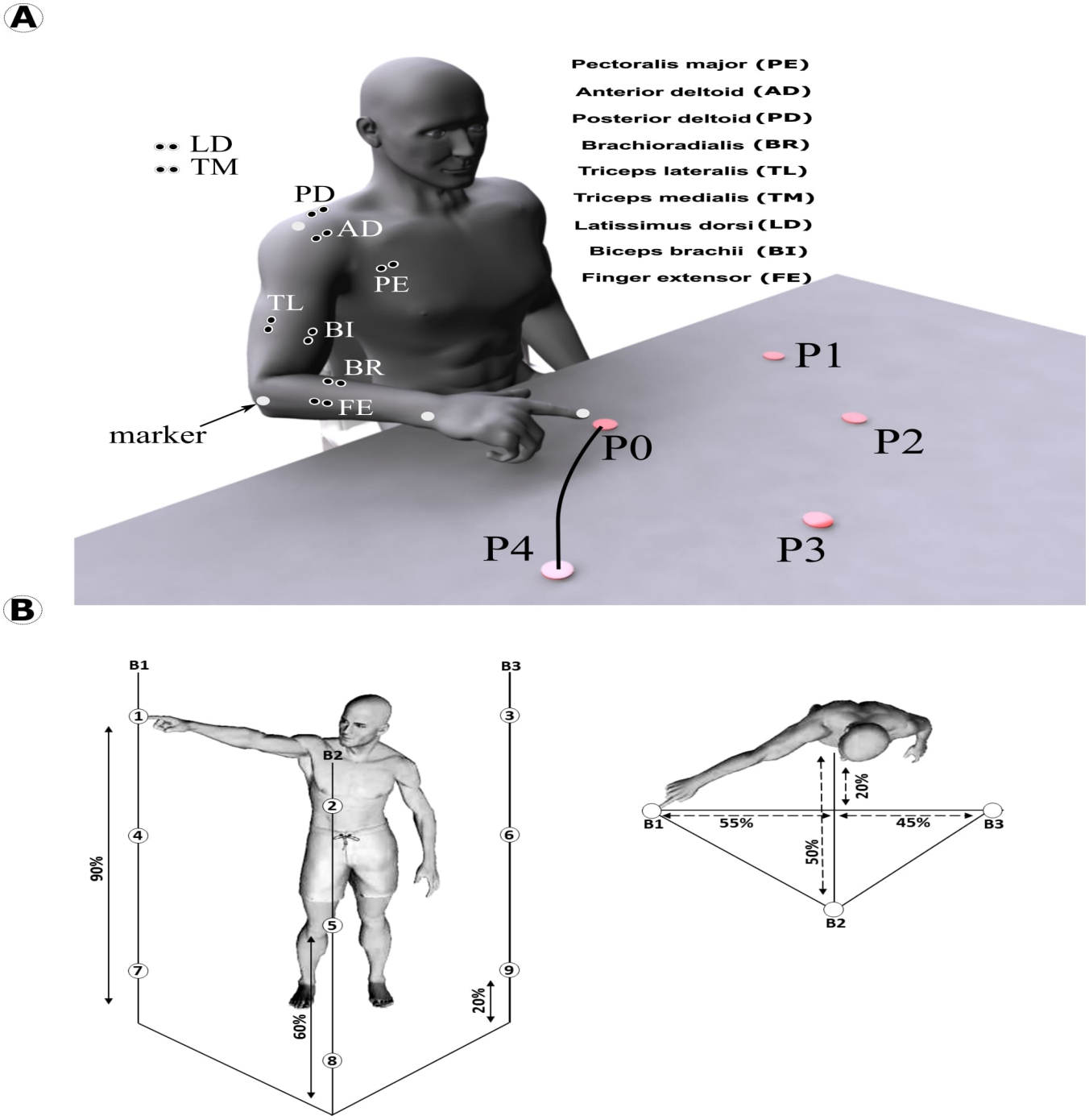

Fig.3 (A): An illustration of the experimental setup for Dataset 1 [23]. 40 repetitions of a tabletop point-to-point reaching movement were performed for each target (P1-P4) were conducted in both forwards/backwards directions and at a fast pace while the activity of the following muscles was recorded: LD: Latissimus dorsi; AD: Anterior deltoid; PD: Posterior deltoid; PE: Pectoralis; TL: Triceps lateral; BI: Biceps brachii (long head); TM: Triceps medial; BR: Brachioradialis; FE: Finger extensors. **(B):** An illustration of the experimental setup for Dataset 2 [82]. Participants were asked to perform whole-body point-to-point reaching movements between pairs of targets. Included were 9 different targets at 3 different heights, totalling 72 possible movement tasks.

2.4 Results

Muscle synergies in point-to-point reaching movements

Spatial synergy model

To identify spatial synergies, i.e. muscle couplings across time within each trial (see Fig.1(A)), we applied the proposed framework to dataset 1 consisting of arm-reaching movements in 8 different directions. In brief, we first computed GCMI between all pairs of muscles for each trial. We then input the single-trial GCMI values of all muscle pairs to the PNMF algorithm to identify couplings between muscles, i.e. muscle synergies, which are consistent across trials (see Fig.2 for an illustration of the full methodology).

Taking a representative example participant, three distinct spatial synergies were found using the community detection procedure (see Materials and Methods for details) with a Q-statistic value of 0.998 (Fig.4(A)). A high co-activation between the medial and lateral triceps was found in S1 along with a lower co-activation of the anterior deltoid. S2 represented a more global activation across the upper-arm and shoulder muscles while the finger extensors and brachioradialis remained inactive. S3 contained couplings between the finger extensors, brachioradialis and biceps brachii. Taking these together, one can interpret their functional grouping as the following: S1 represents elbow extension, S2 proximal stabilisation/shoulder flexion, and S3 is forearm flexion/finger control.

To assess the task-relevance and organisation of the identified synergies, we computed the task information conveyed by the synergy recruitment on each trial (Fig.4(B)) and the noise correlation between synergy recruitment and essential network properties derived prior to dimensionality reduction (Fig.4(C)). Forward vs. backward movements were mainly discriminated by S2 activations (0.26 bits) which implement shoulder flexion. S1 (elbow extension) contained the most information for movement direction across all movements, i.e. P1-P8 (0.51 bits), but also when considering only forward (P1-P4, 0.45 bits) or only backward (P5-P8, 0.52 bits) movements. S3 activations (predominantly of forearm muscles) did not contribute significantly to discrimination of forward movements (P1-P4, 0.16 bits) or forward vs backward direction (0.033 bits) but carried significant information for backward movements (P5-P8, 0.34 bits) which contributed to the overall discriminatory information (P1-P8, 0.29 bits). We also found significant correlations between all three synergy activation coefficients and network-theoretic measures ($p<0.05$) but in opposing directions with positive associations for integration (GE) and negative associations for segregation (Q). Both S2 and S3 shared the highest association with GE ($R= 0.72$), an interesting finding considering these synergies represent the distinct functional grouping of upper- and lower-arm muscles respectively. The activation in S1 reduced the least with positive changes in modularity ($R= -0.11$), likely due to the specificity of this synergy to the medial- and lateral-triceps.

A secondary community structure analysis of the extracted synergies revealed two submodules in S1 and S2 and just one submodule consisting of the lower-arm musculature in S3. In S1, these submodules consisted of the medial- and lateral triceps (green) and anterior deltoid and latissimus dorsi (pink). The medial-triceps and posterior deltoid (yellow) and lateral-triceps, pectoralis major and anterior deltoid (navy) comprised the S2 submodules. These submodules represent the distinct (but often overlapping) co-occurring muscle couplings that contribute consistently across tasks/trials to single-joint or cross-joint actuations.

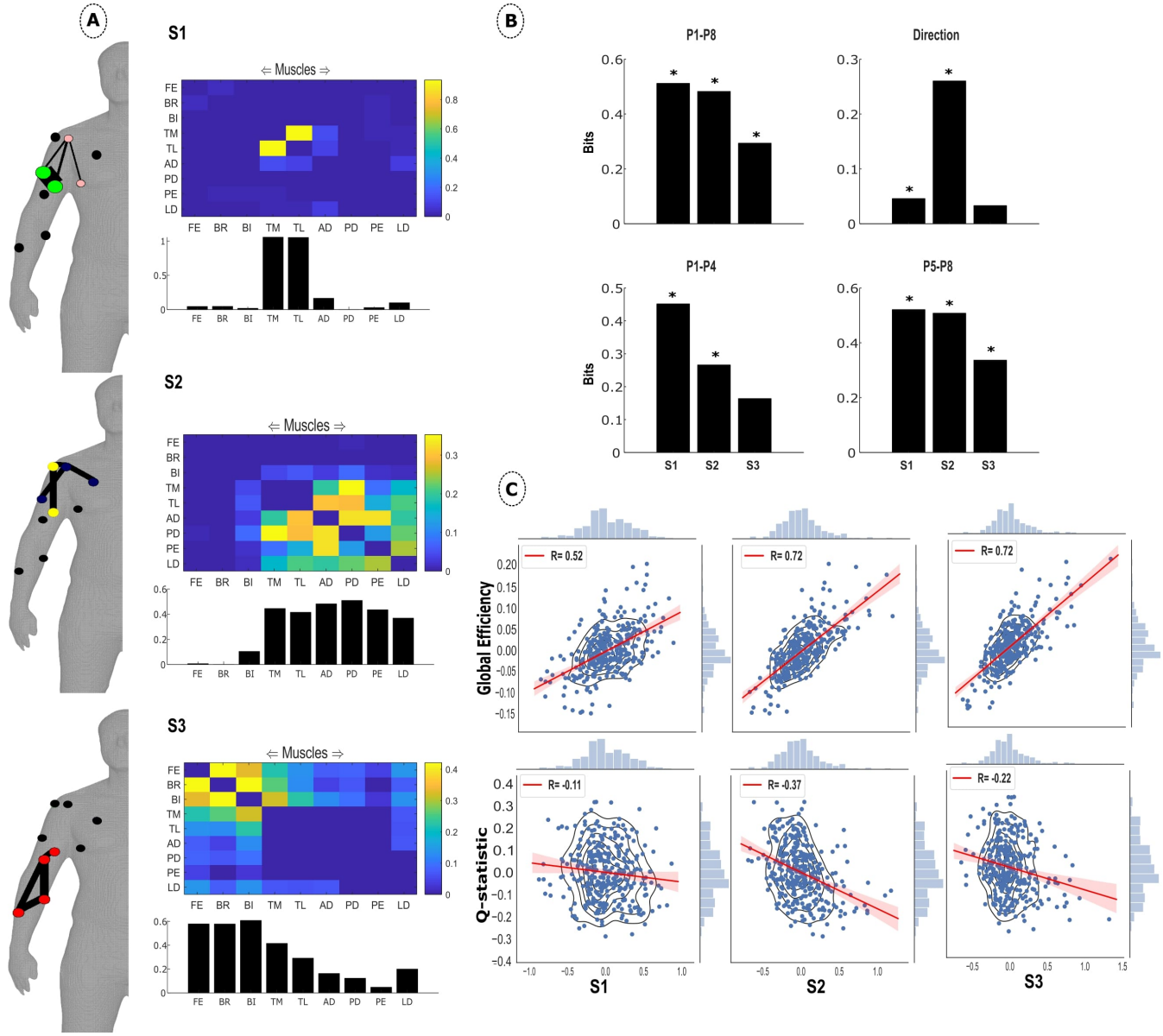

Fig.4:**(A)** The spatial synergies extracted from an example participant in Dataset 1. The community detection criteria found three distinct communities that were extracted using PNMF. The bar graph below represents the average values in each column of the adjacency matrix. The minimally connected human body model illustrates the values in the adjacency matrix with the width of the edges and colour and size of the nodes providing insight into connection strengths, submodular structure and involvement respectively [81]. Submodular structure was identified using the conventional Louvain algorithm on the synergy matrices [72]. Unconnected nodes are in black. **(B)** The encoded information of the three spatial synergies identified in the example participant in dataset 1 for four task attributes: P1-P8, P1-P4, P5-P8 and Direction. Significant information ($p<0.05$) is indicated with *.**(C)** The correlation between trial-to-trial fluctuations in Global Efficiency/Q-statistic for modularity and noise in the spatial activation coefficients. The bars along the axis of each plot are marginal histograms of the x- and y-variables.

Temporal synergy model

To characterise the temporal structure of muscle co-activations, we also applied the GCMI framework in the temporal domain, returning three temporal synergies (Fig.5(A)) for the same example participant that captured temporal associations across muscles. This was produced by computing GCMI between pairs of time-vectors (vectors of activations across all muscles at different time-samples, see Fig.1(B)) within each trial, modelling the output as a multiplex network to identify the optimal community structure and finally extracting these communities using PNMF.

T1 presented dependencies between time-samples for the initial phase of the reaching movement. These dependencies are accompanied by a high dependency between the final (49^{th}-50^{th}) time-samples that is connected to this initial burst through

moderate dependencies among adjacent time samples along the diagonal. T2 illustrates a prominent clustering of dependency from time-samples 15-25 and continuing with strong connection strengths within this time-sample range for the remainder of the movement. T3 presented high dependencies with all time-samples from approximately half-way into the movement until the endpoint.

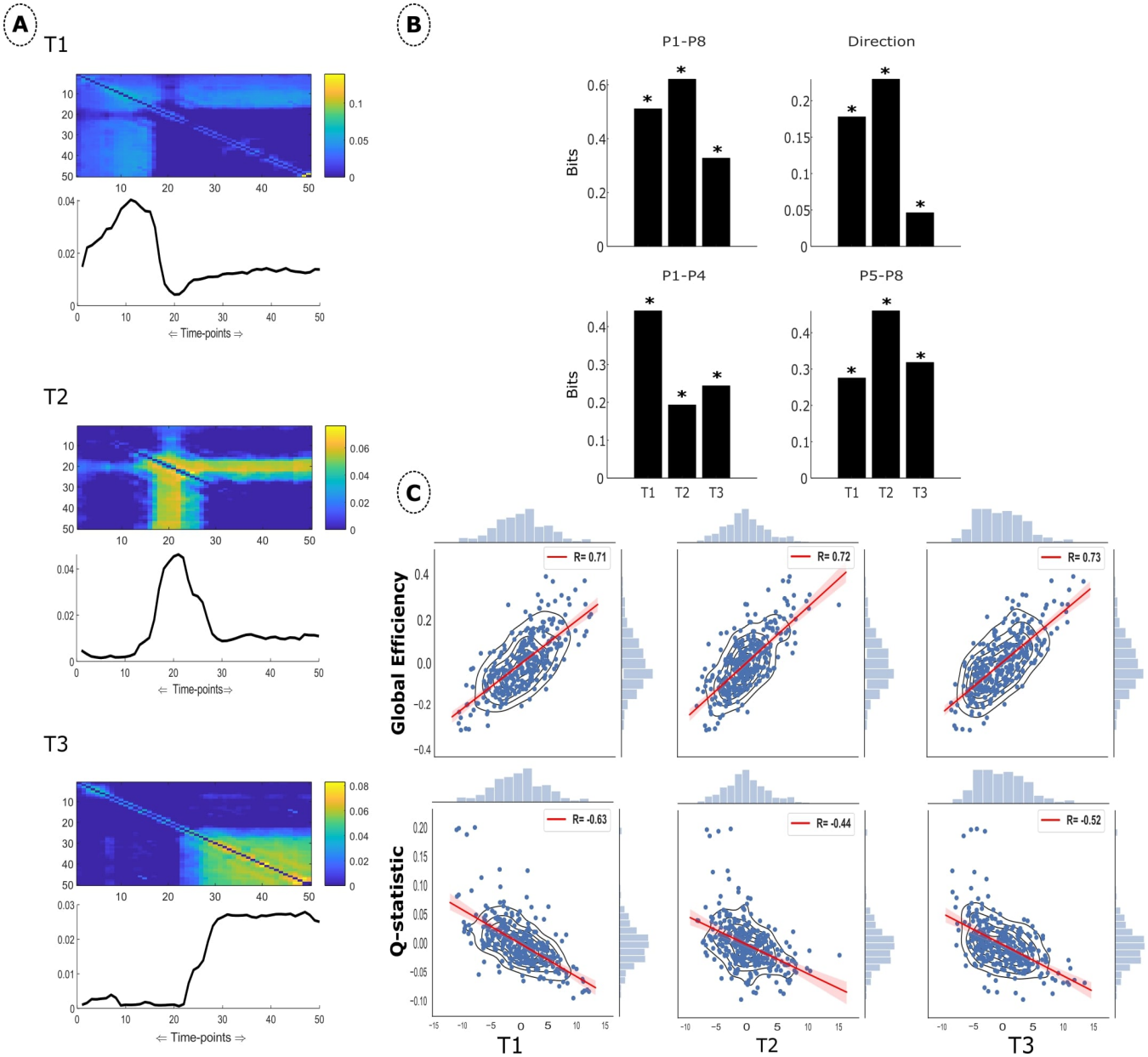

Fig.5:**(A)** The temporal synergies from the example participant in dataset 1. The community detection criteria found three distinct communities that were extracted using PNMF. The line plot below represents the average values within each column of the adjacency matrix. **(B)** The encoded information of the three temporal synergies identified in the example participant in dataset 1 for four task attributes: P1-P8, P1-P4, P5-P8 and Direction. Significant information ($p<0.05$) is indicated with *. **(C)** The correlation between trial-to-trial fluctuations in Global Efficiency/Q-statistic for modularity and noise in the temporal activation coefficients. The bars along the axis of each plot are marginal histograms of the x- and y-variables.

Taken together, a single tonic synergy (T1) was accompanied by a bi-phasic pattern of activation (T2 (acceleration) and T3 (deceleration)) that explained point-to-point reaching movement in this example participant. This observation is supported by an analysis we conducted on the task-dependency of the underlying activation coefficients (Fig.5(B)). Consistent with the differing functional roles of these temporal synergies, differences between forward movements (P1-P4 differing in the respective end-points) were predominantly captured by T1 (peaking at the final time-samples) whereas differences in backward movements (P5-P8 differing in the respective starting points) were predominantly captured by T2 (activating earlier in the movement) which

contained the most information overall (P1-P8, 0.62 bits and direction, 0.23 bits). The noise correlations between all synergy activations and both GE and Q were significant ($p<0.05$) and in opposing directions, with all synergy activations positively related to GE and negatively associated with Q (Fig.5(C)). The tonic synergy (T1) was most sensitive to changes in modularity from trial-to-trial (R= -0.63), while T3 was highest in its association with GE (R= 0.73). The sensitivity to integration in the latter case is likely reflective of the differing muscular involvements required at each reaching end-point position.

Space-Time synergy model

As an extension of the spatial and temporal synergy models, we concurrently extracted these distinct modules in a unifying space-time model, capturing distinct couplings in trial-to-trial dependencies that are consistent across spatial and temporal components. To do this, we first computed GCMI across all muscle pairs and time-samples and then decomposed the identified dependencies into components with distinct spatial and temporal signatures. For the same example participant in dataset 1, we determined an optimal model-rank of three using the community detection procedure with a Q-statistic of 0.97. Fig.6 below illustrates this output with the spatial and temporal synergies corresponding on a 1:1 basis across each row. In other words, the space-time model identified three synergies and characterised their spatial and temporal structure across all trials. The spatial synergies in ST2 and ST3 are relatively robust with those derived from the spatial synergy model previously (Fig.4), demonstrating the consistent coupling of the medial and lateral triceps and within the upper- and lower-arm musculature respectively. Their corresponding temporal synergies represent muscle co-activation throughout the movement and an early-and-late phasic activation that is dynamically involved in the flexion/extension of reaching movements respectively. ST1 presents a strong dependency between the anterior deltoid and latissimus dorsi that is active at the beginning and end of the movement and relatively quiet in the mid-range. This synergy is likely reflective of the alternate roles the anterior deltoid and latissimus dorsi carry out in stabilising the shoulder joint during forward and backwards reaching movements.

A secondary community detection procedure revealed two submodules in each of the spatial synergies that are represented by the colours of individual nodes in the human body model networks. For ST1, the submodules included the anterior deltoid, latissimus dorsi and both the medial- and lateral triceps (cyan) and the finger extensors and brachioradialis of the lower-arm (red). In ST2, the medial- and lateral triceps (orange) and a long range connection between the brachioradialis and posterior deltoid (yellow). Finally, ST3 consisted of the medial-triceps and posterior deltoid (blue), and lateral-triceps and anterior deltoid (green). Both ST1 and ST3 submodules were anatomically compartmentalised and non-overlapping, indicating localised functionalities that were co-occurring and reproducible across trials such as joint stiffness and stabilisation. ST2 submodules represented a more global interaction between overlapping submodules across the arm, coinciding with its corresponding temporal synergy representing a co-activation across the entire movement.

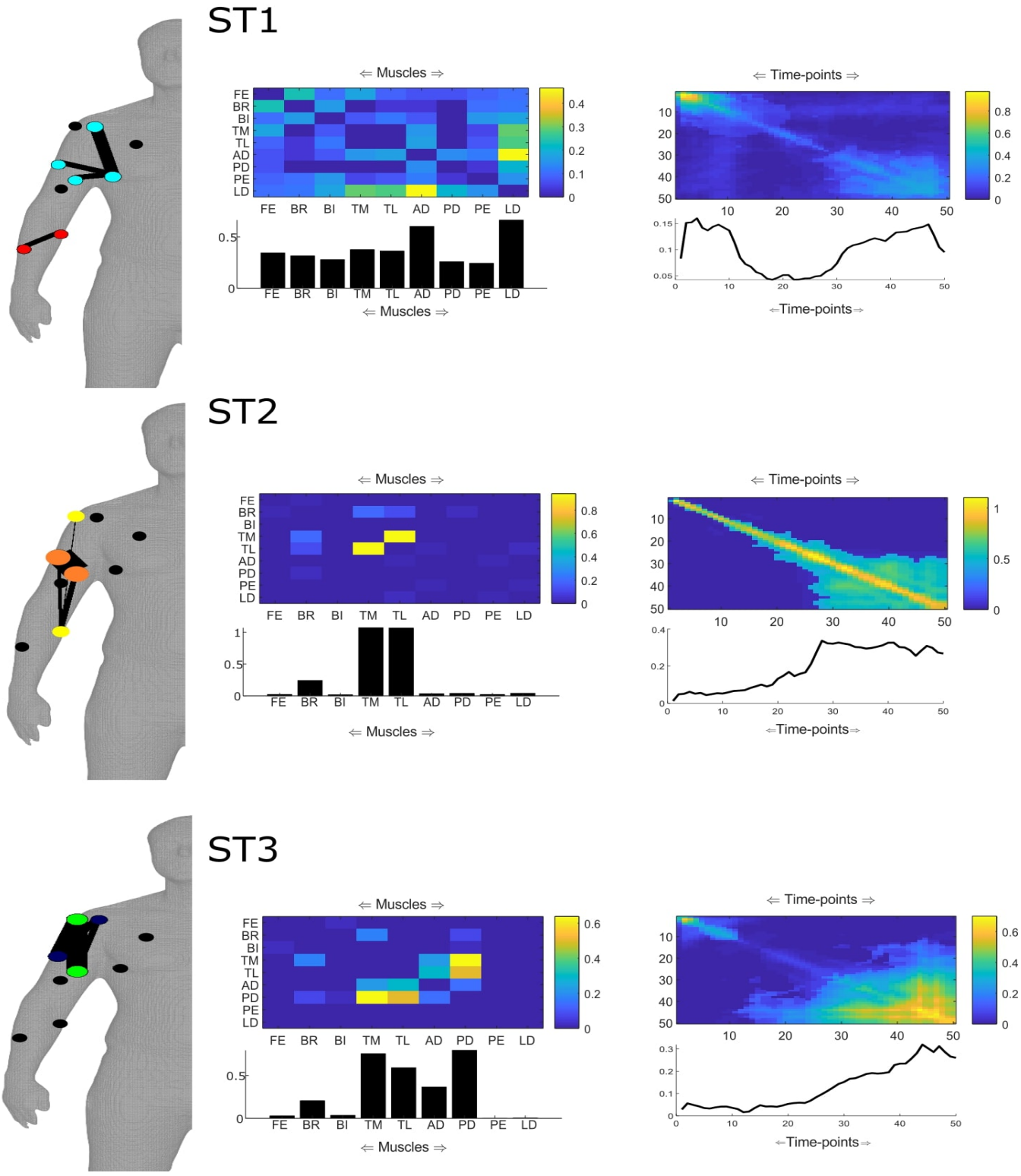

Fig.6: The Space-Time synergies extracted from the example participant in dataset 1. Three communities were identified a priori and then extracted using PNMF. Spatial and temporal synergies correspond on a 1:1 basis here as presented across rows. The bar/line plots below represents the average values within each column of the corresponding adjacency matrix. The connection strengths, submodular structure and involvement of nodes are indicated by the minimally connected human body model via the edge widths, node colour and size respectively [81]. Submodular structure was identified using the conventional Louvain algorithm on the muscle synergy matrices [72]. Unconnected nodes are in black.

Consistency across participants (Dataset 1)

We then sought to determine the similarity of the spatial, temporal and space-time synergies extracted using the GCMI framework across participants. This was conducted by computing a similarity index between pairs of functionally similar synergy weights derived at a representative model rank for the dataset and the average ± standard deviation was found (see Materials and Methods section). Within Dataset 1, we identified 2.4 spatial communities on average (range= 2-3) with a mean Q-statistic of 0.997 and threshold value of 0.13 bits (supplementary materials (Fig.2)). A satisfactory level of consistency was found (R=0.78±0.37). S1 here represents elbow extension primarily with some moderate dependencies across the other muscles. S2 involves a more global activation but particularly between the medial and lateral triceps and between the anterior deltoid and pectoralis. S1 was typically higher in its task information across participants for direction (0.11 bits) and P5-P8 (0.23 bits) while S2 was highest for P1-P8 (0.33 bits) and P1-P4 (0.24 bits). The contrasting relationship between the synergy activations and GE and Q was replicated across participants with S1 presenting the strongest noise correlation for both network properties (supplementary materials (Fig.2(C)).

We identified an average of 3.4 communities (range= 3-4) with an accompanying maximal modularity of 0.93 and threshold value of 0.46 bits on average in the temporal domain across participants in dataset 1. The similarity index revealed a high level of correlation (R=0.83±0.45) although with significant variability. Supplementary materials (Fig.3(A)) illustrates the three representative synergies taken from this procedure along with their mean task-encoded information. T1 presented a low-to-moderate level burst of dependency at the initial phase of movement, but a high dependency in the last two time-sample pairings. T2 had a more idiosyncratic pattern of dependencies across the movement with several bursts along the diagonal. T3 demonstrated a step in activation from the 30^{th} time-sample approximately with dependencies shared across time-samples for the remainder of the movement. In terms of task dependence (supplementary materials (Fig.3(B)), T1 was predominant for P1-P8 (0.31 bits) and P1-P4 (0.22 bits) and also highest for P5-P8 (0.23 bits). T2 contained the highest average task information for forward vs. backward directions (0.11 bits). T1 demonstrated the strongest correlation for both GE (R= 0.86) and Q (R= -0.57) while T3 was weakest in its noise correlation with Q (R= -0.16) (supplementary materials (Fig.3(C)).

For the space-time model, we determined that a model rank of three was representative of dataset 1 participants with a correlation of 0.69±0.33 found (supplementary materials (Fig.4)). The Q-statistic was consistently high across participants, ranging from 0.89-0.99 while the mean threshold value was 0.048 bits. All temporal synergies presented a high dependency between adjacent time-samples and along the diagonal, indicating that co-activations during reaching movements in various directions and points were most consistent across participants when considering trial-to-trial dependencies. The spatial synergies were consistent with those reported already here with ST2 capturing the characteristic dependency between the medial and lateral triceps and the ST3 spatial synergy the dynamic involvement of the upper-arm musculature during reaching. ST1 involved a combination of the anterior deltoid and pectoralis or latissimus dorsi.

A generalisation to whole-body point-to-point reaching movements.

We then sought to generalise the results presented above to a more complex dataset consisting of EMG activity from 30 muscles during whole-body point-to-point reaching movements at various heights and in various directions (82 distinct movements in total, each repeated 30 times) among 5 participants. This new high-dimensional dataset serves to demonstrate the applicability of the proposed framework to characterise the structure of large-scale EMG recordings during 3-dimensional unconstrained movements.

Spatial synergy model

Taking an example participant from dataset 2, we identified three spatial synergies with a maximal modularity of 0.994 (Fig.7(A)). S1 and S2 appear to represent the postural stabilisation activity related to normal stance and during point-to-point reaching respectively. This is indicated in S1 by the greater dependencies found in the lower-limbs and in the lower-limbs and left upper-body in the S2. S3 then completes this picture of whole-body reaching with significant dependencies clustered in the right upper-body. The dependency of these synergies across a number of task attributes including end-point bar and height, start-point bar and height along with the Up-down and left-right directions are also illustrated (Fig.7(B)), and support these functional interpretations. S1 (activating mainly the lower body) carried significant information about the horizontal dimension of movement (start and endpoint bar and left-right displacements) suggesting that its functional role was to drive body rotations. S2 (activating the left upper-body together with parts of the lower body) contained a higher level of task information, mostly for the vertical movement dimension (end-point height [0.242 bits] and the Up-down direction [0.208 bits]) suggesting that its functional role was to support vertical body displacements. Although task information was relatively high for S3 (right arm raising), just one task attribute was found to be significant (end-point height, 0.53 bits), suggesting that this synergy was relevant but highly variable in the information it contained. This could potentially be attributed to the highly variable demands required during upwards vs. downwards reaching movements for example where passive mechanics can be exploited in the latter but not the former. All synergy activations were significant in their trial-to-trial correlations with integrative and segregative network properties ($p<0.05$), and presented contrasting directions in their association, exemplifying the trade-off between these

properties. S2 demonstrated the greatest sensitivity to changes in GE (R= 0.62)and Q (R= -0.41) in its underlying activations. Coinciding with the highly variable task information, S3 presented the least sensitivity to changes in GE (R= 0.29) and Q (R= -0.07).

The submodular structure of these synergies, represented on the human body model by the colour of the nodes shows four submodules for S1 (both erector spinae and the right tibialis musculature (blue), right femoral musculature (navy), left tibialis musculature (red) and both pectoralis major and the left anterior deltoid (yellow)) three submodules for S2 (left arm musculature and right tibialis anterior (pink), right arm and left femoral musculature (grey) and right femoral musculature (orange)) and two submodules for S3 (upper-body musculature (white) and three right femoral muscles (maroon)). The community assignment of these distributed networks provides further evidence as to the underlying function of specific muscle couplings. For example, an interesting long-range connection is found between the right-side lower-limb musculature and erector spinae that belong to the same submodule (S1). This coincides with an overlapping but distinct community among the left-side lower-limb musculature, indicating that the non-reaching side contributes differently to whole-body stability than the reaching side. The predominant submodule in S3 is specific to the reaching arm where a large cluster of strongly weighted connections are present. Long-range connections to distal body parts are also evident in S3, indicating that the whole-body is coupled to the specific activations of the reaching arm.

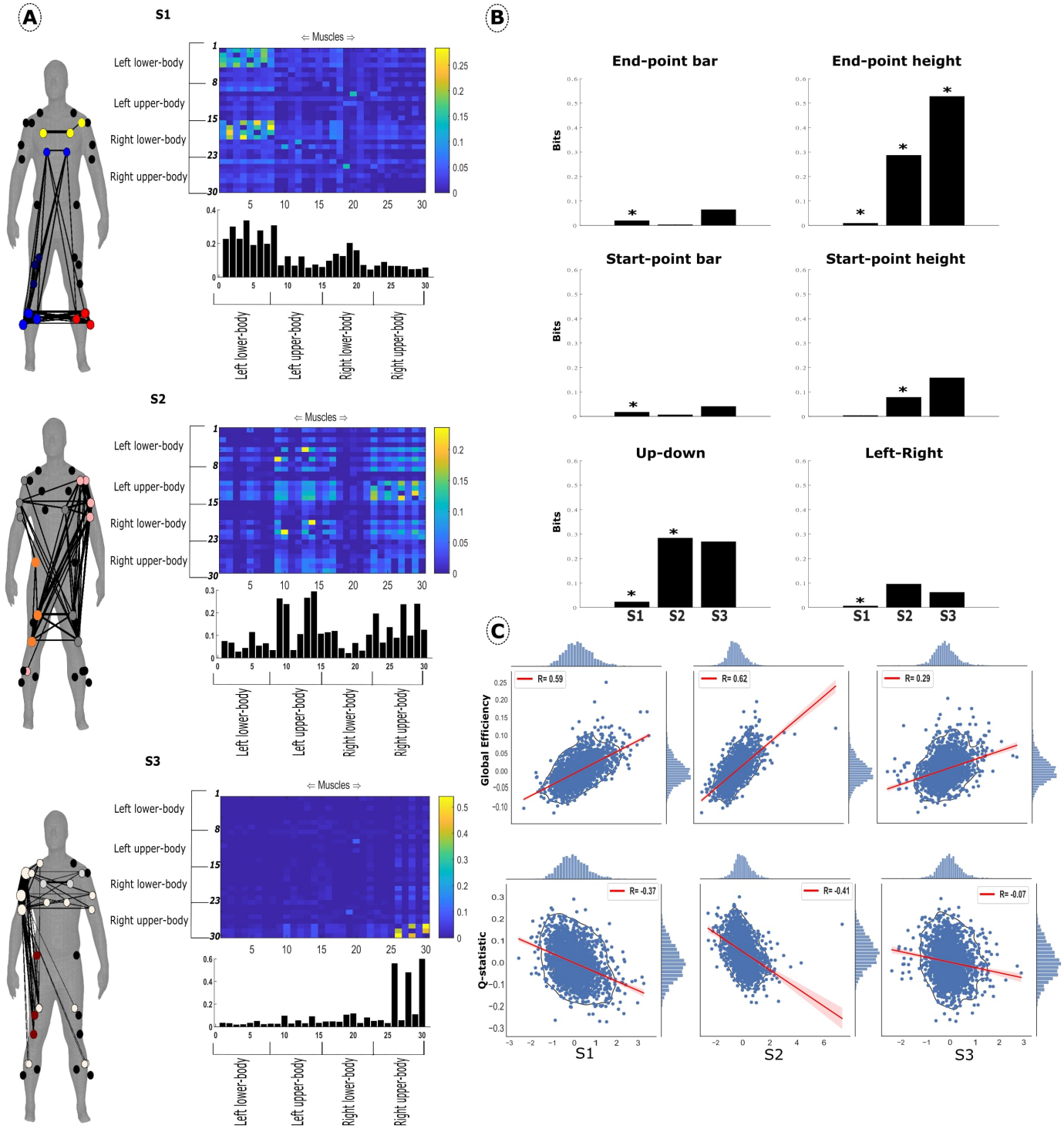

Fig.7:**(A)** The spatial synergies extracted from the example participant in dataset 2. The adjacency matrices are organised so that rows 1-8: left lower-limb, rows 9-15: left upper-body, rows 16-23: right lower-limbs and rows 24-30: right upper-body. The width of the edges on the minimally connected human body model and the size and colour of the nodes indicate the connection strength, node involvement and submodular structure respectively [57]. Submodular structure was identified using the conventional Louvain algorithm on the synergy matrices [72]. Unconnected nodes are in black. **(B)** The information encoded for six task attributes is presented. * indicates significance at p<0.05.**(C)** The noise correlation between spatial synergy activations and trial-to-trial network properties Global Efficiency/Q-statistic for modularity. The bars along the axis of each plot are marginal histograms of the x- and y-variables.

Temporal synergy model

To test how consistent the temporal synergies are when considering more complex motor tasks, we applied the temporal syn-

ergy model to the example participant in dataset 2, revealing three temporal synergies (Fig. 8(A)). T1 here contained moderate proximal dependencies along the diagonal and a gradual increase to a new activation level near movement termination, characteristic of a tonic activation. The initial phasic activation of T2 here is more drawn out along the diagonal and less dependent on time-samples later in the movement. This is likely due to the different heights and directions in point-to-point reaching introduced in this experimental setup, requiring more variable onset-offset timing of phasic muscle activations. T3 consists of a late burst from time-sample 30-40 approximately. We found that all of these temporal synergies were significant for the three task attributes analysed here including start- and end-point and direction (Fig.8(B)). T3 contained the most information regarding the direction of reaching (0.13 bits). All 3 synergies contained similar amount of information about end-point position (0.11, 0.1 and 0.11 bits respectively) while T2 was predominant for start-point position (0.1 bits). The dynamic balance between modularity and small-worldedness was once again captured in the extracted activations (Fig.8(C)), with opposing directions of correlation in the trial-to-trial fluctuations for GE and Q that were all significant ($p<0.05$). T3 activations were most strongly related to integrative changes ($R=0.75$), once again likely reflecting the differing muscular involvement required at end-point position while T2 demonstrated the strongest association with trial-to-trial changes in modularity ($R= -0.83$).

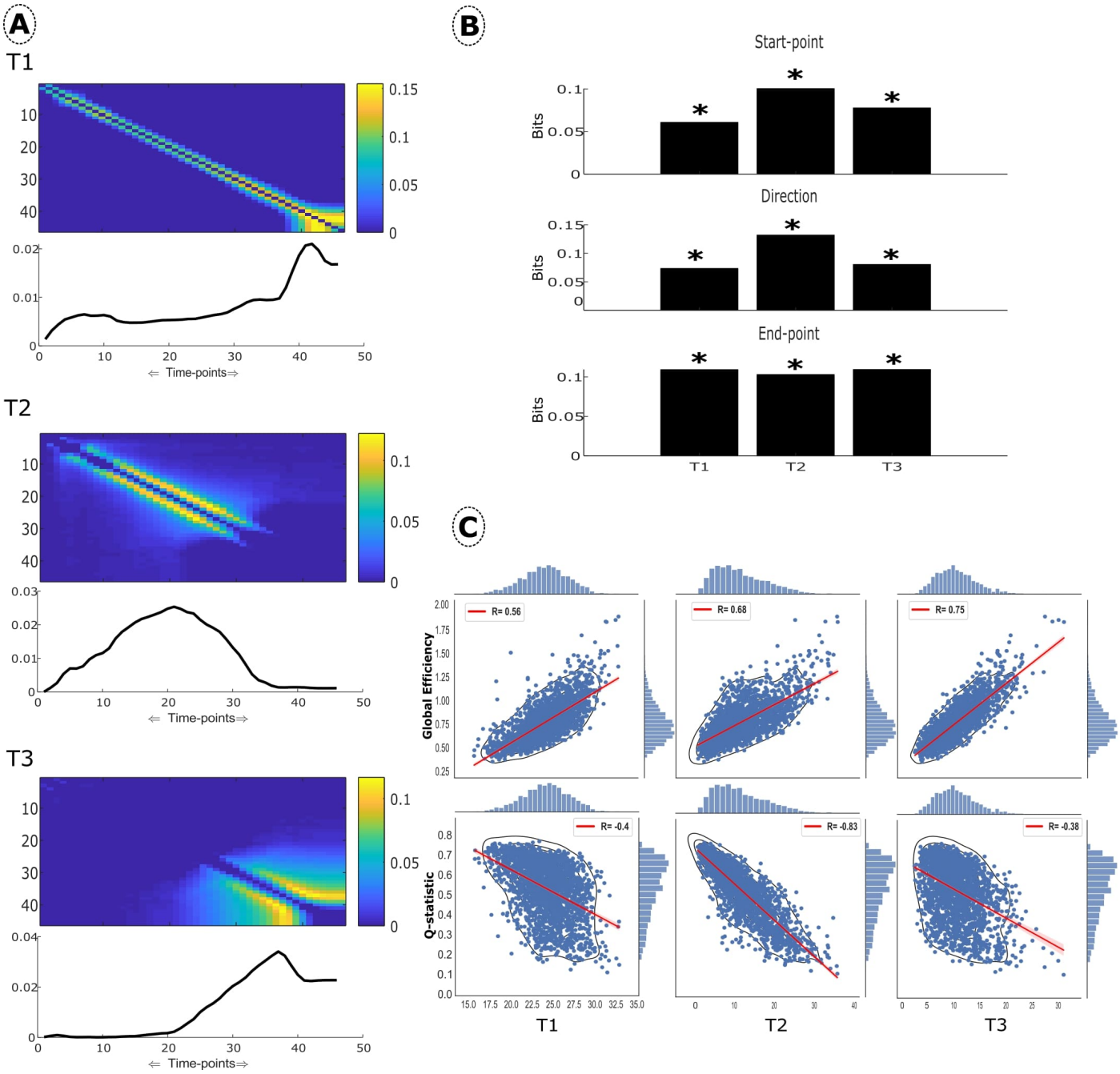

Fig.8: **(A)** Temporal synergies extracted from an example participant in dataset 2. Three communities were identified in the multiplex network and extracted using PNMF. The line plot below represents the average values within each column of the adjacency matrix. **(B)** The task-encoded information is presented in bits. Significant information ($p<0.05$) is indicated with *. **(C)** The noise correlations between each temporal synergy activation and Global Efficiency/Q-statistic. The bars along the axis of each plot are marginal histograms of the x- and y-variables.

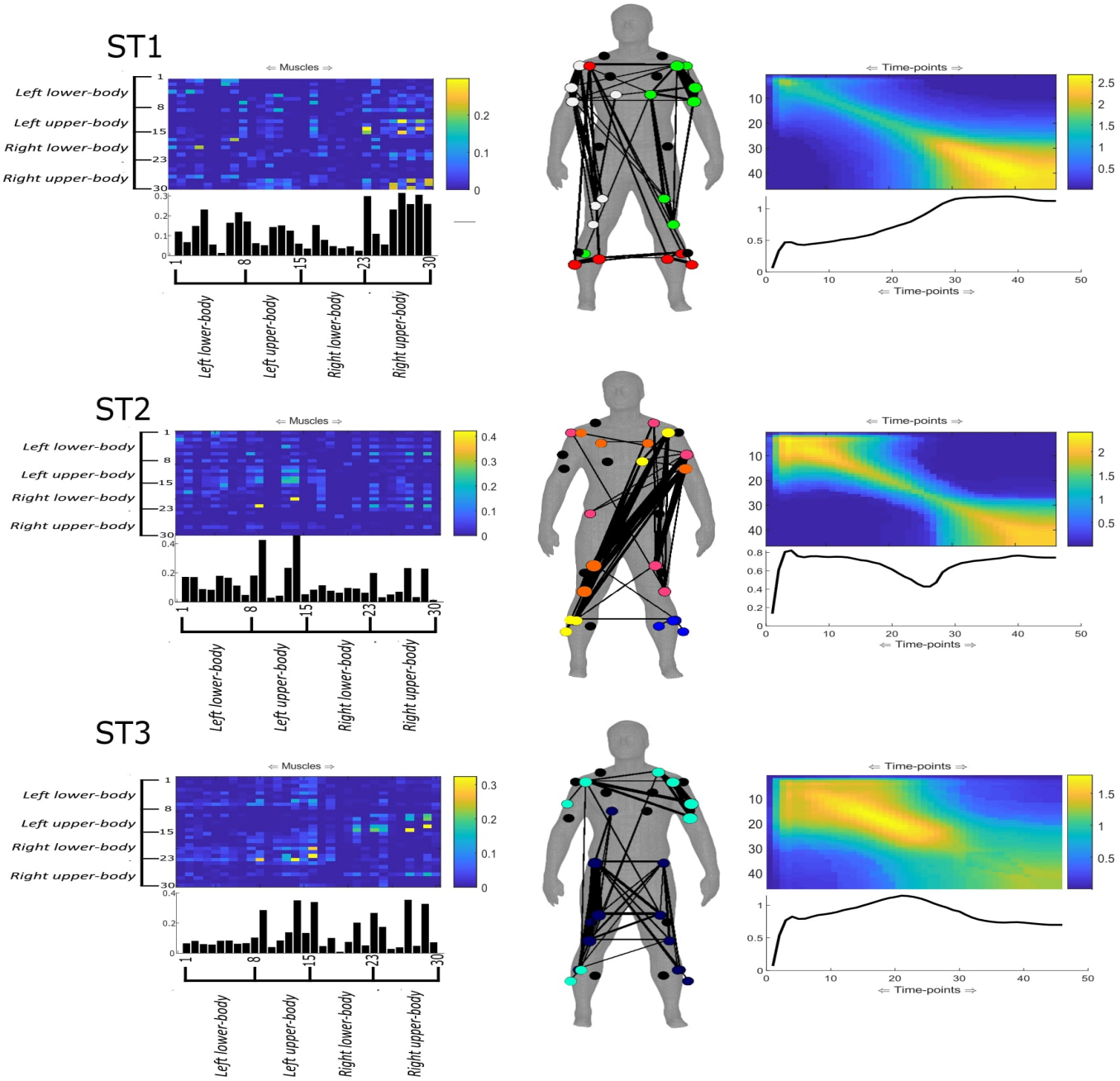

Fig.9: The Space-Time synergies extracted from the example participant in dataset 2. Three communities were identified and extracted using PNMF. Spatial and temporal synergies correspond on a 1:1 basis here as presented across rows. The spatial synergies are organised so that rows 1-8: left lower-limb, rows 9-15: left upper-body, rows 16-23: right lower-limbs and rows 24-30: right upper-body. The bar/line plots below represents the average values within each column of the corresponding adjacency matrix. The connection strengths, submodular structure and involvement of nodes are indicated by the minimally connected human body model via the edge widths, node colour and size respectively [81]. Submodular structure was identified using the conventional Louvain algorithm on the synergy matrices [72]. Unconnected nodes are in black.

We then sought to generalise the space-time synergy model results from dataset 1 to the example participant in dataset 2 (Fig.9). The findings were successfully replicated in a more complex dataset of whole-body reaching where a model-rank of three was found. ST1 here appears to capture the postural stabilisation exhibited predominantly in the upper-body but supported by the femoral muscles at movement onset and increasingly so at movement termination. ST2 is characterised by a phasic activation at movement initiation with a critical muscle (anterior deltoid) identified at the reaching shoulder supported by

dependencies among the lower-limb muscles of both sides that counteract the induced shifts in centre-of-pressure. Following movement initiation, ST3 comes into a greater level of dependency between time-samples 12-28 approximately, accompanied by significant connections between the gluteals and among the right side lower-limb. This synergy then subsides back to its original activation level near movement termination, where the new body position is supported by the sustained activation in ST1. A similar level of dependency is found within the left upper-body and the right anterior deltoid in ST2 with this synergy reflecting the increased demands induced proximally in order to counteract the right arm during the transition to a new position.

A complex submodular structure was found across all three synergies, as exemplified on the human body models where three, five and two submodules were identified by a secondary community detection of ST1- ST3 respectively. The right anterior deltoid and tibialis musculature (red), right arm and femoral musculature (white) and left arm and femoral musculature (green) comprised ST1 submodules. ST2 consisted of strong connections between the left upper- and right-lower body (orange, yellow & wine) and a small cluster among left tibialis musculature (blue). ST3 comprised strong connections among the right lower-limb but also with the left leg (navy) along with a cluster of muscles across the upper-body that contained a long-range connection with the right soleus and anterior tibialis (cyan). Taking ST1 as an example here, the submodular architecture demonstrates the unique functional role of the reaching arms anterior deltoid which shares its community assignment with the lower-limb musculature. This submodular structure is likely representative of the reactive role the lower-limb musculature plays in reacting to stabilise the center-of-pressure against shifts in weight distribution of the reaching arm. The non-reaching arm comprises a submodule in both ST1 and ST3 that overlaps with the reaching arm anterior deltoid, indicating that despite being at rest, the non-reaching arm activations occur in synchrony across trials with the reaching arm and are indeed coupled to some extent.

Consistency of synergies (Dataset 2)

Following synergy extraction, we determined the consistency of identified spatial, temporal and space-time synergies across participants during whole-body reaching movements using a structural similarity index. Starting with the spatial synergy model, 3.4 (range=3-4) synergies were representative of the five participants in dataset 2 with the Q-statistic ranging from 0.997-0.998 and the threshold value 0.26 bits on average. The similarity index revealed a moderate level of correlation (R=0.56±0.19). Supplementary materials (Fig.5(A-C)) illustrates the average spatial synergies we extracted along with their respective task attribute dependencies and correlation with network properties. Despite this reduced similarity, the synergies are readily interpretable in their underlying functionality, likely indicating that the shape of activations rather than functionality was dissimilar across participants. For instance, S1 here consisted of dependencies within both the upper- and lower-body related to normal-stance stability and S2 is related to whole-body postural stability during reaching movements. As the greatest dependencies in S3 lie within the right upper-body, this synergy is representative of the activity in the reaching arm. These observations are supported by the task-encoded information. For instance for S2, the average task information was noticeably higher for start-point height (0.26 bits) and Up-down direction (0.28 bits) over other synergies, likely reflecting the differing postural adjustments required as the reaching arm is either raised up against gravity or down closer to a resting position. The trade-off between GE and Q captured in the activation coefficients was replicated across participants. Interestingly, fluctuations in S3 activations were most sensitive to changes in GE (R= 0.69) and Q (R= -0.57) across the remaining participants.

We then conducted this analysis on the temporal synergies of dataset 2 participants, producing a mean of 3.4 synergies (range=3-4) across participants that exhibited a high degree of concordance (R=0.91±0.57). This high level of concordance was accompanied by significant variability which we posit reflects the varying time-lags and contributions of individual muscles to reaching movements across participants that wouldn't influence the overall shape of the synergy but the composition (i.e. higher/lower magnitude dependencies comparatively). The Q-statistic ranged from 0.97-0.995 while the average threshold value was 1.45 bits. In supplementary materials (Fig.6(A-C)), the representative temporal synergies for this sample are presented along with mean task-attribute and noise correlations with network properties. T2 was most highly modulated by start-point (0.05 bits) and direction (0.07 bits). T1 and T3 shared an equivalent level of modulation by end-point (0.546 and 0.547 bits respectively). The fluctuations in T3 activations were most sensitive to changes in GE (R= 0.69) and Q (R= -0.57), although all synergies demonstrated a high association across participants.

Finally, we applied the space-time model to all dataset 2 participants and their structural similarity was compared using a representative model rank of 2 (mean rank= 2.4, range=2-3). We found a satisfactory level of concordance across participants (R=0.79±0.4). Supplementary material (Fig.7) illustrates these representative synergies where the Q-statistic for modularity ranged from 0.93-0.997 and the threshold values ranged from 0.295-0.385 bits. ST1 functionally represents the deceleration and support of the reaching arm in its new position, which is reflected by the involvement of the upper- and lower-body of the opposing side. ST2 was active during the early to intermediary stages of the movement and mostly consists of couplings between lower-limb muscles, providing postural stabilisation during task execution.

2.5 Discussion

To summarise the findings presented, functionally and physiologically meaningful muscle synergies were extracted using a network-information theoretic framework. Synergies were extracted in the spatial, temporal and spatiotemporal domains, each capturing unique sub-tasks and representing underlying mechanisms in human point-to-point reaching generalisable across two datasets that were consistent in their projections across participants. Along with this, we showed a significant task dependence of synergy activations that closely related to the functional interpretations of the extracted synergies and significant correlations with network properties that captured the dynamic trade-off between modularity and small-worldedness. Both model-rank selection and sparsification procedures were conducted prior to dimensionality reduction in a data-driven and holistic manner that reduces the necessity for post-hoc analyses. Through the determination of dependencies on a within-trial basis between muscles, time-sample vectors or their combination across trials, a novel formulation of muscle synergy was implemented that we suggest can provide important and novel insights into the neural control of human movement. In the following we detail some of the main commonalities of the GCMI framework with existing models along with novel findings and advantages. These commonalities and advantages are summarised in the Supplementary material of this article, where a formal comparison with existing models is provided (supplementary materials Fig.8).

Continuity with previous muscle synergy models

Previous studies have been conducted on the datasets analysed here with interesting commonalities with our results [29, 23, 83]. Functional muscle groupings by the spatial synergy model here were reflective of previous findings (e.g. Dataset 1: elbow extensors (S1), shoulder flexors (S2) and shoulder and elbow extensors (S3); Dataset 2: a single synergy (S3) for the reaching arm along with whole-body functional groupings relevant for postural stability that cannot be explained by anatomical constraints). The spatial synergies presented in the current study were, similarly to previous reports, only moderately similar across participants in their shape but robust in their functional underpinning. This low level of agreement found in dataset 2 is likely related to physical discrepancies among participants (e.g. height, muscle length, motor preferences). The concordance among temporal synergies found in the current study also replicated previous work. Notably however, a high degree of inter-subject variability was reported here. As the temporal synergies consisted of dependencies between time-sample vector pairings across muscles, we posit that in contrast to the shape differences among spatial synergies, the overall shape of the temporal synergies was consistent, but their composition was not. The varying time-lags of individual muscles is likely to have contributed to this difference in composition [24, 84], leading to comparatively higher/lower magnitude dependency at certain time-sample pairs across participants. This demonstrates the capacity for the GCMI framework to effectively capture the idiosyncrasies of individual participants' movement patterns. To exemplify this point further, following a functional similarity analysis of temporal synergies it was noted in [83] that of the four synergies identified, several could be merged into fewer clusters. In the current study, these synergies were indeed merged into a readily identifiable bi-phasic pattern accompanied by an underlying tonic synergy, highlighting the functional relevancy of the synergies extracted here. The ability of GCMI to capture complex, nonlinear associations was advantageous in the merging of functionally synonymous phasic synergies (see 'Materials and methods' section) and exemplifies a step forward in the muscle synergy literature.

In terms of task dependence, significant shared information was observed in the activation coefficients of spatial and temporal synergies with various task attributes. An interesting difference in the task modulation of muscle synergies extracted here to that presented in previous work is that the synergies identified here convey information for several movement phases. This reflects the unique formulation introduced by the GCMI computations where early activations provide relevant task information about future states and vice-versa within the same vector in the input matrices. This allows for individual synergies to provide a more holistic insight into the task performed over existing approaches, representing synergies collectively as a single motor representation that unfolds across space and time. There was also some continuity with previous research. For example in dataset 2, whole-body reaching spatial synergies associated with postural stability were consistently modulated by task attributes that could be said to influence the participants medio-lateral or anterior-posterior centre-of-pressure (e.g. End-point height, Up-Down direction) as formerly observed [83]. The transient but also decelerative temporal synergy in dataset 2 (T2) was highly modulated by reaching direction, a replication of previous work also. The task modulation of space-time synergies has been reserved for investigation in future work.

Novel insights from the GCMI framework

The GCMI framework presents a few advantageous qualities over existing approaches that have provided novel insights in the current study. Firstly, the interactions between pairs of muscles, timepoints or muscle-timepoint pairings is a novel characteristic of the GCMI framework. These pairwise interactions are uniquely present across all three GCMI models and reveal interesting (often overlapping) submodular structures representing the dynamics of muscle couplings at various temporal and spatial scales during movement. Furthermore, the use of GCMI to quantify these pairwise couplings reveals all muscle interactions (even the subtle ones) regardless of muscle amplitudes. This addresses a significant limitation of dimensionality reduction approaches to muscle synergy extraction which put more emphasis on muscles with a predominant role in the movement because these

muscles explain most of the variance in the dataset.

In past work, the separation of tonic and phasic synergies has not been straightforward and commonly involved the subtraction of a linear ramp from EMG waveforms [85, 86]. Within the GCMI framework, these distinct temporal synergy types are both isolated within the same extraction procedure (e.g. T1 in fig.5 and fig.8), leading to a data-driven approach that relaxes the assumption of linearity. In relating the dynamics of movement control in the oculomotor system and the human arm, [87] elucidated a plausible mechanism for subcortical postural control. The integration of cortically generated movement commands by a separate, subcortical postural controller was initially supported in primates and found to be generalizable to healthy human and cortically-impaired populations where this dependence persisted on a within-trial basis only. In the current study, tonic synergies were identified in reaching tasks on a within-trial basis only that consistently presented a pattern of activation indicative of the aforementioned findings. More specifically, a low-to-moderate gradually increasing/decreasing level of dependency was found throughout T1 (fig.5 and fig.8) until a sharp spike in dependency was found consistently across participants at the last few time-sample pairings, potentially representing the integration of the preceding movement activations in the holding response. Further analysis using higher resolution EMG data along with relaxations in rigid temporal alignments may provide further insight into the underlying mechanisms governing motor control. This increased insight is made possible by key advantages provided by this approach in terms of flexibility and multiplexity with findings that may run in parallel to recent innovations in time-warped tensor decompositions [88].

The ability for a self-organising system to re-organise its elemental variables from trial-to-trial to complete a given task is an important attribute of the synergy concept [31]. In the development of this framework, careful consideration for important network properties characteristic of biological systems was made throughout the analysis. We chose to focus on two opposing but essential network properties, fractal modularity and small-worldedness, due to their functional implications and focus in the relevant literature [66, 68, 73, 74, 75, 35]. The preservation of these important network properties in the extracted synergies was confirmed through the identification of significant noise correlations in the underlying activation coefficients with trial-to-trial fluctuations in modularity and global efficiency. The persistent opposing directions and strength of these associations with GE and Q are both reflections of this trade-off and the sensitivity of the extracted synergies to trial-to-trial fluctuations at the network level respectively. These findings are also in line with the current understanding of the phenomena of adaptive breakdowns in modularity in complex systems and findings relating gain modulation to shifts in network topology [35, 89]. Furthermore, the maintenance of fractal modularity in the output of the GCMI framework is exemplified by the consistent presence of functionally meaningful submodules within the extracted synergies. It is likely that many of these submodules were defined by biomechanical constraints and a localised function [50, 51], however, a significant number of long-range connections clearly transcended this constraint (e.g. the right anterior deltoid and lower-limb musculature in the human body models of dataset 2). It is also noteworthy that many of the identified submodules overlapped, indicating that many individual muscles demonstrate a complex functionality that is shared across a distributed subnetwork of muscle couplings, supporting previous findings [50, 51, 52]. We thus suggest that the synergies extracted through the GCMI framework may be useful for investigating the unique contribution of both biomechanical and neural constraints on movement.

The identification of movement phase commencement and cessation has been frequently cited in the literature as difficult, especially during fast-paced movements due to overlapping muscle activations [86, 90]. The orthogonality introduced by PNMF here effectively removes this limitation by minimising the overlap between temporal synergies. The trial-specific activation coefficients produced by the proposed spatial and temporal models here significantly improve the analytical flexibility and convenience of the current models which are difficult to contrast against other variables of interest. The framework is not only convenient for further analysis but can provide novel fundamental insights. For example, in both datasets a novel bi-phasic pattern supported by an underlying tonic synergy was revealed. This bi-phasic pattern is reflective of the bang-bang control policy investigated recently that was found to explain the characteristic tri-phasic activation of reaching movements [90]. The findings presented here support the hypothesis of an intermittent rather than continuous control scheme in human motor control and implicate this control policy as a fundamental mechanism underlying human motor control [91, 92].

Muscle synergy analysis is known to be scale-dependent, in that the number and spread of muscles analysed across the body influences the synergy output, typically by increasing model-rank with increasing dataset complexity [70]. Instead of optimising the variance accounted for criterion, the proposed framework identified a reduced number of spatial and temporal synergies that were invariant to dataset complexity by optimising a more task-relevant modularity criterion. This is a significant progression from existing approaches which rely solely on variance optimisation frequently at the expense of task relevancy [27]. Within the sensory system the multiplex encoding of information across multiple time-scales is well-known [93], allowing for an increased coding capacity and the apparent continuous stream of perception. This multiplexity has more recently been identified in the encoding of task information from low-dimensional dynamics in a motor cortical neural population and put forward as a structural mechanism underlying cognition and self-organisation more generally [94, 95, 96]. Other recent research that has modelled muscle synergies as a multiplex network only identified a single module representing a global co-activation during gait in various coordination modes [53]. This global co-activation may have masked more discrete but important mechanisms that

could not be uncovered by simpler methodologies. In the current study, the multiplexity of human motor control was exhibited through the parsing of several community structures across multiple spatial and temporal scales that demonstrated significant encoding of task information. Therefore, we suggest that the GCMI framework presents as a useful tool for investigating the emergence of complex patterns in motor behaviour.

Future research directions

A key motivation for the development of this framework was to address the limitations of linear assumptions and lack of flexibility in current muscle synergy models. The inclusion of task space variables has recently come into the spotlight in this line of research [19], as the pattern configurations found are required to be constrained by an objective function in order to be functionally relevant and transferable to robotics and prosthetic design [19, 27]. Through the induction of non-parametric statistical tools in information and network theory, the presented formulations are now more amenable to the inclusion of task space variables while more appropriately capturing the non-linearity of the musculoskeletal system. The objective function to constrain these extracted synergies may also involve the inclusion of neural data derived elsewhere in the CNS, producing neurophysiological relevant synergies that are falsifiable [21, 39]. Each muscle synergy model may capture distinct motor features [97], thus investigating their functional underpinning following the inclusion of these constraints may be fruitful. Information theory more generally has found great use in the analysis of complex systems, for instance in identifying synergistic and redundant interactions in the CNS, the integration of cross-modal informational dynamics and providing a framework for understanding causal emergence [98, 99, 100]. Quantifying informational dynamics among muscles in space and time may allow for the identification of task-relevant and irrelevant spaces, providing a bridge between neurophysiological and purely computational frameworks [101, 102].

Chapter 3

Dissecting muscle synergies in the task space

David Ó' Reilly, Ioannis Delis (2023) Dissecting muscle synergies in the task space eLife 12:RP87651

3.1 Abstract

The muscle synergy is a guiding concept in motor control research that relies on the general notion of muscles '*working together'* towards task performance. However, although the synergy concept has provided valuable insights into motor coordination, muscle interactions have not been fully characterised with respect to task performance. Here, we address this research gap by proposing a novel perspective to the muscle synergy that assigns specific functional roles to muscle couplings by characterising their task-relevance. Our novel perspective provides nuance to the muscle synergy concept, demonstrating how muscular interactions can '*work together'* in different ways: a) irrespective of the task at hand but also b) redundantly or c) complementarily towards common task-goals. To establish this perspective, we leverage information- and network-theory and dimensionality reduction methods to include discrete and continuous task parameters directly during muscle synergy extraction. Specifically, we introduce co-information as a measure of the task relevance of muscle interactions and use it to categorise such interactions as task-irrelevant (present across tasks), redundant (shared task information) or synergistic (different task information). To demonstrate these types of interactions in real data, we firstly apply the framework in a simple way, revealing its added functional and physiological relevance with respect to current approaches. We then apply the framework to large-scale datasets and extract generalizable and scale-invariant representations consisting of subnetworks of synchronised muscle couplings and distinct temporal patterns. The representations effectively capture the functional interplay between task end-goals and biomechanical affordances and the concurrent processing of functionally similar and complementary task information. The proposed framework unifies the capabilities of current approaches in capturing distinct motor features while providing novel insights and research opportunities through a nuanced perspective to the muscle synergy.

3.2 Introduction

Human movement is a highly complex behaviour, with a broad spectrum of multiplexed spatiotemporal dynamics typically exhibited for basic activities-of-daily-living [103, 104]. How the central nervous system controls movement in the face of this inherent complexity to ensure efficient and reliable navigation of the environment and task performance is a nontrivial question currently under investigation in the motor control field [105, 8]. The muscle synergy hypothesis is a long-withstanding proposition on the underlying neural constraints producing coordinated movement, stating that this complexity is offset by the allocation of computational resources to the spinal-level in the form of motor primitives [105, 8, 16, 15]. These motor primitives modularly activate functional groups of muscles that are flexibly combined for the efficient construction of a movement. The conceptual underpinning of the '*muscle synergy'* entails the idea of combinations of muscles '*working together'* for the purpose of effective goal-orientated behaviour [31]. This emergent cohesion involves the following qualifying attributes: a repeatable muscle activation pattern common across trials and participants, a reciprocal relationship among functional muscle groups such that changes occur in one group to compensate for changes in another, and task dependence (i.e. the pattern of interdependencies among muscles must map onto task performance) [31, 106]. A common approach to analyse the neural constraints underlying these motor patterns is to apply unsupervised machine-learning algorithms to electromyographic (EMG) data [70, 43], with the aim of extracting a latent, low-dimensional representation.

In [107], we considered, key limitations among current approaches to muscle synergy analysis in extracting functionally relevant and interpretable patterns of muscle activity [19]. We proposed a combinatorial approach based on information- and network-theory and dimensionality reduction (the network-information framework (NIF)) that significantly improved the generalisability of the extraction process by, among others, removing restrictive model assumptions (e.g. linearity, same mixing coefficients) and the reliance on variance-accounted-for (VAF) metrics [19]. By determining the pairwise mutual information between muscles, this innovation paved the way for the appropriate mapping of muscular interactions to the task space. To elaborate on the significance of this development, the extraction of motor patterns in isolation of the task space often comes at the expense of functional and physiological relevance [19, 27]. Furthermore, effective methods for mapping large-scale physiological dynamics to behaviour is a current gap across the neurosciences [11]. Thus, here we build on this work by, for the first time, directly including task space parameters during muscle synergy extraction. This enables us, in a novel way, to dissect the concept of the muscle synergy and therefore quantify interactions between muscle activations with shared or complementary functional roles.

Further to the above, in its currently defined state, the muscle synergy concept describes the role of common neural drives to functional muscle groupings working redundantly towards a common task-goal [105, 16, 8, 31, 21]. However, recent influential works have highlighted several other important mechanisms involved in this low-dimensional control strategy that are not well recognised by the muscle synergy concept [108, 50, 52, 51, 109, 110, 102, 111, 7]. Such insights include the partitioning of motor variability by the nervous system into task-relevant and -irrelevant spaces and the cooperation between functionally distinct muscle groupings in the form of cross-module functional connectivities. These observations highlight the need for a refinement of the muscle synergy concept to comprehensively describe diverse muscle interactions during movement, including their partitioning into task-relevant and –irrelevant spaces and the characterisation of their functional roles.

We thus motivate the development of a more nuanced perspective to the muscle synergy concept and the general notion of '*working together'* that comprehensively describes the muscle interactions underlying motor behaviour. To do so, we propose an information-theoretic approach (based on the NIF pipeline) that characterises the contributions of muscle couplings to task performance. In other words, we frame the notion of '*working together'* in more specific terms of shared information between pairs of spatiotemporal muscle activations ($[m_x,\ m_y]$ (Fig.1.3(a))) (red and green sets respectively) and a corresponding task parameter (τ) (blue set) (see Venn diagrams in Fig.1.3(b) below). Among current approaches to muscle synergy analysis, the shared information between muscles (yellow and white area in Fig.1.1(a)) is quantified, using dimensionality reduction, as common patterns of variability. These common patterns are essentially task-agnostic and may contain patterns of variability a) present in specific tasks (i.e. task-relevant (white shaded area in Fig.1.1(a)) as well as b) shared across tasks (i.e. task–irrelevant (yellow shaded area in Fig.1.1(a)). Our proposed approach dissects patterns of muscle variability in space, time and across trials in terms of their task-relevance and functional similarity in a generalizable manner using mutual information (MI) (Fig.1.3(a-c)). This enables us to decompose muscle activations into muscle pair – task parameter couplings and characterise their combined functional roles. We can then extract low-dimensional representations of these muscle couplings, i.e. muscle networks with specific spatial and temporal signatures, across participants and tasks (Fig.1.3(c)).

Crucially, using this novel framework, we can separately quantify the task-irrelevant (i.e. muscle interactions present across tasks) information conveyed by a muscle coupling (yellow intersection in Fig. 1.1(b)) from the task-relevant information (pink-and-orange shaded area in Fig.1.1(b)). These task-relevant interactions can be either sub-additive/redundant (i.e. the muscle coupling provides less information about the task compared to the sum of the individual muscle patterns) or super-additive/synergistic (i.e. the muscle coupling conveys more task information than the sum of individual muscle-task encodings).

Conceptually, the information a muscle interaction provides is considered redundant when all the information can essentially be found in one of the muscles (pink shaded area (Fig.1.2(a)). This redundant task information thus reveals a functional similarity between muscle activations. Alternatively, we can also identify muscles that act synergistically towards complementary task goals, meaning their variations provide different information about a motor behaviour. A key, quantifiable attribute of this complementary interaction is the emergent task information ('*synergy*') they provide when considered together (orange shaded area (fig.1.2(b)). From this novel perspective, muscle activations can '*work together'* not just similarly towards a common task-goal but also complementarily towards different aspects of motor behaviour and concurrently towards objectives functionally irrelevant to overt task performance, thus providing a comprehensive view of the muscle interactions governing coordinated movement.

To illustrate this novel conceptual and analytical framework, we conducted two example applications to data from human participants performing naturalistic movements. These applications demonstrate the added utility of this framework to current muscle synergy analysis in terms of functional and physiological relevance and interpretability. We then applied it to three large-scale datasets, extracting generalizable and functionally interpretable space-time muscle networks with respect to both discrete and continuous task spaces. We have also made available open-source Matlab routines for readers to apply this approach to their own data (https://github.com/DelisLab/EMG2Task).

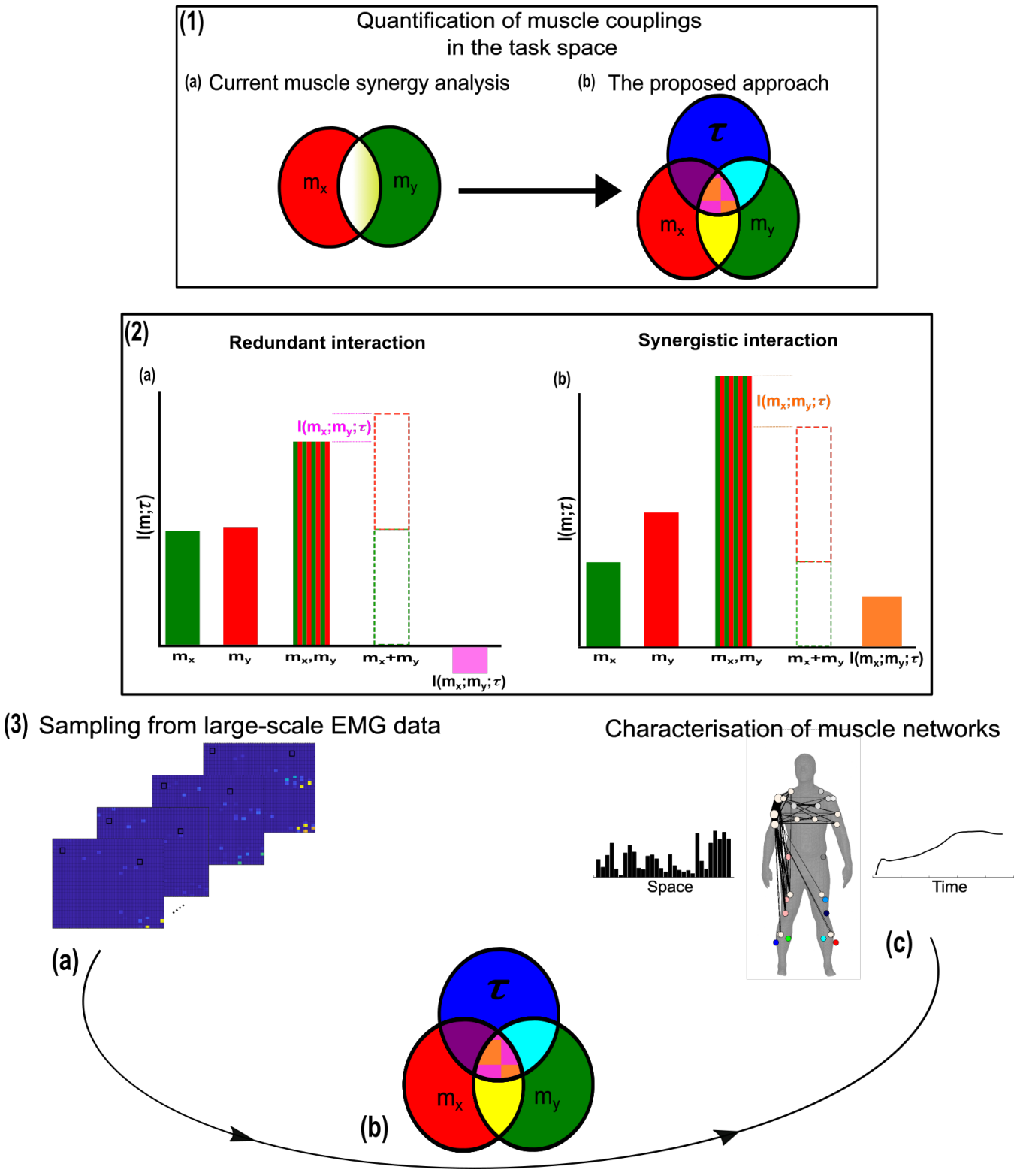

Fig.1: A general outline of the proposed approach. **(1.1(a-b))** We propose a novel approach to mapping muscle couplings to the task space. Among current muscle synergy analysis approaches, muscle couplings are quantified in isolation of the task solely using dimensionality reduction. Using our approach, the functional characteristics of muscle interactions can be quantified in terms of the similarity of their encoded task information. We do so by determining the coupling between $[m_x,\ m_y]$ and a corresponding task parameter (τ) using mutual information (MI). From this perspective, task-redundant muscle couplings (pink shaded area in pink-orange intersection) represent muscles cooperating towards similar task goals, while task-synergistic muscle couplings (orange shaded area in pink-orange intersection) encapsulate the task information provided by a muscle pairing acting towards complementary task goals. Muscle couplings present across tasks (i.e., task-irrelevant) are quantified by conditioning

the MI between $[m_x,\ m_y]$ pairs with respect to τ (yellow intersection). **(1.2)** A description of redundant and synergistic interactions. **(a)** Net redundant interactions are defined by a greater amount of information generated by the sum of individual observation of m_x and m_y ($[m_x + m_y]$) than their simultaneous observation ($[m_x,\ m_y]$). **(b)** In a net synergistic interaction, $[m_x,\ m_y]$ provides more information than $[m_x + m_y]$. **(1.3(a-c))** An overview of the approach. Spatiotemporal muscle activation samples are extracted across trials from large-scale EMG datasets and concatenated into vectors, forming $[m_x,\ m_y]$ pairs.The derived muscle couplings are then run through the NIF pipeline [107], producing low-dimensional, multiplexed space-time muscle networks.

3.3 Results

Our primary aim here is to characterise muscle synergies in task space by quantifying the contributions of muscle couplings to task performance. To achieve this, we essentially reverse the analytical approach typically used in muscle synergy studies (i.e. muscle groupings are identified and inferences then made about their functional roles) [70]. More specifically, we firstly identify functional couplings between paired muscle activations by evaluating their task-relevance and then extracting representative patterns of such couplings using dimensionality reduction methods. This enables us to distinguish task-irrelevant from task-relevant muscle couplings. Of the muscle couplings that demonstrate task-relevance, we can then characterise their functional roles as either redundant or synergistic. Fig.2 illustrates a simulation to facilitate interpretations of what informational redundancy and synergy mean when applied to muscle activities in the context of task performance. Redundant task information is generated when m_x and m_y carry identical predictive information about τ. This is distinct from current muscle synergy analysis which would consider m_x and m_y to share information about τ if their magnitudes are equivalent. Here, τ is always L when m_x is on and when m_y is off and R when vice versa. Thus, all the task information can be found in either m_x or m_y alone, generating 1 bit of redundant information. Synergistic task information on the other hand is predictive task information generated only when observing both m_x and m_y together. In the simple example shown, τ can be L when both m_x and m_y are active or inactive. However, we can see that when both muscles are active or inactive then τ is L. Thus, no predictive task information is provided by either m_x or m_y alone but the full 1 bit of information available is generated when observing both muscles together.

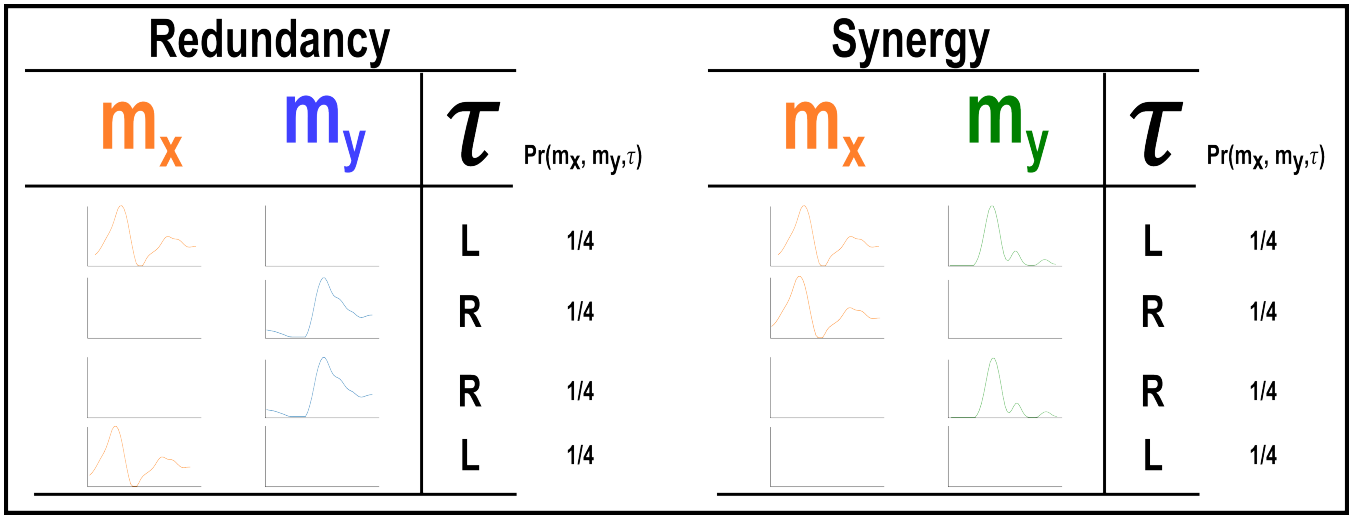

Fig.2: A simulation demonstrating how informational redundancy and synergy can be interpreted when applied to the muscle space. Four observations of a given muscle pair (m_x and m_y) that can fall into two equiprobable on and off activation states and a corresponding task parameter (τ) describing left (L) or right (R) movement direction. Observing either m_x or m_y in the redundancy example gives 1 bit of information while observing both m_x and m_y together in the synergy example gives 1 bit of information.

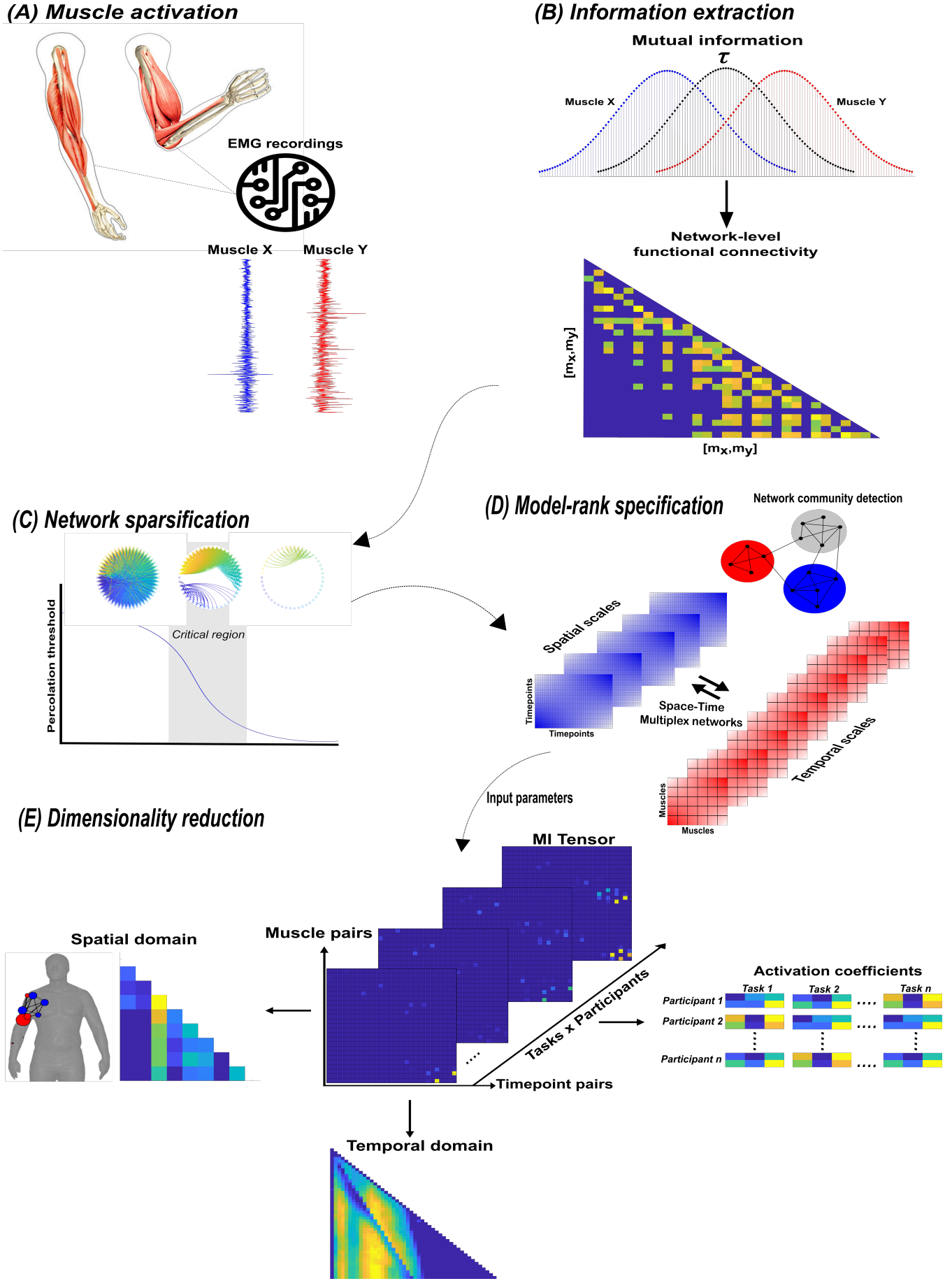
(A) Muscle activation
EMG recordings
Muscle X
Muscle Y
(B) Information extraction
Mutual information
τ
Muscle X
Muscle Y
Network-level
functional connectivity
[mx,my]
[mx,my]
(C) Network sparsification
Percolation threshold
Critical region
(D) Model-rank specification
Network community detection
Spatial scales
Timepoints
Timepoints
Space-Time
Multiplex networks
Temporal scales
Muscles
Muscles
Input parameters
(E) Dimensionality reduction
MI Tensor
Spatial domain
Muscle pairs
Tasks x Participants
Timepoint pairs
Activation coefficients
Task 1
Task 2
Task n
Participant 1
Participant 2
Participant n
Temporal domain

Fig.3: A summary of the NIF pipeline. (**A**) Large-scale datasets of EMG signals are captured while participants perform various motor tasks [25–27]]. (**B**) The MI between all unique muscle-timepoint vector ($[m_x, m_y]$) combinations with respect to a corresponding task parameter (τ) is determined [59], forming a network of functional connectivities. (**C**) These adjacency matrices are then analysed in terms of statistical significance and modular structure using percolation theory [66]. (**D**) The optimal spatial and temporal model-ranks are determined using generalised, consensus-based network community detection methods [72, 71, 112, 79]. (**E**) The optimal model-ranks are used as input parameters for dimensionality reduction, where space-time muscle networks along with their underlying activation coefficients are concurrently extracted [23].

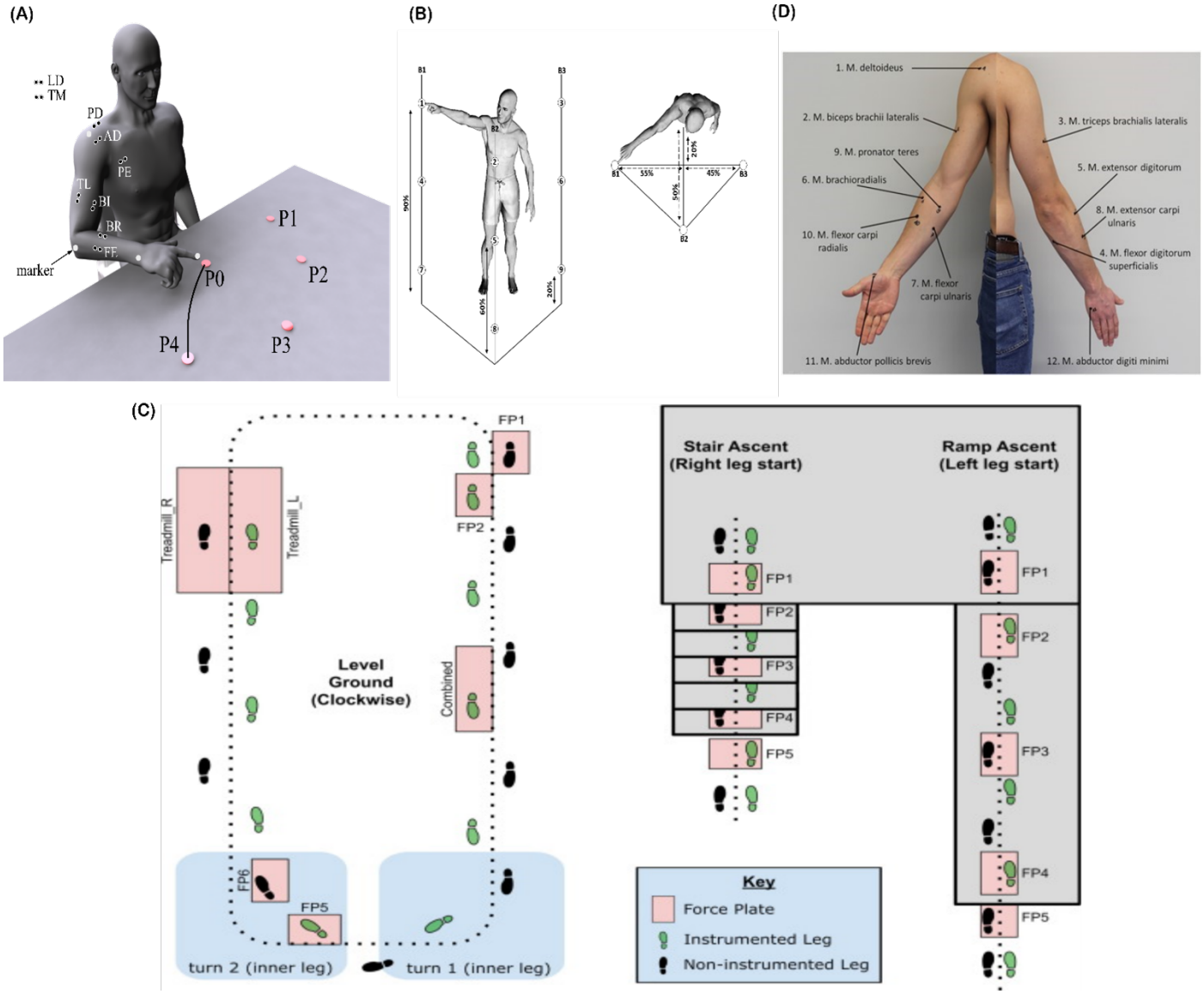

Fig.4: Graphical illustrations of each of the datasets analysed in the current study. **(A)** Dataset 1 consisted of participants executing table-top point-to-point reaching movements (40cm distance from starting point P0) across four targets in forward (P1-P4) and backwards (P5-P8) directions at both fast and slow speeds (40 repetitions per task) [23]. The muscles recorded included the finger extensors (FE), brachioradialis (BR), biceps brachii (BI), medial-triceps (TM), lateral-triceps (TL), anterior deltoid (AD), posterior deltoid (PD), pectoralis major (PE), latissimus dorsi (LD) of the right, reaching arm. **(B)** For dataset 2, the activity of 30 muscles was recorded while participants performed whole-body point-to-point reaching movements across three different heights and bars and in various directions, accumulating to 72 unique reaching tasks [82]. **(C)** The circuit navigated by participants in dataset 3 as they executed various locomotion modes is illustrated, of which level-ground walking, stair- and ramp- ascent/descent were analysed in the current study [113]. Several sub-conditions were undertaken by participants for each locomotion mode including different walking-speeds, clockwise vs. counter-clockwise direction, different stair heights and ramp inclines etc. Participants executed these tasks while the EMG of 11 muscles on the right leg ((Gluteus medius (GlutM), right external oblique (Obl), semitendinosus (ST), gracilis (GR), biceps femoris (BF), rectus femoris (RF), vastus lateralis (VL), vastus medialis (VM), soleus (SO), tibialis anterior (TA), gastrocnemius medialis (GM)) along with kinematic, dynamic

and IMU signals were captured. (**D**) The EMG placement for dataset 4 Deltoideus pars clavicularis (DC), Biceps brachii (BB), Triceps brachii (TB), Flexor digitorum superficialis (FDS), Extensor digitorum (ED), Brachioradialis (BR), Flexor carpi ulnaris (FCU), Extensor carpi ulnaris (ECU), Pronator teres (PT), Flexor carpi radialis (FCR), Abductor pollicus brevis (APB), Abductor digiti minimi (ADM) [114]. A single-trial was taken from 25 healthy and 20 post-stroke participants performing a unilateral pointing movement with the index finger and arm outstretched (task 9 of the Softpro protocol (MHH)).

Building on current approaches to muscle synergy analysis

Current approaches to muscle synergy analysis based on non-negative matrix factorisation (NMF) have a proven use case in the extraction of functionally- and physiologically relevant motor patterns [105, 19, 17, 30, 115]. To demonstrate that the proposed framework adds to this current utility, here we firstly provide a simple example output from the proposed and current approaches (see fig.5(A-D)). This example was derived from the EMG recordings of a single-trial of a participant walking on level-ground in the counter-clockwise direction around the circuit depicted in fig.4(C) [113]. For the proposed approach, the muscle couplings were determined with respect to a single, continuous task parameter, the heel kinematic marker in the anterior-posterior direction. For the application of the current approach, we applied the spatial muscle synergy model across the same single-trial EMG recordings [42], extracting one component.

The simplified representations from the proposed approach reveal the functional role of muscular interactions with respect to the heel marker and provide intuition on the types of muscle couplings that can be identified, including task-irrelevant (A) -redundant (B) and –synergistic (C) interactions. Their submodular structure are illustrated via the node colour on the accompanying human body models [81], describing muscles that have a closer functional relationship. For example, a) the hamstring muscles (ST and BF) controlling knee flexion work redundantly together with muscles involved in hip abduction (GR, GlutM and Obl) to move the heel around the circuit (Fig.4(B)), and b) calf muscles involved in ankle flexion (GM, TA) cooperatively determine heel position in synergy with the same hamstring muscles (Fig.5(C)). Moreover, these hamstring muscles together with their antagonist RF also form a task-irrelevant network, i.e. their couplings are not predictive of heel position (Fig.5(A)). Overall, task-irrelevant muscle couplings primarily capture interactions between co-agonist and agonist-antagonist muscles that are indiscriminative of heel marker position. Also, task-redundant and -synergistic couplings reveal functionally similar and dissimilar muscle combinations respectively that provide sub-additive (i.e. shared or redundant) and super-additive (i.e. complementary or synergistic) information about heel marker position.

The NMF representation (fig.5(D)) conveys important information about gait in a task-agnostic manner, thus it may contain both task-relevant and -irrelevant interactions. Intuitively, SO, GM and Obl of the outer, right-side are most prominently weighted here, perhaps representing their functional role in accelerating the body in the counterclockwise direction around the circuit whilst maintaining upright posture (fig.4(C)). This observation can only be inferred indirectly however as, amongst current approaches, no direct association is made with other muscles or with task performance. Indeed, with respect to heel position, the proposed approach reveals that SO is functionally similar to Obl and GM whilst also containing task-synergistic and -irrelevant information with GM (fig.5(A-C)). From the perspective of existing approaches, the knee flexors and extensors play a minor role during turning gait (as indicated by their relatively low weighting (fig.5(D))). However, the proposed approach conveys a central role for these muscles suggesting that the proposed framework enables targeted dissections of muscle functionality with respect to a chosen task parameter, thus revealing subtle couplings with potentially important behavioural consequences.

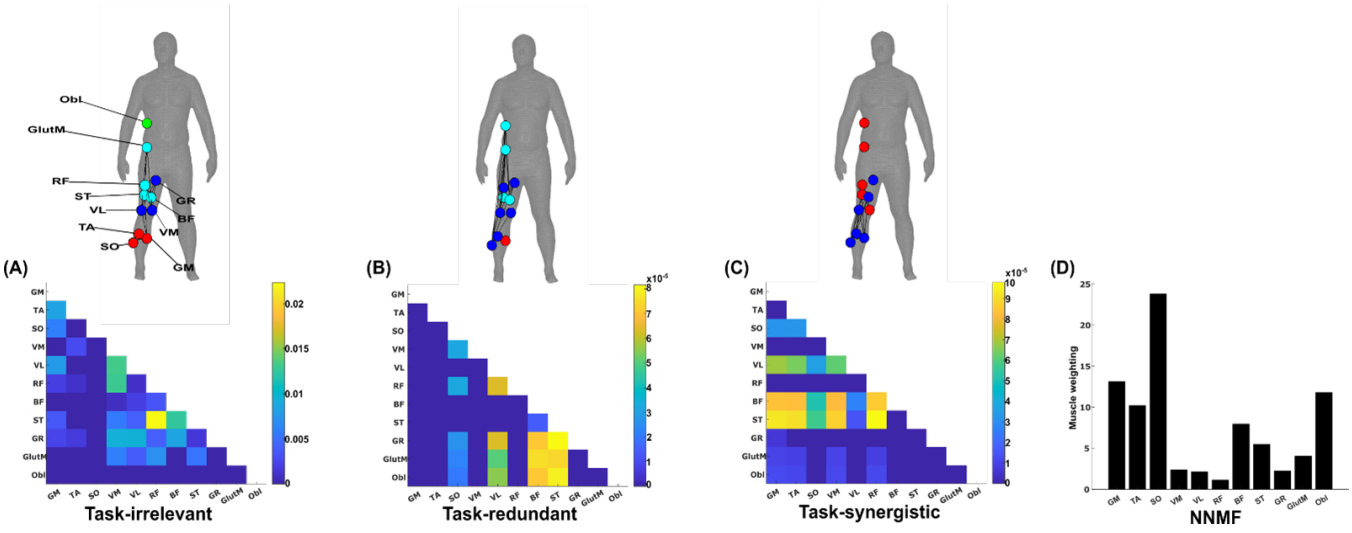

Fig.5: A simplified example output from the proposed framework applied to a single trial of turning gait from Dataset 3. (**A**)

Task-irrelevant, (**B**) Task-redundant and (**C**) Task-synergistic synchronous muscle couplings were quantified (the unit of shared information is 1 bit) with respect to the heel kinematic marker (anterior-posterior direction). Human body models accompanying each spatial network illustrate their respective submodular structure with node colour and size and edge width indicating community affiliation [72], network centrality and connection strength respectively [81, 116]. (**D**) A corresponding synergy representation from a single trial of turning gait from dataset 3 extracted using the spatial model from current approaches [42]. Each bar represents the relative weighting of each muscle in the synergy component.

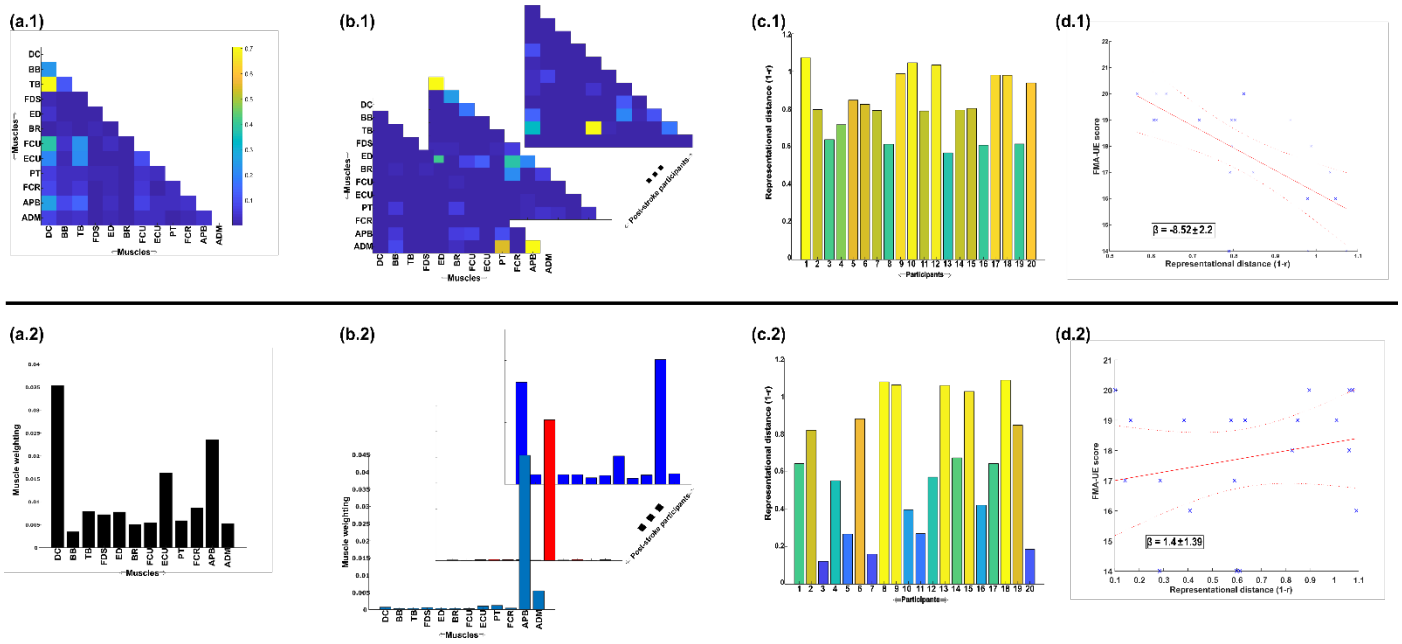

Fig.6: A simple demonstration of the physiological relevance of the proposed approach (**a.1-d-1**) and the traditional, NMF-based approach (**a.2-d.2**). From dataset 4 [114], we took the EMG signals and WRBA kinematic from 20 post-stroke and 25 healthy participants. We extracted a single normative reference of healthy controls task-redundant muscle couplings with respect to WRBA (**a.1**) and a corresponding normative reference using NMF only (**a.2**). We then extracted a single component from each post-stroke participant and compared them individually with the corresponding normative reference, computing distance values (1-r) (**b-c**). We finally determined the predictive relationship of these distance values with a measure of upper-extremity motor impairment derived from the Fugl-meyer assessment (FMA-UE) (**d**).

Next, to demonstrate the additional physiological relevance the proposed methodology brings to current muscle synergy analysis, we applied the proposed framework to single trials of pointing movements performed by 20 participants with stroke and 25 healthy controls from dataset 4 (fig.4(D)) ('MMH' task 9 [114]). Specifically, we determined MI from a randomly selected trial of healthy and post-stroke participants with respect to the 3D position of the anterior wrist kinematic marker (WRBA) of the pointing arm. We chose WRBA as the task variable here due to its sensitivity to hand orientation. For the purpose of this simplified demonstration, we focused on a comparison between task-redundant (with respect to WRBA) and NMF-based muscle representations. We firstly generated a normative representation of this pointing motion by extracting the first component across the healthy controls using the proposed approach (Fig.6(a.1)) and NMF (Fig.6(a.2)). We then quantified the similarity of muscle representations extracted from each post-stroke participant individually to this normative reference (obtained across all healthy participants) using Pearson's correlation and converted these values to distances (i.e. 1-r) (Fig.6(b-c)). Finally, we determined if these distances from healthy control values were predictive of the stroke survivor's motor impairment, measured using the upper-extremity section of the Fugl-Meyer assessment (FMA-UE) (Fig.6(d)).

To briefly summarise the results, the distance of post-stroke participants from healthy controls was found to be predictive of motor impairment for the proposed approach (β= -8.52±2.2, p=0.0012) but not the NMF-based approach (β= 1.4±1.39, p=0.33). This finding suggests, intuitively, that the proposed approach captures redundant muscle couplings that support robust motor control and that deviations from this normative pattern of motor redundancy are linearly related to the degree of impairment. Importantly, this result was obtained using only one randomly selected trial for each participant. This simple example conveys the physiologically-relevant targeted insights that can be generated from the proposed framework. Although current approaches have demonstrated significant linear relationships with motor impairment [45, 117, 118], these assessments generally rely on large numbers of trials and participants and don't point to specific underlying muscle interactions as provided here.

Together, through two example applications, we have demonstrated attributes of the proposed methodology that provide novel

capabilities to current muscle synergy analysis. In the following, we sequentially present in more detail the three types of muscular interactions in the spatiotemporal domain across three datasets and then show the robustness of the approach and its outputs.

Representations of motor behaviour in muscle couplings

To begin, we derived pairs of muscle activation vectors $[m_x,\ m_y]$ from benchmark datasets of human participants executing naturalistic movements, namely arm reaching (dataset 1), whole-body point-to-point reaching (dataset 2), and various locomotion modes (dataset 3) [23, 82, 113, 114] (see Fig.4 for the experimental design of each dataset and '*Materials and methods'* for an outline of the experimental setups and EMG data pre-processing) (fig.3(A)). For datasets 1 and 2, we determine the MI between $[m_x,\ m_y]$ vectors with respect to several discrete task parameters representing specific task attributes (e.g. reaching direction, speed etc.), while for dataset 3 we determined the task-relevant and -irrelevant muscles couplings in an assumption-free way by quantifying them with respect to all available kinematic, dynamic and inertial motion unit (IMU) features.

Having extracted the muscle pair-task interdependencies representing a specific intersection in fig.1.1(b), we next sought to find a parsimonious representation of motor behaviour that is consistent across tasks and participants for dataset 1-3 (fig.3(E)) [107, 23]. To produce this sparse, low-dimensional representation, we undertook the following intermediary steps:

We modelled the MI values as adjacency matrices in the spatial or temporal domain and identified dependencies that were statistically significant using percolation theory (fig.3(C)) [66, 119]. By assuming the muscle networks operate near a state of self-organised criticality [120], we effectively isolated dependencies that were above chance-level occurrence, thus empirically sparsifying the networks.

To empirically determine the number of components to extract in a parameter-free way, we then concatenated these adjacency matrices into a multiplex network and employed network community-detection protocols to identify modules across spatial and temporal scales (fig.3(D)) [72, 71, 112, 79, 121]. Having detected the spatiotemporal modular structure, we then returned the sparsified networks to their original format and used the number of modules identified as input parameters into dimensionality reduction (fig.3(E)) [23].

By optimising a modularity-maximising cost-function [67, 122], the community detection protocols we employed consistently identified three spatial (S1-S3) and two temporal (T1-T2) modules as representative of the underlying task-redundant, -synergistic and -irrelevant informational dynamics. Following their extraction, we further analysed the spatial networks from each dataset in terms of their submodular structure by applying network-theoretic tools [72, 79, 116]. In doing so, we identified subnetworks within each spatial network and interesting patterns of network centrality, i.e. the relative importance of a node in a network. The spatial and temporal networks of each dataset output are illustrated in panels A and B (fig.7-12) of the following sections. They are accompanied by human body models where node colour and size indicate subnetwork community affiliation and network centrality respectively [81]. The networks we extracted operate in parallel within spatial and temporal domains while having an all-to-all correspondence across domains, i.e. any spatial component can be combined with any temporal component via a task-specific coefficient (illustrated in panel C for dataset 1 and 2 outputs and in the supplementary materials for dataset 3) [23]. Unlike similar muscle synergy extraction approaches, dimensionality reduction in the NIF pipeline doesn't seek to approximate the variance of recorded EMG data but to identify sets of muscles that share the same type of interaction. Thus, the multiplexing coefficients extracted in this framework are instead interpreted as the participant- and task-specific scaling of information overlap.

Task-irrelevant muscle coupling

To quantify the task-irrelevant contributions of muscular interactions to motor behaviour, we conditioned the MI between $[m_x,\ m_y]$ with respect to τ (see '*Materials and methods'* section) [59]. This conditioning effectively removes the task-relevant information, leaving information produced by pairwise muscle variations that are task-indiscriminative. Following a run through the NIF pipeline (fig.3) [107], the output from dataset 2 and 3 are presented in fig.7-8 respectively while the output from dataset 1 is presented in Fig.7-supplementary materials 1. The task-irrelevant space-time muscle networks we extracted from dataset 1 and 2 shared several structural features with their task-agnostic counterparts extracted in the preliminary study [107], supporting recent work showing that functional muscle network structure are heavily influenced by task-irrelevant factors such as anatomical constraints [12]. The functional connectivities identified here captured known contributions of spatiotemporal muscular interactions to aspects of motor behaviour common across tasks and participants which we outline briefly here.

The temporal networks from dataset 1 and 2 captured mostly co-activations from movement onset – mid-movement and movement cessation, indicating that some co-contraction mechanisms were consistently task-irrelevant across trials. The temporal networks for dataset 2 were more diffuse compared to dataset 1, probably reflecting the more variable role of passive forces in generating movements to different heights captured in this dataset's experimental design [82, 123]. Furthermore, this co-contraction mechanism was more parsimoniously represented as a single network in dataset 3 (T1 in fig.8B), where passive forces in contrast likely played a consistently resistive role during locomotion. Interestingly, T1 for dataset 3 corresponded

equivalently high for all three task spaces when corresponding with S2 which consisted of upper-leg extensors (see Fig.8-supplementary materials 1). Muscle couplings indicative of agonist-antagonist pairings were also identified as separate subnetworks in S3 of dataset 3 (fig.8A). More specifically, their functional segregation appeared to be based on their distinct functional roles in forward propulsion (red nodes) and deceleration (blue nodes) during the mid-stance phase of gait, as indicated by the prominent correspondence with T2 across task spaces (see Fig.8-supplementary materials 1). This finding reflects the consistent agonistic and antagonistic contributions of muscular interactions across locomotive tasks.

The gross motor function of muscle couplings was another characteristic of task-irrelevant muscle couplings that pervaded across the datasets analysed here. For instance, AD had a central role in S2 of dataset 1 while also displaying a unique pattern of connectivity with tibial musculature in S3 of dataset 2. Similarly, GlutM had a central role in S1 of dataset 3 (fig.8A). We further found a common pattern of task-irrelevant connectivity in S2 across datasets, namely the musculature about a hinge joint (elbow in dataset 1 and 2, knee in dataset 3) coupled with proximal shoulder or hip musculature, indicative of their biomechanical affordances. Finally, the passive, left-arm was connected with the tibial musculature of S3 in dataset 2 (green nodes (Fig.7(A)). To probe the underlying function of this connectivity in the left-arm, we inspected the original EMG signals. We observed periodic, tonic activations across tasks, reflective of reciprocal inhibition of contralateral limb musculature that enables unilateral movement [124].

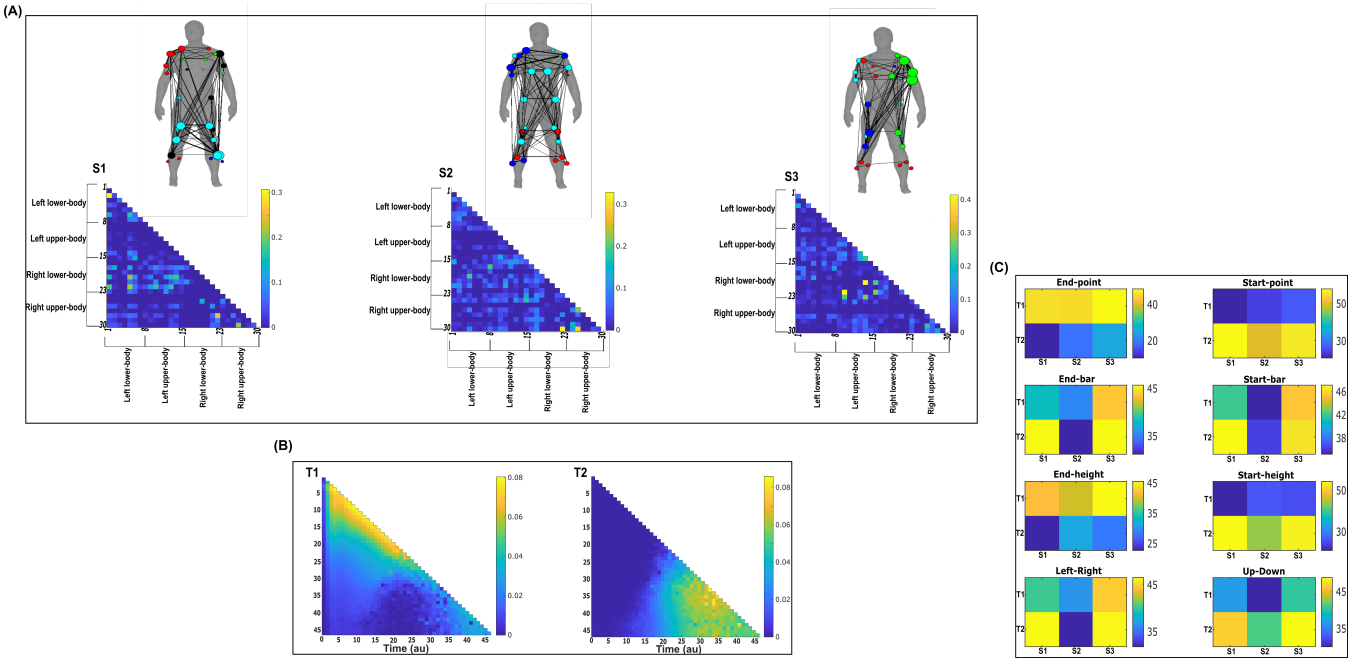

Fig.7: Three spatial (**S1**-**S3**) and two temporal task-irrelevant muscle networks (**T1**-**T2**) were empirically identified and extracted across participants and task parameters from dataset 2 using the NIF pipeline (Panel **A**-**B**) [107, 82] (Panel **C**) Activation coefficients are presented to the right of the networks, indicating their task parameter-specific scaling averaged across participants. Human body models accompanying each spatial network illustrate their respective submodular structure with node colour and size and edge width indicating community affiliation [72], network centrality and connection strength respectively [81, 116].

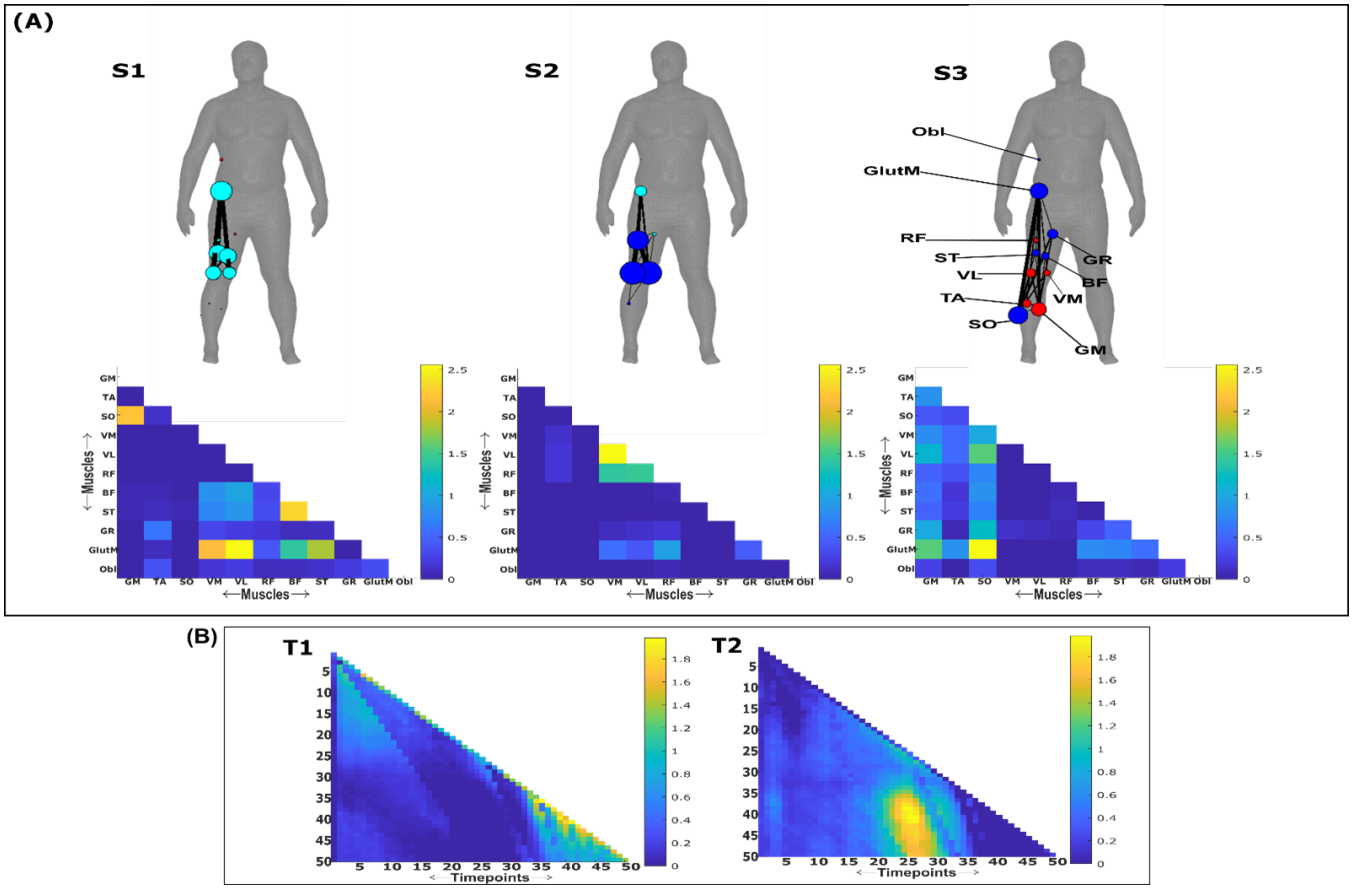

Fig.8: Three spatial (**S1**-**S3**) and two temporal task-irrelevant muscle networks (**T1**-**T2**) were empirically identified and extracted across participants and task parameters from dataset 3 using the NIF pipeline (Panel **A**-**B**) [107, 113]. Activation coefficients are presented in supplementary materials 1, indicating their task parameter-specific scaling averaged across participants in the dynamic, IMU and kinematic spaces. Human body models accompanying each spatial network illustrate their respective submodular structure with node colour and size and edge width indicating community affiliation [72], network centrality and connection strength respectively [81, 116].

Task-redundant muscle couplings

To characterise the functional role of task-relevant muscle couplings, we employed a higher-order information-theoretic concept known as co-information (co-I) [59, 125, 126]. This metric quantifies the MI between three random variables and may take on positive values (net synergistic) and negative values (net redundant) (see Fig.13 of '*Materials and methods*' section). Co-I quantifies the task-relevant information shared between $[m_x,\ m_y]$ independently of the information generated by task-irrelevant muscular interactions. In doing so, it also defines the functional relationship between $[m_x,\ m_y]$ overall as redundant or complementary. Following the quantification of co-I for all $[m_x,\ m_y]$ and corresponding τ (pink area in orange-and-pink intersection (fig.1.3(B)), we parsed the negative values indicating redundancy into a separate matrix and rectified them. In fig.9-10, we illustrate the output following the extraction of task-redundant space-time muscle networks from datasets 2-3 across tasks and participants respectively while the output for dataset 1 is presented in Fig.9-supplementary materials 1. In the co-I formulation, task-redundant muscle couplings can be interpreted as muscle couplings that overall shared a common task-relevant functional role. For example, with reference to Figure 9 here, muscles in the networks presented in S1 (fig.9A) carry redundant information about the movement endpoint (fig.9C) with the temporal profile T1 (fig.9B) whereas S3 (fig.9A) contains muscle networks carrying redundant information about the starting point (fig.9C) with the same temporal profile T1 (fig.9B).

Both dataset 1 (Fig.9-supplementary materials 1) and dataset 3 (fig.10) outputs display similar patterns of muscle couplings at the same spatial scale of an individual, task-relevant limbs' musculature, with an emphasis on the coupling of specific muscles with all other muscles. For dataset 1, FE, BI and BR displayed this integrative pattern across S1-S3 respectively while BF, TA and ST demonstrated this pattern in dataset 3 also. The muscle networks encapsulated several functionally interpretable couplings such as the agonist-antagonist pairings of the BI and TM of S2 (dataset 1 (Fig.9-supplementary materials 1(A)) and the task redundancy of ankle dorsi-flexors, and knee/hip flexors during sloped walking for example in S2 of dataset 3 (fig.10(A)) [127]. The functional interpretation of these muscle connectivity patterns was in line with the extracted task-

specific activations. For instance, S2 of dataset 1 was modulated most prominently by reaching direction when corresponding with T2, commensurate with the biomechanical affordances of this upper-arm muscle network. Furthermore, S2 of dataset 3 was specifically modulated by the right-thigh kinematic marker along the y-axis (up-down direction) for both T1 and T2 (see Fig.10-supplementary materials 1). The centrality of task-redundant muscle couplings in dataset 1 and 3 suggests particular muscle activations drive the task-specific variations in the reaching arm and stepping leg muscle activities towards a common behavioural goal. It is also worth noting that the magnitude of these functional connectivity patterns appeared to be proportional to anatomical distance, as evidenced by the magnitude of connection strengths, a finding supportive of previous related research [12].

Meanwhile at the greater spatial scale of dataset 2 (fig.9(A))), task-redundant muscle couplings were anatomically compartmentalised to the upper- and lower-body. This functional segregation was emphasised at the subnetwork level also, where the upper- and lower-body musculature of S3 for instance formed distinct submodules (blue and red nodes). Amongst the task-specific activations in dataset 2, S1 carried redundant task information about end-point target, -height and up-down direction when corresponding with T1. T2 for dataset 2 on the other hand contained mostly temporally proximal dependencies along the diagonal, suggestive of co-contraction mechanisms, which became more diffuse near movement cessation. These endpoint trajectory and co-contraction related temporal patterns were qualitatively similar to T1 and T2 of both dataset 1 and 3 respectively (see fig.10 and Fig.9-supplementary materials 1 respectively).

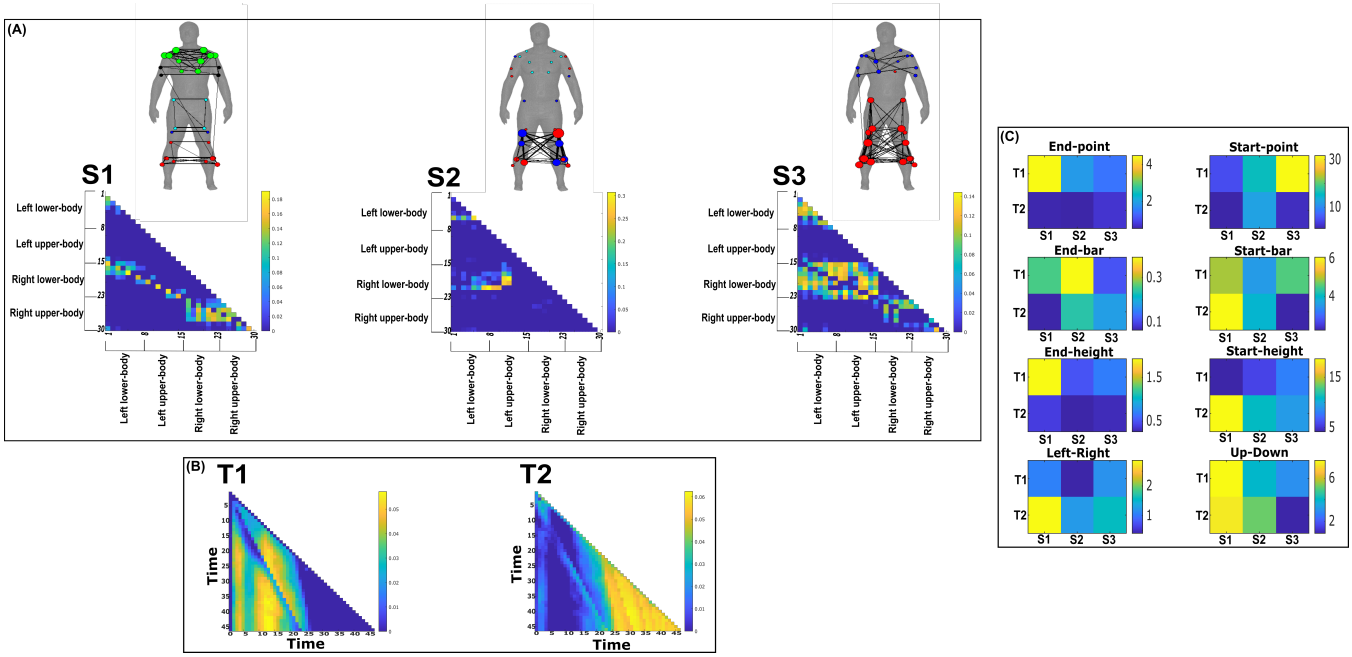

Fig.9: Three spatial (**S1**-**S3**) and two temporal task-redundant muscle networks (**T1**-**T2**) were empirically identified and extracted across participants and task parameters from dataset 2 using the NIF pipeline (Panel **A**-**B**) [107, 82]. (Panel **C**) Activation coefficients are presented to the right of the networks, indicating their task parameter-specific scaling averaged across participants. Human body models accompanying each spatial network illustrate their respective submodular structure with node colour and size and edge width indicating community affiliation [72], network centrality and connection strength respectively [81, 116].

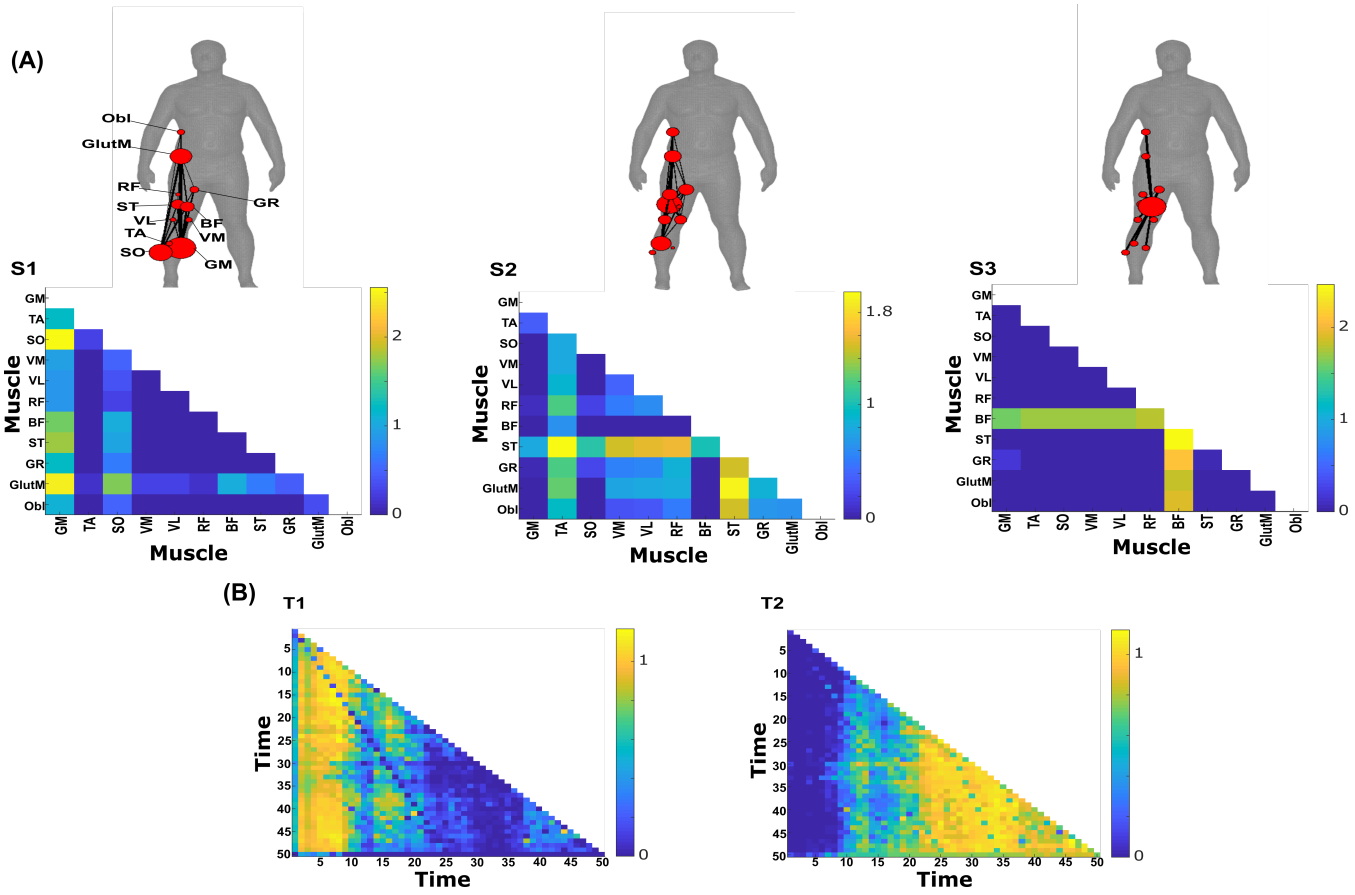

Fig.10: Three spatial (**S1**-**S3**) and two temporal task-redundant muscle networks (**T1**-**T2**) were empirically identified and extracted across participants and task parameters from dataset 3 using the NIF pipeline (**A**-**B**) [107, 113]. Activation coefficients are presented in supplementary materials 1, indicating their task parameter-specific scaling averaged across participants in the dynamic, IMU and kinematic spaces. Human body models accompanying each spatial network illustrate their respective submodular structure with node colour and size and edge width indicating community affiliation [72], network centrality and connection strength respectively [81, 116].

Task-synergistic muscle couplings

Similarly, we isolated task-synergistic muscle couplings by parsing, instead, the positive co-I values from the computations conducted across all $[m_x,\ m_y]$ and corresponding τ into a sparse matrix where all redundant couplings were set to zero (see Fig.13 of '*Materials and methods'* section). Task-synergistic muscle couplings here can be interpreted as a $[m_x,\ m_y]$ pair that provide complementary (i.e. functionally dissimilar) task information, thus more information is gained by observing $[m_x,\ m_y]$ together rather than separately (orange area in orange-and-pink intersection (fig.1.3(B)). In Fig.11-12, we illustrate the task-synergistic space-time muscle networks from datasets 2-3 respectively (dataset 1 output is presented in Fig.11-supplementary materials 1).

Across datasets, muscle networks could be characterised by the transmission of complementary task information between functionally specialised muscle groups, many of which were identified among the task-redundant representations (Fig.9-10 and Fig.9-supplementary materials 1). The most obvious example of this is the S3 synergist muscle network of dataset 2 (Fig.11), which captures the complementary interaction between task-redundant submodules identified previously (S3 (Fig.9)). A particularly consistent structural feature was the emphasis of an individual muscles' connectivity with all other muscles which was evident among synergistic couplings in dataset 3 (see VM, VL and RF of S1, GR, TA and SO of S2 and GlutM of S3 in fig.12A). This structural similarity demonstrates that parallel and synchronous exchanges of redundant and synergistic task information underlie task-specific variations across trials (e.g. S3 of dataset 2 in fig. 9A and fig.11A). Interestingly, despite the similarity between the redundant and synergistic muscle networks, the way they are combined to encode task information differs depending on the type of interaction (synergistic vs. redundant, e.g. panel C of fig.11 in comparison to panel C of fig.9).

Concerning the temporal activations of these networks, the task-synergistic structure of dataset 2 (fig.11B) was also relatively unchanged compared to the task-redundant structure (fig.9B). This suggests that the task end-goal and co-contraction related mechanisms provided both redundant and synergistic task information concurrently during whole-body reaching movements.

In contrast, a different view of synergistic information exchange is provided in datasets 1 and 3 (Fig.11-supplementary 1 and fig.12 here respectively), where T1 and T2 consist of more idiosyncratic activations that together appear to reflect the task end-goal related patterns found elsewhere. More specifically, in both datasets we found two distinct patterns of task-end goal related activity where early and late timepoints during movement initiation operated in parallel to provide complementary task information (see Fig.12B and Fig.11-supplementary materials 1(B)).

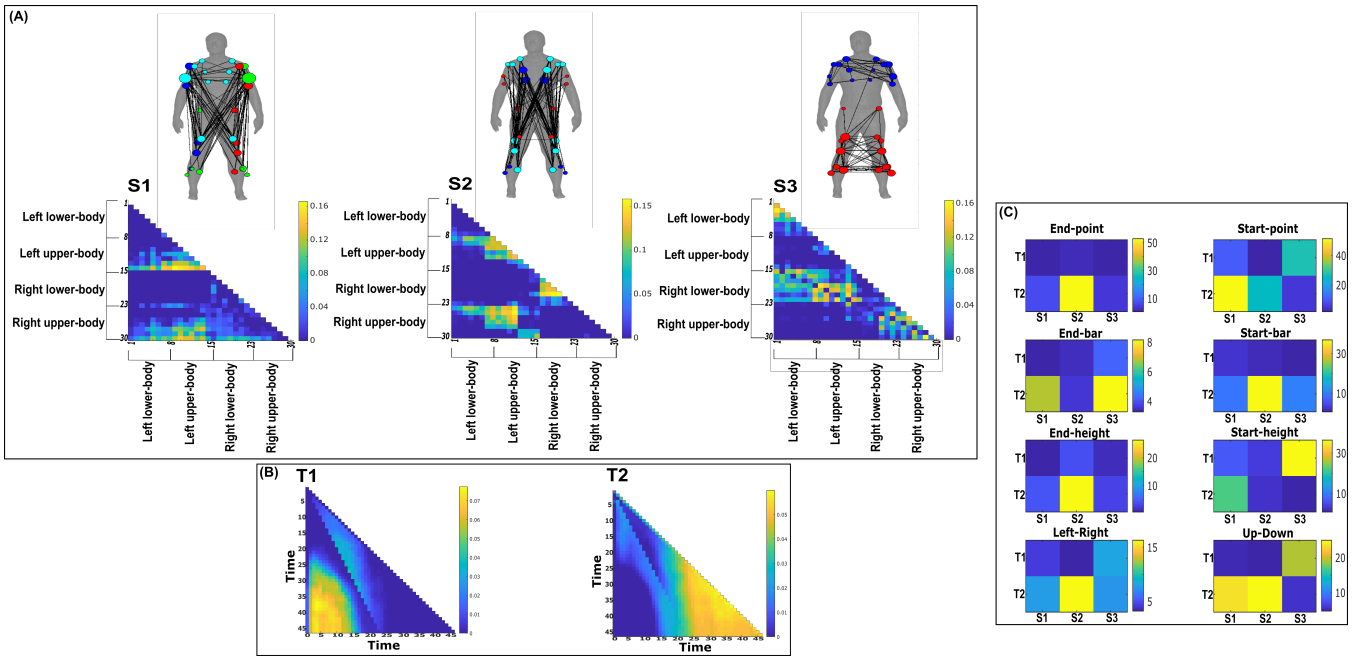

Fig.11: Three spatial (**S1**-**S3**) and two temporal task-synergistic muscle networks (**T1**-**T2**) were empirically identified and extracted across participants and task parameters from dataset 2 using the NIF pipeline (Panel **A**-**B**) [107, 82]. (Panel **C**) Activation coefficients are presented to the right of the networks, indicating their task parameter-specific scaling averaged across participants. Human body models accompanying each spatial network illustrate their respective submodular structure with node colour and size and edge width indicating community affiliation [72], network centrality and connection strength respectively [81, 116].

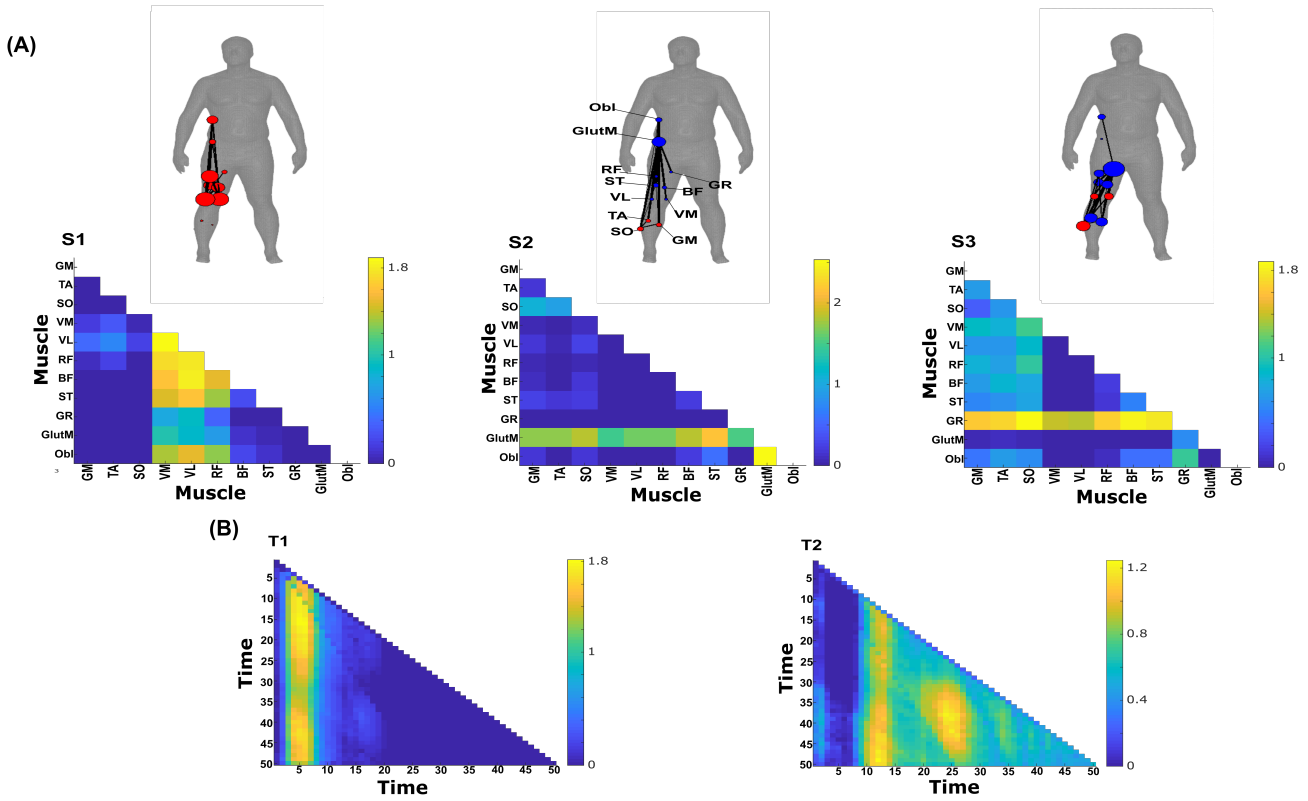

Fig.12: Three spatial (**S1**-**S3**) and two temporal task-synergistic muscle networks (**T1**-**T2**) were empirically identified and extracted across participants and task parameters from dataset 3 using the NIF pipeline (Panel **A**-**B**) [107, 113]. Activation coefficients are presented in supplementary materials 1, indicating their task parameter-specific scaling averaged across participants in the dynamic, IMU and kinematic spaces. Human body models accompanying each spatial network illustrate their respective submodular structure with node colour and size and edge width indicating community affiliation [72], network centrality and connection strength respectively [81, 116].

Generalisability of the extracted space-time muscle networks

To ascertain the generalisability of the extracted representations presented here beyond any subset of the input data, we conducted a similarity analysis through a leave-n-out cross validation procedure. In more detail, we compared the space-time networks extracted from the full dataset (illustrated in fig.4-9 and corresponding supplementary materials) to the networks extracted from a subset of the data (see '*Materials and methods'* section). Across datasets, a high level of concordance was found on average (~0.9 correlation, see table1). This trend was evident across all datasets and for task-redundant, -synergistic and -irrelevant spatial and temporal networks. Dataset 1 and 2 findings demonstrate that the extracted networks are generalisable beyond any individual participant or task. Dataset 3 results go further by demonstrating that the extracted patterns are generalizable beyond any randomly selected and randomly sized subset of the input data. The highest correlations on average were consistently among temporal networks, replicating previous findings [107, 83, 128]. Although the spatial networks demonstrated a lower average correlation, this was substantially higher compared to previous applications of datasets 1 and 2 [107, 83, 23], suggesting that the inclusion of task parameters here captures the inter-participant differences more effectively. When comparing representations extracted from each continuous task space in dataset 3, kinematic features consistently had the highest average correlation and lowest variability compared to dynamic and IMU feature spaces. These findings support our change in the interpretation of the extracted activation coefficients away from conventional approaches where representational biases towards particular participants and/or tasks are inferred.

To further probe how the underlying assumption of an all-to-all correspondence between spatial and temporal representations made by sNM3F influenced the generalisability of the extracted networks, we compared its performance to non-negative Canonical-Polyadic (CP) tensor decomposition, which assumes an opposing one-to-one correspondence between components. We found that although CP has demonstrated a considerable capacity to de-mix neural data into simplified and interpretable low-dimensional components [129], its application here resulted in poor generalisability of the extracted patterns (~0.5 correlation on average). This finding suggests that the all-to-all correspondence implemented by sNM3F identifies a more generalizable representation and should be favourably considered in future applications of this framework.

	Dataset 1				Dataset 2				Dataset 3					
	Spatial		Temporal		Spatial		Temporal		Spatial			Temporal		
	Participants	Tasks	Participants	Tasks	Participants	Tasks	Participants	Tasks	Kinematics	Dynamics	IMUs	Kinematics	Dynamics	IMUs
Task-redundant muscle couplings	0.95±0.23	0.89±0.28	0.98±0.19	0.89±0.27	0.82±0.42	0.94±0.27	0.99±0.03	0.96±0.28	0.92±0.28	0.91±0.32	0.86±0.31	0.93±0.21	0.92±0.24	0.87±0.29
Task-synergistic muscle couplings	0.95±0.23	0.73±0.26	0.98±0.19	0.91±0.3	0.79±0.37	0.96±0.25	0.92±0.3	0.99±0.1	0.97±0.16	0.9±0.27	0.96±0.19	0.99±0.04	0.98±0.13	0.95±0.18
Task-irrelevant muscle couplings	0.84±0.1	0.85±0.1	0.79±0.15	0.95±0.04	0.84±0.15	0.99±0.01	0.93±0.1	0.99±0.06	0.9±0.34	0.83±37	0.8±0.33	0.995±0.04	0.98±0.1	0.97±0.15

Table.1: A summary table illustrating the findings from an examination of the generalisability of the muscle networks extracted from each dataset. The spatial and temporal representations extracted from the full input data in each muscle-task information subspace were compared using Pearson's correlation against functionally similar representations extracted from a subset of the input data.

3.4 Discussion

The aim of the current study was to dissect the muscle synergy concept and offer a novel, more nuanced perspective on how muscles '*work together'* to achieve a common behavioural goal. To do so, we introduced a computational approach based on the NIF pipeline (fig.3), enabling the effective decomposition of muscle interactions and the comprehensive description of their functional roles. Through the direct inclusion of task parameters in the extraction of muscle synergies, a novel perspective was produced where muscles '*work together'* not just towards a common task-goal, but also concomitantly towards complementary task objectives and lower-level functions irrelevant for overt task performance. The functional architectures we uncovered were comprised of distributed subnetworks of synchronous muscle couplings and driven by distinct temporal patterns operating in parallel. Example applications to simple real and simulated EMG datasets revealed the additional capabilities provided by the proposed framework to current muscle synergy analysis in terms of functional and physiological relevance and interpretability. When applied to large-scale data, the proposed methodology extracted representations scale-invariant to dataset complexity and motor behaviours whilst being generalizable beyond any subset of the data. We thus present this framework as a useful analytical approach for mechanistic investigations on large-scale neural data through this novel perspective to the muscle synergy.

The '*muscle synergy'* is a major guiding concept in the motor control field [105, 8, 16, 15, 31, 21], providing a conceptual framework to the problem of motor redundancy that centres around the general notion of '*working together'*. In its current conceptualisation, '*working together'* describes how the nervous system functionally groups muscles in a task-dependent manner through common neural drives to simplify movement control. This idea has undergone continued refinement since its early conception [105, 15, 31], with a notable progression being the introduction of the qualifying attributes: a sharing pattern, reciprocity and task dependence [31]. Nonetheless, recent influential works revealing other important mechanisms for the simplification of motor control highlight the generality of the current perspective offered by this concept [108, 50, 52, 51, 109, 110, 102, 111, 7]. We thus sought to provide greater nuance to the notion of '*working together'* by defining motor redundancy and synergy in information-theoretic terms [15, 130]. In our framework, redundancy and synergy are terms describing functionally similar and complementary motor signals respectively, introducing a new perspective that is conceptually distinct from the traditional view of muscle synergies as a solution to the motor redundancy problem [105, 15, 31]. In this new definition of muscle interactions in the task space, a group of muscles can '*work together'* either synergistically or redundantly towards the same task. In doing so, the perspective instantiated by our approach provides novel coverage to the partitioning of task-relevant and -irrelevant variability implemented by the motor system along with an improved specificity regarding the functional roles of muscle couplings [109, 110, 102]. Our framework emphasises not only the role of functionally redundant muscle couplings that result from the underlying degeneracy of the motor system, but also of complementary, synergistic dependencies that are important for communication and integration across specialised neural circuitry [131, 132]. Thus, the present study aligns the muscle synergy concept with the current mechanistic understanding of the nervous system whilst offering an analytical approach amenable to the continued advances in large-scale data capture [11, 133].

Among current approaches to muscle synergy analysis, the established synchronous, temporal and time-varying muscle synergy models are understood to each characterise unique motor features [97]. More specifically, the synchronous model captures agonist-antagonist muscle pairings, the temporal model decomposes EMG signals into functionally distinct temporal phases

and the task-specific modulation of spatiotemporal invariants are quantified in the time-varying model. In a unifying framework, here we quantify space-time muscle networks that concurrently capture many of these salient motor features in a holistic and principled way whilst mapping their functional consequences to motor behaviour. These salient features included, among others, agonist-antagonist pairings and functionally meaningful inter-limb couplings that consistently appeared across task-redundant, -synergistic and -irrelevant spaces. Thus, in dissecting the muscle interactions governing coordinated movement, our framework revealed their parallel and synchronous processing of functionally similar, complementary, and task-irrelevant information. This insight aligns with several recent works also demonstrating this distributed neural architecture of parallel information processing units [103, 131, 132].

Our framework also revealed novel characteristics of the motor system. For instance, the task-redundant and -synergistic networks we extracted appeared to be structured around the coupling between a prime-mover muscle and several supporting muscles, supporting recent work showing the nonhomogeneous sharing of neural drives within modules [134]. These novel spatial characteristics were driven by parallel temporal patterns representing endpoint trajectory and co-contraction related mechanisms, an insight supportive of recent work showing their parallel innervation [108, 123, 135]. Together, these representations encapsulated the functional interplay between task end-goal requirements and biomechanical affordances, a dynamic frequently highlighted in object manipulation experiments [136]. In other words, the task-relevant networks reflected how muscles 'work together' both redundantly and synergistically towards a desired end-goal state whilst, in parallel, continually controlling the present trajectory of the system. Meanwhile, the task-irrelevant networks demonstrated that these muscle couplings also work concomitantly towards lower-level objectives assigned mostly during the transition to this desired end state. Although distinguishing task-irrelevant muscle couplings may capture artifacts such as EMG crosstalk, our results convey several physiological objectives of muscles including gross motor functions [137], the maintenance of internal joint mechanics and reciprocal inhibition of contralateral limbs [124, 51]. Thus, task-irrelevant muscle interactions reflect both biomechanical- and task-level constraints that provide a structural foundation for task-specific couplings. The separate quantification of these muscle interaction types opens up novel opportunities in the practical application of muscle synergy analysis, as demonstrated in the current study through the identification of a significant predictor of motor impairment post-stroke from single-trials [16, 19, 18]. For instance, these distinct representations may encapsulate different neural substrates that can be specifically assessed at the muscle-level for the purpose of bodily restoration and augmentation [138]. Uncovering their neural underpinnings is an interesting topic for future research.

Indeed, in future work, we aim to complement this study's combinatorial perspective to the muscle synergy by dissecting the unique contribution of individual muscles to motor behaviour and how they may work independently towards task performance (see magenta and cyan intersections in fig.1.3(B)). More broadly, our work here parallels related information-theoretic approaches to decomposing task-relevant brain activity [126, 57], whilst addressing a current research gap across the neurosciences in effective methods to mapping large-scale, spatiotemporal neural activity to behaviour [133, 11]. Future applications of this framework should include large-scale, multi-modal data captured from participants performing a wide range of natural behaviours.

In sum, this study introduced a novel perspective to the muscle synergy concept and a computational framework to extract muscle couplings that map their pairwise contributions to motor behaviour. We suggest that this approach offers novel research opportunities for investigating the underlying neural constraints on motor behaviour and the fundamental structure-function relationships generated by agent – environment interactions [21, 139].

3.5 Materials and Methods

Quantifying muscle couplings in the task space

To quantify muscle couplings we used MI, a non-linear measure of dependence that captures any type of relationship between random variables. Here to estimate MI, we used a Gaussian copula-based approximation [59]. This semi-parametric estimator exploits the equivalence between MI and the negative entropy of the empirical copula (c), a function that maps a multivariate set (e.g. $[m_x, m_y]$ representing activities of muscles X and Y) to their joint distribution (Equation 1.1) [59].

$$I\left(m_x; m_y\right) = -H(c) \qquad \text{Equation 1.1}$$

Thus, to determine task-irrelevant muscle couplings ($I\left(m_x; m_y|\tau\right)$), we conditioned the negative entropy of the empirical copula for $[m_x,\ m_y]$ with respect to a task variable τ (Equation 1.2). As mentioned, $[m_x,\ m_y]$ are continuous vectors composed of individual muscle amplitudes at specific timepoints across trials while τ is a corresponding discrete (e.g. movement direction for datasets 1 and 2) or continuous (e.g. movement kinematics in dataset 3) task parameter. For discrete task variables, τ takes one value for each trial and the MI is calculated across trials using a Gaussian mixture model [59]. In the case of continuous task variables, τ varies in time within a specific trial. Thus, we compute MI at each timepoint *t* using the muscle activity $m_x(t)$

and the task variable value $\tau(t)$ at this time point using a closed-form parametric estimator [59].

$$I\left(m_x; m_y|\tau\right) = -H(c|\tau) \qquad \text{Equation 1.2}$$

To evaluate the task-relevance of the identified muscle couplings, we used a higher-order information theoretic measure known as co-information (co-I) (Equation.1.3) (fig.11), which quantifies the relationship between three random variables, here $[m_x, m_y]$, and τ. Co-I implements the inclusion-exclusion principle of combinatorics [125], whereby the sum of MIs between individual m vectors and τ ($I\left(m_x;\tau\right) + I\left(m_y;\tau\right)$) is compared against their composite MI ($I\left(m_x, m_y;\tau\right)$) as follows:

$$-I\left(m_x; m_y;\tau\right) = I\left(m_x;\tau\right) + I\left(m_y;\tau\right) - I\left([m_x, m_y];\tau\right) \qquad \text{Equation 1.3}$$

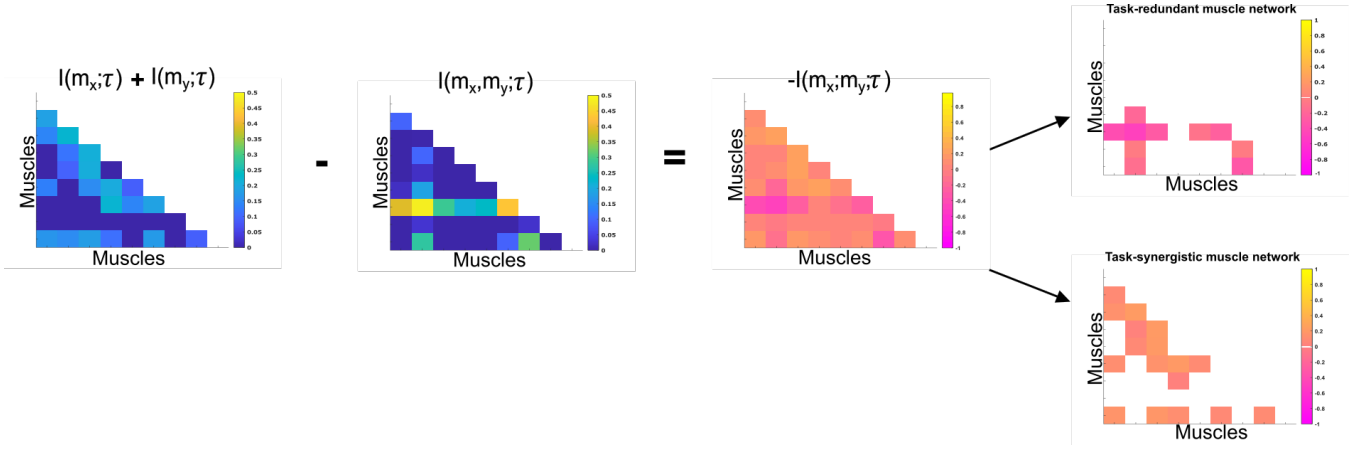

Fig.13: Co-I determines the difference between the sum total information shared with τ *in* m_x *and* m_y when observed separately and the information shared with τ when they are observed together. The adjacency matrices show how this calculation is carried out for all unique $[m_x, m_y]$ combinations. Redundant and synergistic muscle couplings are then separated into two equivalently sized networks. The accompanying colour bars indicate the values present in the adjacency matrix.

Negative $I\left(m_x; m_y;\tau\right)$ corresponds to a net redundant coupling between $[m_x,\ m_y]$ about τ while positive $I\left(m_x; m_y;\tau\right)$ indicates a net synergy. To analyse these distinct couplings separately, we parsed redundant and synergistic $I\left(m_x; m_y;\tau\right)$ into two equivalently sized matrices and rectified the redundant couplings to make them suitable for non-negative dimensionality reduction.

Then, to produce a multiplexed view of the muscular interactions across trials, we iterated these MI computations over all unique combinations of $[m_x,\ m_y]$ and τ. The resulting MI estimates collectively form A, a symmetric adjacency matrix (i.e. $A^T A = I$) that represents the functional connectivities between all muscle activations (fig.10). When repeated across all available task variables τ and participants, A is of dimension [$No.\ of\ muscle\ pairs$ x $No.\ of\ timepoint\ pairs$ x $No.\ of\ \tau$ x $No.\ of\ participants$]. Thus, by applying network-theoretic statistical tools to A, we can identify functional modules carrying the same type of (redundant/synergistic) task information (fig.2(B)).

Estimating the statistical significance of muscle couplings

To isolate statistically significant dependencies, we applied a modified percolation analysis to each A [66]. This method sparsifies functional connectivities in A with respect to its percolation threshold (P_c). P_c is a critical value that specifies the probability of a nodes' occupation in A with respect to the networks size. In random networks, a '*giant component*' comprised of long-range connections exists above P_c but disappears as P_c tends to zero [119], while it is thought that living systems optimise adaptability by fluctuating around P_c in a state of self-organised criticality [120]. Preliminary testing of this method showed it to be at least equivalent to permutation-testing each MI value in the network and thus, much more computationally efficient. P_c was therefore iteratively specified for each layer of A relative to equivalently sized random networks and utilised to remove insignificant network edges up to a stopping-point where this giant component begins to become affected (fig.3(C)). This procedure was carried out for each layer of A separately configured as muscle-wise couplings across temporal scales (i.e. a 3-D tensor of dimension [$No.\ of\ muscles$] x [$No.\ of\ muscles$] x [$No.\ of\ timepoint\ pairings$ x $No.\ of\ \tau$ x $No.\ of\ participants$]) and vice versa as timepoint-wise couplings across spatial scales (fig.3(D)). The separate sparsification of each individual network layer in both alternative network configurations produced discrepancies in the output, as some connections were found to be significant in only one domain. To ameliorate this discrepancy, we employed a conservative heuristic where dependencies must be significant in both space and time to be included in the final input matrix for dimensionality reduction. Thus, the sparsified input matrices to dimensionality reduction were comprised of significant spatiotemporal task-redundant, -synergistic or -irrelevant muscle couplings.

Model-rank specification

To determine the optimal number of modules to extract, we implemented two alternative community detection algorithms generalised to multiplex networks [72, 71, 121]. Both forms seek to optimise a modularity criterion known as the Q-statistic that quantifies the proportion of within-community network edges compared to what would be expected from a network consisting of random connections [67]. More specifically, for a particular division of a single layer network (Equation 2.1), let $\delta(g_i, g_j)$=1 if node i and j belong to the same group (g) and 0 otherwise and A_{ij} be the number of edges between node i and j. The equivalent of A_{ij} from a randomised network (P_{ij}) is expected to be $\frac{k_i k_j}{2m}$ (Newman-Girvan null model) [67], where k_i and k_j are the node degrees and $m = \frac{1}{2}\sum_{ij} A_{ij}$. The typical output of the Q-statistic is found within the range [0,1] with 1 indicating maximum modularity [67].

$$Q_{monolayer} = \frac{1}{4m}\sum_{ij}\left(A_{ij} - P_{ij}\right)\delta(g_i, g_j) \qquad \text{Equation 2.1}$$

In its generalised multilayer form, the Q-statistic is given an additional term to consider couplings between layers l and r with intra- and inter-layer resolution parameters γ and ω (Equation 2.2). Here, μ is the total edge weight across the network and γ and ω were set to 1 in the current study for classical modularity [71], thus removing the need for any hyperparameter tuning.

$$Q_{multilayer} = \frac{1}{2\mu}\sum_{ijlr}\left[\left(A_{ijl} - \gamma_l P_{ijl}\right)\delta_{lr} + \delta_{ij}\omega_{jlr}\right]\delta(g_{il}, g_{jr}) \qquad \text{Equation 2.2}$$

We chose to implement two complementary model-rank specification approaches to address limitations related to stochasticity and scalability present in the multilayer formulation and the inability to consider inter-layer dependencies present in the monolayer formulation [52, 122]. To apply these algorithms to our data, we grouped the set of A into multiplex networks configured with respect to spatial or temporal scales (fig.3(D)). We then applied these algorithms to both space-time network configurations for individual participant/tasks. This procedure generated a binary adjacency matrix from the resulting community partition vector in each case where 1 indicated the nodes belonged to the same community and 0 otherwise [121]. Following a consensus-based approach [112], we then grouped these binary adjacency matrices into a new multiplex network and re-applied the two alternative community detection algorithms to find an optimal spatial and temporal model-rank.

Extraction of low dimensional representations

Following the specification of an optimal model-rank in the spatial and temporal domains, we used these values as input parameters into dimensionality reduction (fig.3(E)). To extract a low-dimensional representation of motor behaviour across muscle couplings, we applied a sample-based non-negative matrix tri-factorisation method (sNM3F) with additional orthogonality constraints to the matrices consisting of vectorised and concatenated A [23]. More specifically, we decomposed the input three-mode tensor A of dimension [K = No. of unique muscle pairs (m) x (L = No. of time-sample pairs (t) x No. of participants + tasks)] into a set of spatial (V) and temporal (W) factors and the participant- and task-specific weighting coefficients (S) reflecting the amount of information carried by each combination of spatial-temporal factors for each participant and task parameter (Equation 3.1). In equation 3.2, this factorisation is also illustrated in vector sum notation for a single participant and task variable:

$$A \approx WSV \qquad \text{Equation 3.1}$$

$$\begin{pmatrix} (m^1 t^1) & \cdots & (m^1 t^L) \\ \vdots & \ddots & \vdots \\ (m^K t^1) & \cdots & (m^K t^L) \end{pmatrix} \approx \begin{pmatrix} \mathbf{w}_i^{t^1} & \cdots & \mathbf{w}_i^{t^L} \end{pmatrix} \bullet \begin{pmatrix} s_{v_1}^{w^1} \cdots s_{v_j}^{w^1} \\ s_{v_1}^{w^i} \cdots s_{v_j}^{w^i} \end{pmatrix} \cdot \begin{pmatrix} \mathbf{v}_j^{m^1} \\ \vdots \\ \mathbf{v}_j^{m^K} \end{pmatrix} + residuals \qquad Equation\ 3.2$$

Examining the generalisability of extracted representations

To determine the generalisability of the extracted space-time muscle networks, we implemented a representational similarity analysis where we compared representations extracted from the full dataset 1-3 to equivalent networks extracted from a subset of the respective datasets. We computed the similarity between pairs of representations using Pearson's correlation.

For dataset 1 and 2 (see below), we removed from the input data an individual participant or task at a time and compared the similarity of the decomposition outputs with those obtained from the full dataset. We repeated this for all participants and task variables and reported the average similarity as a measure of robustness of the decomposition.

For dataset 3 (see below), due to the greater number of participants and task parameters, we implemented a more stringent examination. More specifically, we firstly extracted representations from each task space individually and, using these representations as a reference, compared them against functionally similar outputs after removing randomly sized portions of randomly selected vectors in the input data (up to the no. of column vectors - 1). We repeated this procedure for 50 itera-

tions, and computed summary statistics by converting the coefficients to Fisher's Z values, computing the average and standard deviation, and then reverting these values back to correlation coefficients.

Subnetwork analysis

To illustrate the relative importance of individual muscles within each network, we determined the total communicability ($C(i)$) of individual nodes (i) in each network (A). $C(i)$ is defined as the row-wise sum of all matrix exponentials (e) in the adjacency matrix (A) that consider the number of walks between each pair of nodes i and j (Equation 4.1) [116, 140]:

$$C(i) = \sum_{j=1}^{N} \left[e^{A}\right]_{ij} \qquad \text{Equation 4.1}$$

To emphasise salient functional connectivities in the spatial networks, we sparsified all dependencies with a below average network communicability and illustrated the output on the accompanying human body models [81, 140]. To uncover salient subnetwork structures consisting of more closely functionally related muscle activations, we applied the monolayer community detection algorithm in equation 2.1 to the extracted spatial networks [72, 79].

Data acquisition and processing

To illustrate our framework, we applied it to three datasets of EMG signals recorded during different motor tasks. In dataset 1 (fig.4(A)), 7 adult participants (age: 27 ± 2 years, height: 1.77 ± 0.03 m) performed table-top point-to-point reaching movements in both forward and backwards directions and at fast and slow speeds while the activity of nine muscles on the preferred right, reaching arm (finger extensors (FE), brachioradialis (BR), biceps brachii (BI), medial-triceps (TM), lateral-triceps (TL), anterior deltoid (AD), posterior deltoid (PD), pectoralis major (PE), latissimus dorsi (LD)) were captured for a total of 640 trials per participant [23]. To enable the quantification of shared information across muscles with respect to specific task attributes, we formulated four discrete task parameters of length equal to the number of trials executed. These discrete variables represented the trial-to-trial variation in reaching direction (fwd vs bwd), speed (high vs low), and reaching target [P1-P8] (fig.3(A)).

In dataset 2 (fig.4(B)), 3 participants performed whole-body point-to-point reaching movements in various directions and to varying heights while EMG from 30 muscles (tibialis anterior, soleus, peroneus, gastrocnemius, vastus lateralis, rectus femoris, biceps femoris, gluteus maximus, erector spinae, pectoralis major, trapezius, anterior deltoid, posterior deltoid, biceps and triceps brachii) across both hemi-bodies were captured [82]. Like dataset 1, we formulated task parameters each representing a specific task attribute across trials (~2160 trials per participant). In this case, we formed eight discrete task parameters representing start- and end-point target, -bar, and -height and both up-down (vertical) and left-right (horizontal) reaching directions.

Dataset 3 consisted of multiple trials from 17 participants performing level-ground walking, stair- and ramp-ascents/descents with various sub-conditions (walking speed, clockwise/counter-clockwise direction, different stair/ramp inclines etc.) (fig.4(C)) [113]. These locomotion modes were performed while 11 EMG signals were captured from the right lower-limb (Gluteus medius (GlutM), right external oblique (Obl), semitendinosus (ST), gracilis (GR), biceps femoris (BF), rectus femoris (RF), vastus lateralis (VL), vastus medialis (VM), soleus (SO), tibialis anterior (TA), gastrocnemius medialis (GM)), XYZ coordinates were captured bilaterally from 32 kinematic markers and 4 IMUs and a force-plate captured accelerations and dynamic features among the lower-limbs also. More detailed breakdowns of the experimental design for each dataset can be found at their parent publications [23, 82, 113].

For all datasets, we processed the EMG signals offline using a standardised approach [43]: the EMGs for each sample were digitally full-wave rectified, low-pass filtered (Butterworth filter; 20 Hz cut-off; zero-phase distortion), normalised to 1000 time-samples and then the signals were integrated over 20 time-step intervals yielding a waveform of ~50 time-steps. To match the time-series lengths, we resampled the kinematic, dynamic and IMU recordings of dataset 3 using cubic-spline interpolation to match the EMG signals.

Data Availability

Data from datasets 1 and 2 is available on reasonable request. Data from datasets 3 and 4 are freely available as online [113, 114]. The matlab codes to implement the proposed framework are available here: `https://github.com/DelisLab/EMG2Task`.

Chapter 4

Quantifying the diverse contributions of hierarchical muscle interactions to motor function

O'Reilly D, Shaw W, Hilt P, de Castro Aguiar R, Astill SL, Delis I. Quantifying the diverse contributions of hierarchical muscle interactions to motor function. bioRxiv. 2023 Dec 1:2023-11.

4.1 Abstract

The muscle synergy concept suggests that the human motor system is organised into functional modules comprised of muscles '*working together*' towards common task-goals. However, recent innovative work has added further nuance to this idea, showing how muscles may also work together towards functionally different and independent task-goals, representing crucial attributes of flexible motor behaviour. Here we probed this proposed functional neural architecture by building upon an established theoretical framework to characterise distinct types of muscle interactions, i.e. functionally similar, complementary and independent, across scales. Through a novel application of the Partial Information Decomposition to large-scale muscle activations, we unveiled complex networks of inter- and intra-muscular interactions with distinct functional roles as well as independent muscle contributions to task performance. We showcased the effectiveness of this approach by extracting hierarchical and functionally diverse motor components that were a) generalisable across participants and tasks and b) predictive of balance performance across trials and of differences in motor variability between young and older adults. In aligning muscle synergy analysis with the forefront of understanding on human movement modularity, our findings suggest the proposed methodology can offer novel biological insights into the neural control of movement and research opportunities towards health and engineering applications.

4.2 Introduction

Hierarchical modularity is a ubiquitous characteristic of complex living systems such as the human nervous system [68, 3]. The constituent parts (i.e. individual neurons, muscles etc.) at each level interact in a goal-directed manner [141], forming functionally specialized modules that cooperate towards common task-goals. The putative interactions within these modules include a common selectivity (i.e. redundancy) for task information along with unique contributions by individual parts to the processing of task information. To exemplify this point in the context of motor control, in seminal work Ivanenko and colleagues noted: "*... We can think of (*electromyographic*) EMG waveforms as being dependent on two aspects. First, there are some underlying common waveforms shared by the muscles. Second, each muscle also captures a unique aspect of activation that is not addressed by any other muscle"* [22]. However, for a set of muscle activity patterns to form an emergent whole (i.e. a coordinated movement), the integration of redundant and unique muscle constituents in the form of cross-module, synergistic muscle interactions is necessary. Synergistic interactions combine information across functionally heterogeneous modules, therefore serving as important channels of communication for the integration of information in the nervous system [131, 66]. The complementary information generated by these interactions is super-additive, emerging from the union of lower-level constituents [142]. Indeed, from a more coarse-grained view, these emergent functional modules themselves, through hierarchies of complementary interactions [143], form parts of greater wholes (i.e. submodules-within-modules) [144].

Motor control research, has focused primarily on deciphering how the many redundant degrees-of-freedom of the human body are coordinated for everyday tasks [31, 15]. This avenue of research uses the '*muscle synergy*' as a guiding concept [105, 8], where the cohesive interactions between groups of muscles ('*muscle synergies*') map to common task-goals, and in doing so simplify movement execution. This definition of synergy hinges on covariations between muscles and is distinct from the information-theoretic based description we have previously provided. To avoid confusion in the use of the synergy term, here we refer to muscle covariations as couplings or interactions and, based on our framework presented below, we separate these further into "redundant" (i.e. functionally similar) and "synergistic" (i.e. functionally complementary) types of interaction. Thus, unlike the traditional definition of synergy in motor control [105], here synergy is a specific type of muscle interaction where muscles cooperate towards different, complementary aspects of task performance. This distinction in muscle interaction types is inspired by recent influential works suggesting that a more nuanced functional architecture underlies human motor control [50, 52, 51, 134]. For instance, anatomically proximal musculature thought to have equivalent task efficacy have, in fact, demonstrated a partial decoupling and sharing of common drive with distal musculature [50, 52]. Moreover, the identification of independent functional modules indicates that multiple sources of common drive are present in the muscle space [134]. Altogether, this recent perspective proposes that functional modularity exists both between and within muscles, simplifying the control of movement by enabling the flexible compliance of muscles towards multiple task-objectives [37]. It also integrates independent muscle control as a fine-grained control mechanism into the conceptual perspectives on course-grained motor control, importantly broadening the context of human movement modularity for the research field. It is therefore prescient for the field to develop new analytical approaches to comprehensively understand human movement modularity from this novel perspective. Hence, an objective of this study is to specifically address this research gap by providing a bridge between theoretical and computational frameworks within the motor control field.

In [145], we addressed this research gap by proposing a computational framework that dissects task information into task-irrelevant (i.e. present across all tasks), -redundant (functionally similar) and -synergistic (functionally complementary) muscular interactions. In doing so, we aligned current analytical approaches with this novel perspective of flexible motor control. However, the separate quantification of the task-relevant information that is not shared or complementary between muscles (i.e. provided uniquely by a muscle), is not possible using current analytical approaches. Intuitively, this task information encodes the functionally independent muscle activations that contribute uniquely to task performance, generated potentially by both central and peripheral sources [22, 37, 146]. Although independent motor control mechanisms are well-established and can improve with training [147, 36], the inclusion of this attribute in recent theoretical work marks a significant departure from traditional perspectives [37]. Thus, here we will address an important current research gap by developing a methodology for the comprehensive quantification of unique task information in the muscle space.

A second consideration we address here concerns the coverage given by the muscle synergy concept to the contribution of whole muscle groups, rather than individual muscles, towards task-objectives. The motor redundancy problem motivating this concept describes how common neural inputs map to the task space through inter-muscular components [8]. However, the end-effectors of this mapping operation are in fact individual muscles with their own unique anatomical attachments and activation timings [51, 148], thus, as recognized by several lines of recent research [144, 52, 37, 149], the muscle group may not be the smallest unit of modular control. Only more recently has the muscle synergy concept been formally applied at the intramuscular level [149], revealing that intramuscular synergies are independent of the muscles' compartmentalized structure and may be complementary to inter-muscular analyses as a window into the neural control of movement [150, 151].

In the current study, through a principled methodology, we aimed to probe the hierarchically structured functional architecture

of the motor system, revealing salient features of movement modularity at multiple scales. To this end, we built upon traditional approaches by directly including task parameters during muscle synergy extraction but here, as a first for the field, by employing a partial information decomposition (PID) (Fig.1.1). With this novel implementation into an established pipeline (Fig.1.2), we can separately quantify redundant, synergistic, and unique task information. Intuitively, synergistic information (orange shaded area (Fig.1.1) and orange bar (Fig.1.2)) is the information shared by a given muscle pair ($[m_x, m_y]$) about a task parameter (τ) that can only be gained by observing m_x and m_y together. On the other hand, redundant information (pink intersection (Fig.1.1)) and pink bar (Fig.1.2)) is the task information shared by m_x and m_y that can be found in either alone. Finally, unique information (magenta and cyan intersections and bars in fig.1.1-2 respectively) is the task information provided by either m_x or m_y that is not found in the other.

Towards this aim, we applied the framework to three datasets of human movement (whole-body reaching – Dataset1, balancing on a balance board – Dataset2 and an object lifting task – Dataset3), revealing generalizable patterns of diverse task information processing both between and within muscles that encode distinct features of motor behavior. To supplement the work presented here, we provided Matlab code for readers to apply this framework to their own data: `https://github.com/DelisLab/Muscle_PID`.

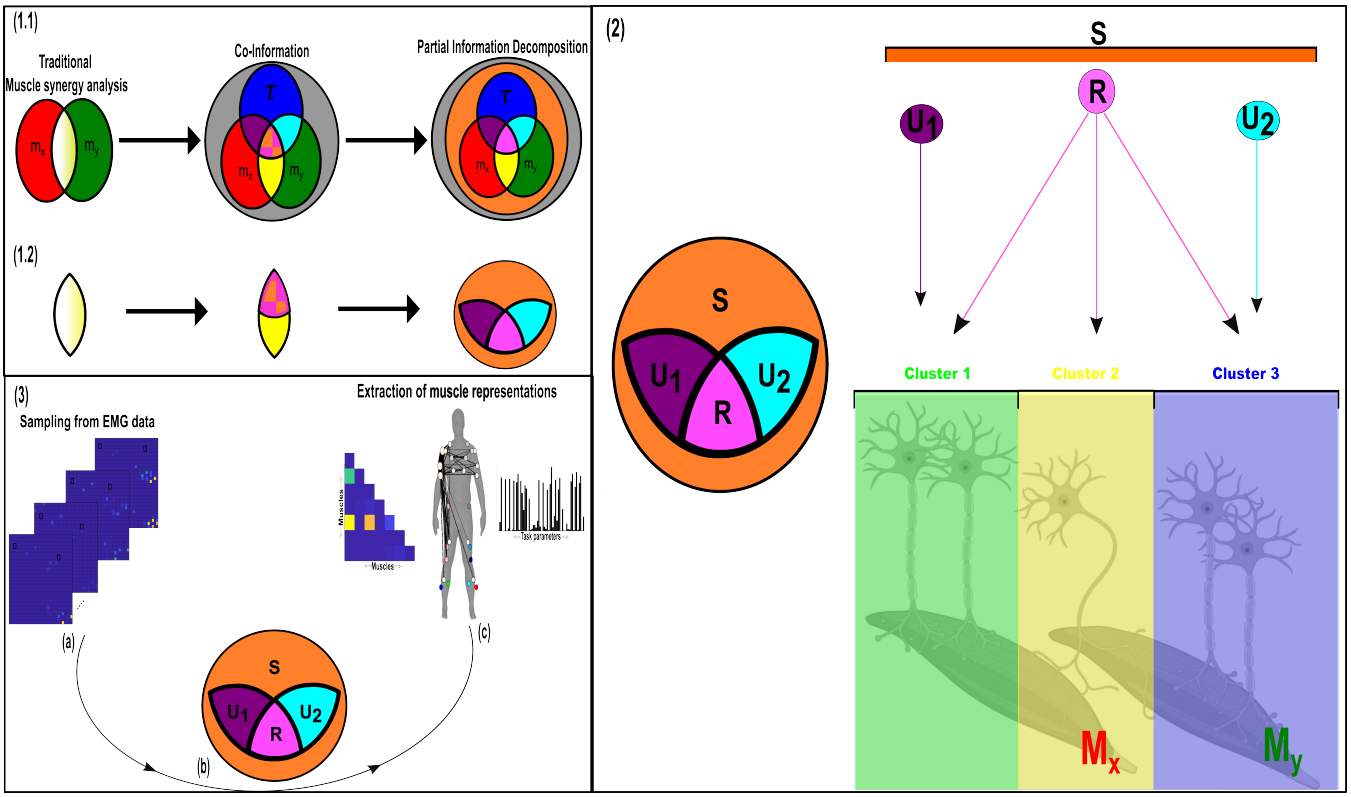

Fig.1: **(1.1)** Building on traditional muscle synergy analysis based on dimensionality reduction and a recent computational framework introducing an information-theoretic measure of net redundancy/synergy (pink-orange intersection) known as Co-Information [125], here we introduce Partial Information Decomposition (PID) [152], to more comprehensively quantify and functionally characterize muscle interactions. **(1.2)** The underlying premise of this framework builds on current approaches that quantify muscle covariations as shared variability and our previous work that dissects the task-relevant information from the task-irrelevant information (yellow intersection) and characterizes it as either functionally redundant (pink shading) or synergistic (orange shading) [145]. By employing PID, here we introduce the novel capability of separately quantifying redundant (pink intersection), synergistic (orange shaded area) and unique information (magenta and cyan intersections) from the information a given muscle pair ($[\mathbf{m_x}, \mathbf{m_y}]$) shares about a task parameter (τ). **(2)** This innovation aligns with recent theoretical developments on movement modularity by enabling the principled decomposition of their shared information into four non-negative quantities representing the functionally redundant, ($\mathbf{R}$), synergistic ($\mathbf{S}$) and unique ($\mathbf{U_1}$,$\mathbf{U_2}$) informational components at both inter- and intra-muscular scales (cluster 2 and both 1 and 3 respectively) [37]. **(3)** An overview of the proposed framework. (**a**) EMG data along with corresponding task parameters are recorded from human participants performing naturalistic movements. (**b**) PID is applied to all $[m_x, m_y]$ and τ combinations, with the resulting information atoms then input into an established pipeline [145, 107]. (**c**) The output of this framework is low-dimensional components consisting of pairwise dependencies between muscles and their task- and participant-specific activations.

4.3 Results

Our primary aim here is to probe the functional architecture of the motor system by establishing a principled method for quantifying task-redundant, -synergistic and unique informational dynamics underlying motor behavior. To achieve this, we firstly develop a novel computational framework and apply it to pairs of EMG signals across time ($[m_x,\ m_y]$) and a corresponding, continuous task parameter (τ) (e.g. kinematics, dynamics etc.) (see '*Quantifying functionally diverse muscular interactions*' section in the Materials and methods) [152]. The basic premise behind this approach is that the direct mapping of muscle interactions to task performance is crucial for understanding and principally quantifying their functional underpinnings. Unlike current approaches which first identify muscle couplings and then relate them to task performance, our proposed methodology first quantifies the task information carried by each muscle activation and then builds networks of common task information across muscles. The proposed Partial Information Decomposition (PID) framework parses the effects on τ by a pair of muscle activations ($[m_x,\ m_y]$) into four separate atoms of information (i.e. task-redundant (R), -synergistic (S) and two unique information components (U_x and U_y)) by decomposing their joint mutual information (JMI). R is the predictive information between $[m_x,\ m_y]$ about τ that can be found in either alone (sub-additive task information), encapsulating the portion of the $[m_x,\ m_y]$ pairing that has a similar functional consequence. S on the other hand, is the predictive information provided by $[m_x,\ m_y]$ about τ that is produced only when m_x and m_y are observed together (super-additive task information), capturing the functional complementarity within the interaction. Finally, U_x and U_y is the predictive information within $[m_x,\ m_y]$ about τ that is only present in m_x or m_y alone, capturing the unique contributions of the individual muscles within the functional interaction (e.g. m_x predicts a 'L' result in irrespective of the state of m_y and vice versa for predicting an 'R' outcome (Fig.2)). Thus, in contrast to the traditional conception of muscle synergies as co-variations across muscles, here instead we firstly extract shared task information between individual muscles, decompose each muscle interaction into the different types of functional muscle covariation (see Fig.2), and then finally determine common patterns of functional interactions across the muscle network (see Fig.3).

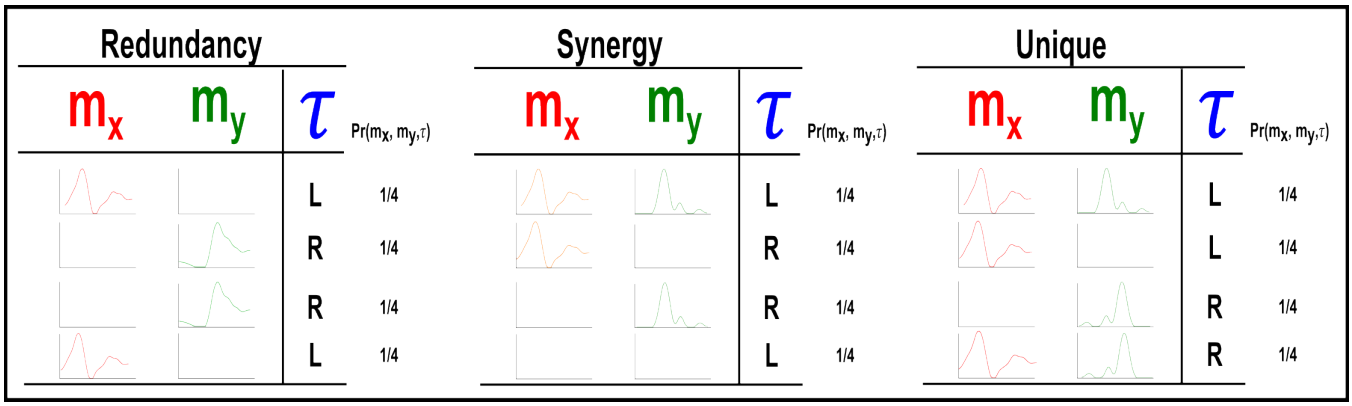

Fig.2: A toy simulation demonstrating how redundant, synergistic, and unique task information can be interpreted from the application of the PID approach to the muscle space. Four observations of a given muscle pair (m_x and m_y) that can fall into two equiprobable on and off activation states and a corresponding task parameter (τ) describing left (L) or right (R) movement direction. Observing either m_x or m_y in the redundancy example gives 1 bit of information while observing both m_x and $_y$ together only in the synergy example gives 1 bit of information. Turning to the unique information example, when m$_y is active in a specific way, it predicts a R outcome irrespective of the state of m_x$ and vice-versa. Thus, both m_x and m_y each provide task information that cannot be found in the other. In summary, the PID approach enables the principled quantification of all types of functional relationships between muscles, including similar, complementary and independent interactions.

Following this decomposition, we then ran these separate PID atoms through an established pipeline [145, 107], referred to as the Network-Information framework (NIF) (Fig.3(A-E)) (see Materials and methods for detailed breakdown). The purpose of the NIF is to produce functionally and physiologically relevant and interpretable low-dimensional components of muscular interactions underlying coordinated movements. The following briefly summarizes the main steps of the pipeline:

1. To produce a comprehensive network of functional muscle interactions, we applied the PID framework over all unique $[m_x,\ m_y]$ and τ combinations for each participant (Fig.3(B)). This iterative procedure results in a multiplex network, with each layer consisting of all functional dependencies between muscle pairs for a particular PID atom, τ and participant.
2. To determine the statistically significant interactions, we applied a modified percolation analysis to each layer of the multiplex network (Fig.3(C)) [66].
3. To determine the optimal number of clusters to extract from structurally nested networks, we employed a link-based community detection protocol based on a modularity maximization cost-function (Fig.3(D)) [72, 153].

4. The optimal cluster count was then used as the input parameter into dimensionality reduction, namely a projective non-negative matrix factorization (PNMF) algorithm [63], to extract patterns of muscle connectivity along with their task- and participant-specific activations (Fig.3(E)).

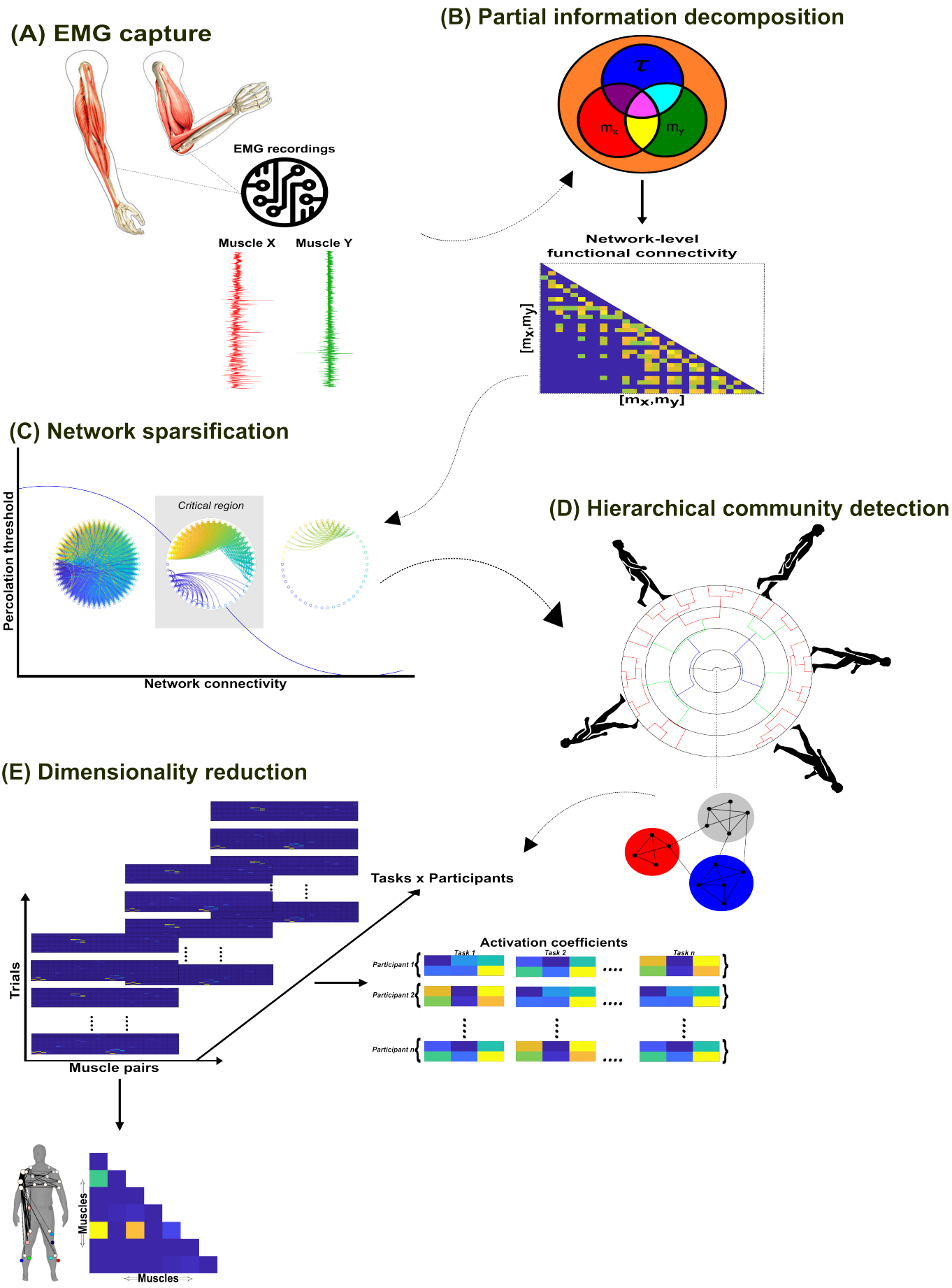
(A) EMG capture
EMG recordings
Muscle X
Muscle Y
(B) Partial information decomposition
τ
mx
my
Network-level
functional connectivity
[mx,my]
[mx,my]
(C) Network sparsification
Critical region
Percolation threshold
Network connectivity
(D) Hierarchical community detection
(E) Dimensionality reduction
Trials
Muscle pairs
Tasks x Participants
Activation coefficients
Task 1
Task 2
Task n
Participant 1
Participant 2
Participant n
Muscles
Muscles

Fig.3: A summarized overview of the NIF pipeline. **(A)** EMG data is captured from human participants performing naturalistic movements. **(B)** The joint mutual information (JMI) between all muscle pair and continuous task parameter combinations is decomposed using the partial information decomposition framework, resulting in separate networks of redundant, synergistic, and unique muscle interactions. **(C)** Each network is sparsified with respect to its percolation threshold, identifying statistically significant functional connections. **(D)** A novel hierarchical community detection essentially unravels and identifies overlapping clusters of network dependencies. **(E)** The optimal number of clusters identified serves as the input parameter into dimensionality reduction, where low-dimensional components of muscular interactions along with task- and participant-specific activations are extracted.

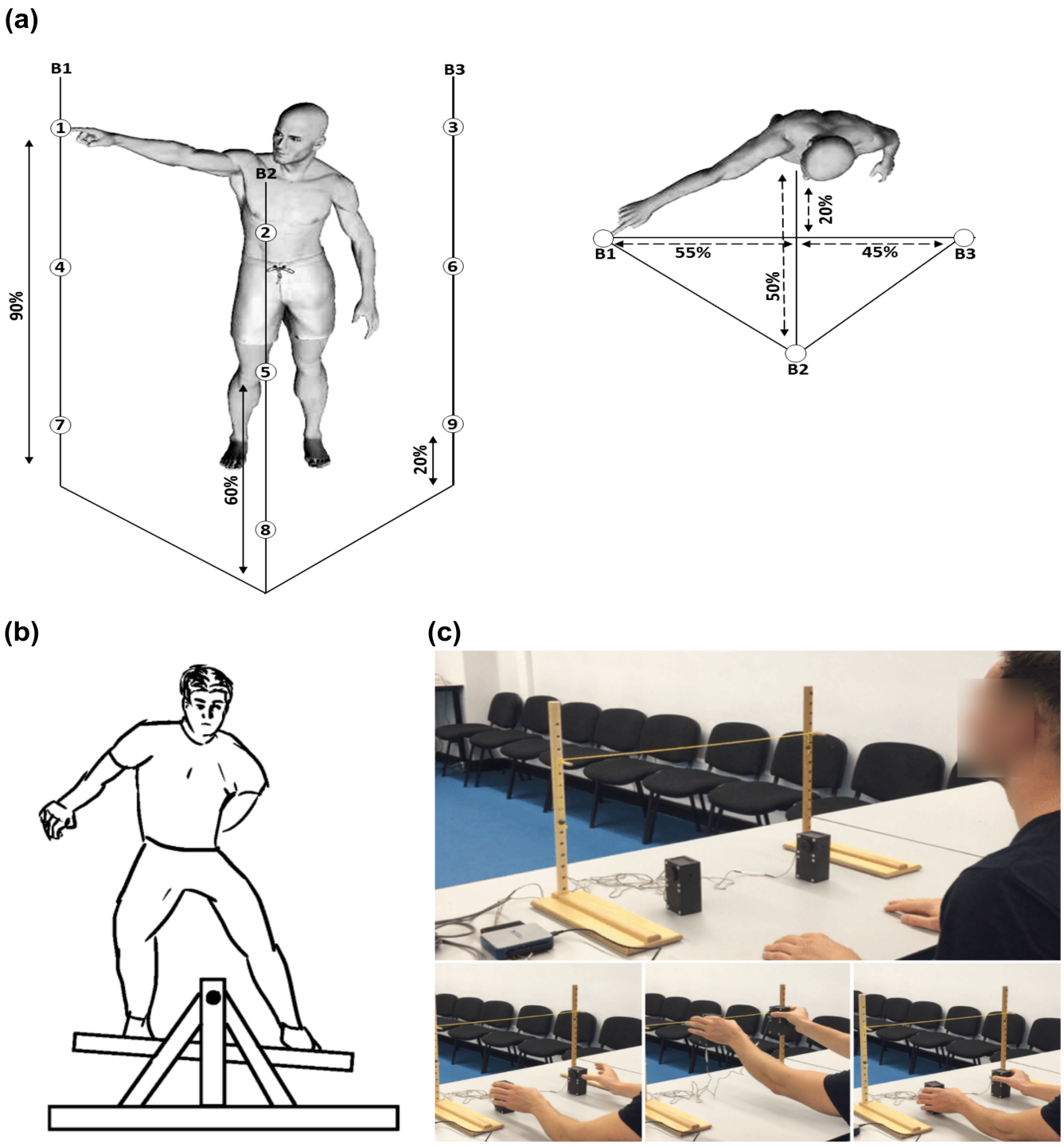

Fig.4: The datasets used in the application of the proposed framework in the current study. **(a) Dataset 1:** Healthy adult participants performed whole-body reaching tasks in various heights and directions while EMG and kinematics were captured across the body [82]. **(b) Dataset 2:** Healthy adult participants performed 10 trials of balancing on a balance board while EMG

was captured among the bilateral lower-limb flexors and extensors simultaneously to the horizontal angular displacement of the balance board. **(c) Dataset 3:** Healthy younger and older adults performed a reach-grasp-lift-hold and replace task of both light and heavy objects while EMG from the arm musculature bilaterally were captured along with load and grip forces on the grasped object [154]. For full details on the experimental setup of these datasets, see *'Data acquisition and experimental conditions'* section of the Materials and methods.

Hierarchical and functionally diverse muscular interactions underlie motor behavior

To demonstrate the proposed PID approach, we present an example output from an application to the EMG recordings of a single participant (across all trials) from Dataset 1 with respect to the reaching finger anterior-posterior kinematic coordinate. This participant was instructed to perform a total of 72 different randomly selected whole-body point-to-point reaching tasks for ~2160 trials (see fig.4(a)) and *'Data acquisition and experimental conditions'* section of the Materials and methods section). In fig.5, we illustrate the redundant (R – 5b), synergistic (S - 5c), and unique (U_x and U_y - 5d) interactions between muscles, as well as their sum total which they are all normalized by, (i.e. JMI -5a). Human body models accompanying each of the JMI, R and S muscle networks illustrate the strongest interactions between muscles (indicated by edge-width) [81], the muscle subnetworks (node color) and the network centrality (a measure of a muscle's relative importance indicated by node size) (see '*Subnetwork analysis'* section of Materials and methods) [72, 79, 116]. The U_x and U_y terms are not considered as a muscle coupling, as they encode the task information present in one muscle that is not present in another and vice versa, and so instead the average unique information (U_{xy}) for each muscle is presented as a bar graph.

The JMI network contains several reaching arm muscles including the anterior- and posterior deltoid and biceps and triceps brachii that form anatomically defined subnetworks (red and blue nodes) with multiple contralateral upper-limb and bilateral lower-limb muscles in the anterior-posterior direction (fig.4(a)). When these dependencies are decomposed into their PID components (fig.4(b-d)), we reveal a more complex functional architecture underlying whole-body reaching movements. These functionally diverse components consist of multiple subnetworks widespread across the body that are driven by prime-mover muscles such as the right biceps brachii and trapezius (fig.4(b-c)). Interestingly, these prime-movers did not contain much unique task information (fig.4(d)), while muscles displaying considerable functional independence did not feature prominently in the redundant and synergistic networks (e.g. right triceps brachii, anterior and posterior deltoid), indicating that the PID approach characterized distinct muscle networks with different functional roles. The structural similarity of redundant and synergistic networks here suggests that across the many trials and reaching tasks of dataset 1, patterns of functional muscle redundancy and synergy converge on a similar network structure, although the magnitudes of these contributions favour synergistic interactions (see Fig.5 adjacency matrices). This finding also provides further evidence towards the basic premise of this framework in mapping muscle interactions to task performance, illustrating the diverse types of functional interaction occurring concomitantly among muscles that links well with emerging findings in the field [50, 52].

Next, to elucidate the functional interactions within muscles underlying whole-body reaching movements, we applied the proposed methodology to pairwise combinations of amplitude signals from six frequency-bands ($[f_x,\ f_y]$) (Delta [0.1-4 Hz], Theta [4-8 Hz], Alpha [8-12 Hz], Beta [12-30 Hz], Low-Gamma (Piper rhythm) [30-60 Hz], High Gamma (Gamma) [60-80 Hz]) (see '*Quantifying diverse muscular interactions in the task space'* and '*Data pre-processing'* sections of the Materials and methods) extracted from the right anterior deltoid muscle. This computation serves as a novel, nonlinear measure of coherence decomposed into its task-relevant informational constituents, which we used here to determine the multifarious effects of $[f_x,\ f_y]$ on the right, reaching finger anteroposterior kinematic (Fig.5). The intramuscular JMI network comprised of a mixture of dependencies between distinct oscillations (Fig.5(a)), most prominently between the Delta-Theta rhythms. When we decomposed their shared task information, the rhythmic activities of the right anterior deltoid presented a more distinguishable encoding of task performance. Gamma amplitudes were functionally similar in their encoding of the finger kinematic with respect to all other frequency bands while a separate Delta-Theta coupling was also had functionally similar consequences (Fig.5(b)). The Piper rhythm comprised of task-synergistic information in the anterior deltoid muscle when coupled with the Theta and Alpha oscillations (Fig.5(c)). Meanwhile, the amplitude of beta oscillations provided the most functionally independent information about the reaching finger kinematic on average, followed by Delta and Theta amplitudes (Fig.5(d)).

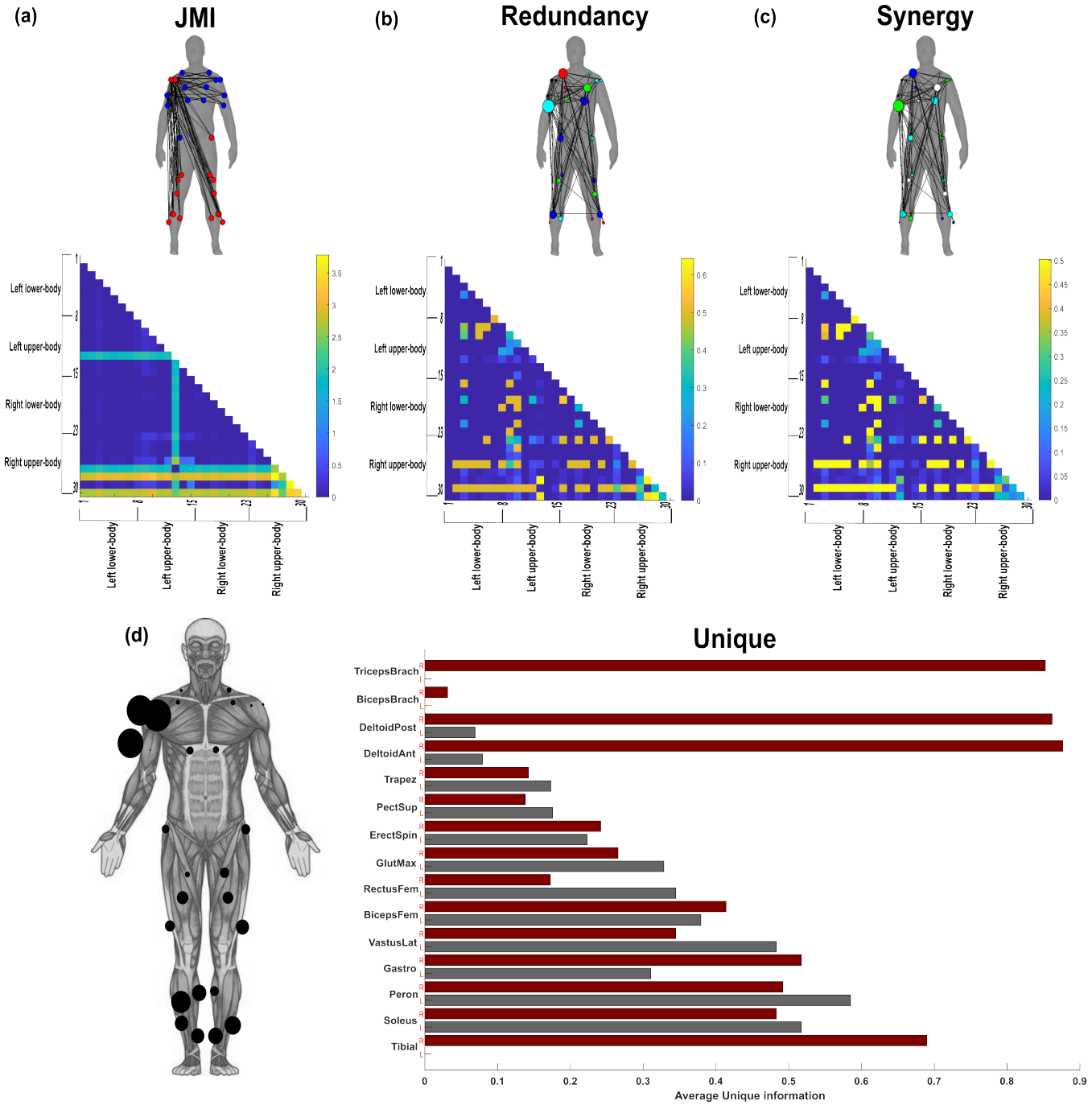

Fig.5: Application of the proposed framework to the intermuscular space of a single participant performing multiple trials of various whole-body reaching tasks (dataset 1). The Joint mutual information (JMI) **(a)** and its informational components**,** redundant **(b)**, synergistic **(c)** and unique information **(d)** were determined with respect to the reaching finger anterior-posterior kinematic coordinate. Values for R, S and U_{xy} were normalised with respect to the presented JMI values [155]. Human body models accompanying each representation in **(a)**-**(c)** illustrate the strongest connectivities (edge-width) [81], the subnetwork community structure (node color) and network centrality (relative node size) [72, 79, 116]. The U_x and U_y terms are not considered as a muscle coupling, as they encode the task information present in one muscle that is not present in another and vice versa, and so instead the average unique information (U_{xy}) for each muscle (left-side=grey, right-side=maroon) is presented as a bar graph. The accompanying human body model to the left illustrates the predominant muscles (black nodes) that encoded unique information about the right, reaching finger kinematic.

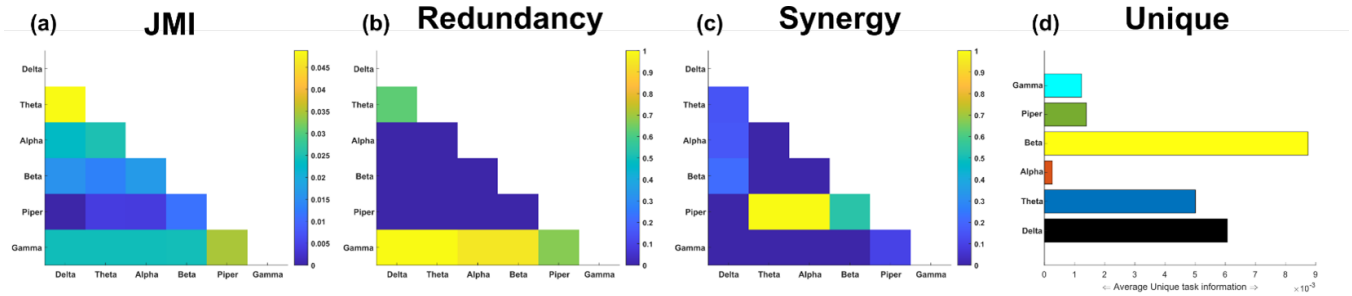

Fig.6: Application of the proposed framework to frequency-specific amplitudes in the reaching side anterior deltoid muscle of a single participant performing multiple trials of various whole-body reaching tasks (Dataset 1). The Joint mutual information (JMI) **(a)** and its informational components**,** redundant **(b)**, synergistic **(c)** and unique information **(d)** were determined with respect to the reaching finger anterior-posterior kinematic coordinate. Values for R, S and U_{xy} were normalised with respect to the presented JMI values [155]. The U_x and U_y terms are not considered as a coupling, as they encode the task information present in one oscillation that is not present in another and vice versa, and so instead the average unique information (U_{xy}) for each frequency-band are presented together as a bar graph.

Generalizable components of functionally diverse inter and intra-muscular interactions

Having demonstrated the presence of the parallel processing of R, S and U_{xy} between and within muscles, we then sought to extract motor components that are generalizable beyond any individual participant and task.

Beginning with intermuscular components, we identified four R and S (R1-R4 and S1-S4) and three U_{xy} (U1-U3) components with respect to the XYZ (anterior-posterior, medio-lateral vertical directions) coordinates of 21 kinematic markers (21 x 3 dimensions = 63 task parameters in total) across the body of three participants performing whole-body reaching movements (>2000 trials each). For brevity here, we provide illustrations of the output in the supplementary materials (Supp. Fig.1-3). To examine the generalizability of these components, we removed an individual task parameter or participant from the input data and then re-extracted the same number of components and computed the average correlation between corresponding components (see *'Examining the generalizability of the extracted components'* section of the Materials and methods). We found an almost perfect concordance between the presented intermuscular components and those extracted from a subset of the data (~0.99 average correlation). The robustness of these components exceeds previous implementations of the NIF [107, 145], where a high level of concordance was also found.

Turning to the intramuscular space, applying the proposed approach within all 30 muscles with respect to 63 kinematic coordinates from the three participants of Dataset 1 revealed four R (R1-R4 (Supp. fig.4)) and three S (S1-S3, (Supp. Fig.5)) and three U_{xy} (U1-U3 (Supp. fig.6)) components. The generalizability of these intramuscular components was proven at the intramuscular level with ~0.99 correlation typically for both individual tasks and participants among R and S networks. A slightly lower concordance among U_{xy} (r=0.9) was found when an individual participant was removed from the input data.

Hierarchies of functional muscle interactions encode distinct motor features

Finally, having quantified diverse types of functional muscle interaction at both inter- and intra-muscular scales, we then investigated the functional relevance of the extracted muscle networks at each of these scales. Specifically, we asked if the identified muscle interactions are predictive of motor performance (balance – Dataset 2) and motor decline with age (object lifting – Dataset 3).

Functionally diverse intermuscular interactions reflect balance performance

To begin with dataset 2, we identified and extracted five R, four S and four U_{xy} intermuscular components. We then used the trial-specific activations from the extracted components for each participant (normalized with respect to their corresponding JMI) to predict motor performance in each trial (i.e. the total balance board error calculated as the sum of absolute deviations from 0 degrees on the horizontal plane of the balance board) (Error) (see '*Salient features of motor performance'* of the Materials and methods section). As multiple observations for the same participant were present within these vectors (n=10 trials each), we determined associations using repeated measures correlation [156], a measure of linear correlation that models participant-specific clustering in the data.

We found two intermuscular interactions (S2 with synergistic couplings between both BF-R and MGN-R, and the left tibialis anterior (TA-L), r=0.64,p=0.000256 and R2 with redundant couplings between the right medial-gastrocnemius (MGN-R) and biceps femoris (BF-R) and BF-R and left rectus femoris (RF-L), r=0.638489,p=0.000256) (Fig.7(A)). Interestingly, muscle couplings representing redundant and synergistic interactions here did not appear prominently in the motor component U4 contributing uniquely to task performance. In contrast, the unique task information in the right rectus femoris (RF-R) and to a lesser extent TA-L (together possibly representing their important roles in crossed-extensor reflex actions) was related to a

significant reduction in Error (r=-0.44, p= 0.019621), i.e. predicting better balance performance (Fig.7(A)).

Functionally similar intramuscular interactions reflect balance performance

Turning to the intramuscular space, we identified and extracted five R and three S and U_{xy} from Dataset 2 and found three of these components significantly correlated with Error across trials (see *Salient features of motor performance'* of the Materials and methods section) (Fig.7(B)). These components all represented redundant amplitude couplings (R2-R4), consisting exclusively of specific coherences between the gamma band and other lower frequency amplitudes (delta and theta in R2, beta and piper in R3 and, alpha in R4), and were negatively correlated with ΣError (i.e. increased involvement of intramuscular modules resulted in improved balance performance, r=-0.454, p=0.0153 for R2, r=-0.509, p=0.005665 for R3, and r=0.415, p=0.0282 for R4).

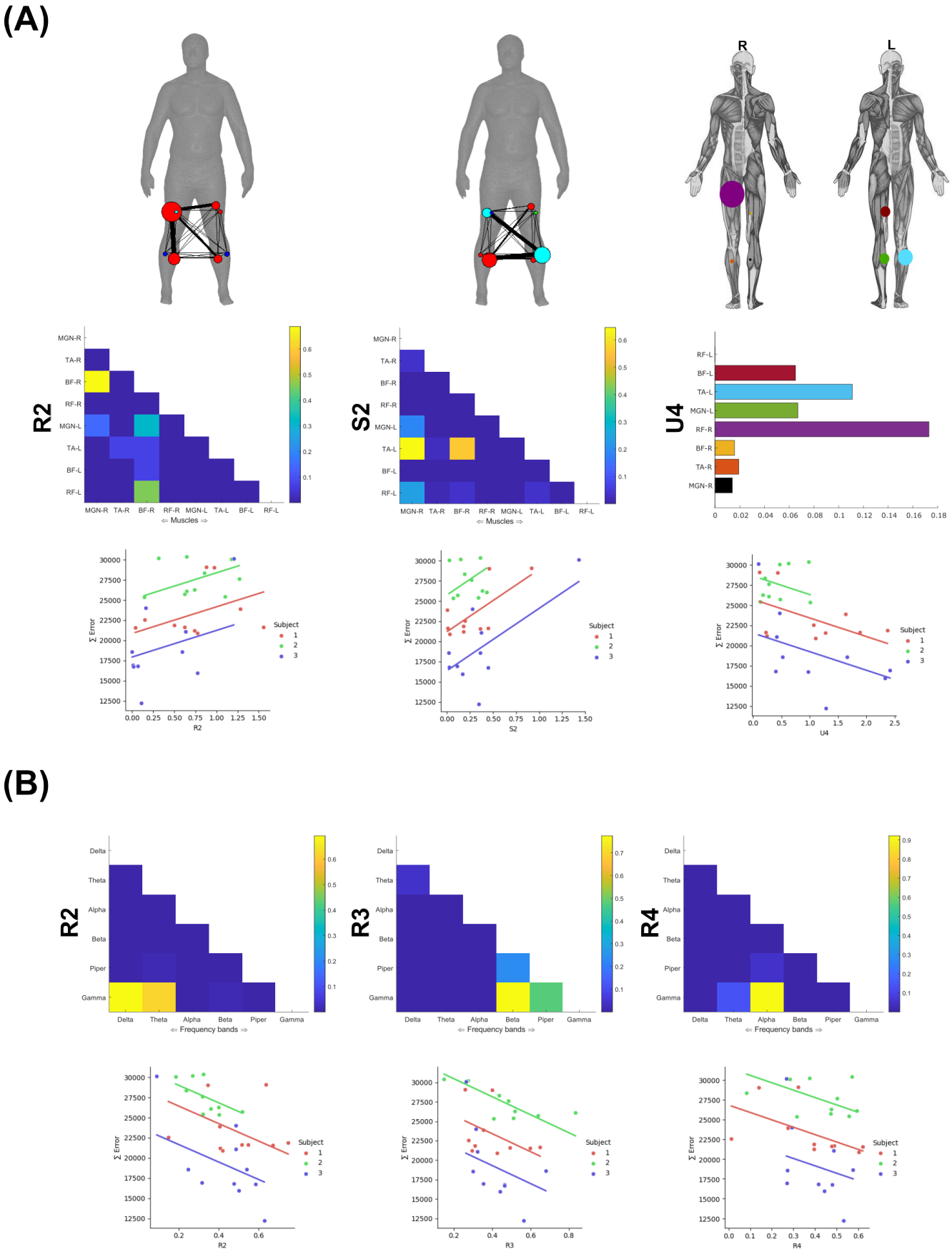

Fig.7:(**A**) The intermuscular components (R2, S2 and U4) determined to have a significant (P<0.05) correlation with balance

performance (Σ Error) across trials in Dataset 2. Top: each adjacency matrix, the human body models illustrate the network structure with relative edge thickness, node size and color reflecting connection strength, importance and sub-modularity respectively[72, 79, 116]. Bottom: Scatterplots illustrating the corresponding repeated measures correlation with balance performance. **(B)** Top: The intramuscular components (R2, R3 and R4) determined to have a significant (P<0.05) correlation with balance performance (ΣError) across trials in dataset 2. Bottom: Scatterplot of the corresponding repeated measures correlation outputs.

The activation variability of a combination of bilateral muscle networks predicts age differences in bimanual object-lifting

Next, we asked which muscle interactions may underpin differences in motor performance resulting from ageing. In the motor control literature, older adults have been shown to exhibit greater motor variability compared to young cohorts [157], leading to behavioral inconsistency. To answer this question, we applied our proposed approach to Dataset 3 [154], consisting of EMG recordings (8 upper-limb muscles bilaterally) from healthy young (N=14) and older (N=18) participants performing a bimanual reach-grasp-hold task of both light and heavy objects (see fig.3(c) and '*Data acquisition and experimental conditions'* section of the Materials and methods).

Applying PID to all pairs of EMG signals to predict the bilateral grip and load forces (i.e. 4 task parameters) the participants exerted, we identified and extracted five R, seven S and three U_{xy} intermuscular components. To investigate how this variability would manifest in the extracted functional muscle patterns, we defined a measure of motor variability in the activation of muscle or frequency couplings (ΣError) and applied it to the extracted components (see *'Salient features of motor performance'* of the Materials and methods section). These vectors were then employed as the predictors in a binary logistic regression model against participants' age group (Young=0 vs. Old=1). This procedure indicated that a combination of the 5$^{\text{th}}$ R (β= -2.12±0.801, p<0.01), 7$^{\text{th}}$ S (β= 1.36±0.704, p=0.053) and 3$^{\text{rd}}$ U_{xy} (β= 0.964±0.445, p<0.05) motor components were optimal in predicting age group (Fig.7(A)), classifying 75% of participants correctly.

The activation variability of a combination of functionally diverse intramuscular rhythms predict age differences in bimanual object-lifting

When applied in the same way to the corresponding intramuscular level of Dataset3, we identified and extracted five R, four S and four U_{xy} rhythmic components. Participants' age group was optimally predicted by a combination of the 4$^{\text{th}}$ R (β= -0.557±0.313, p=0.075), the 2$^{\text{nd}}$ S (β= -11.75±4.6, p=0.011) and the 1$^{\text{st}}$ U_{xy} (β= 1.94±0.982, p<0.05), which classified 84.4% of participants correctly (Fig.7(B)). Taken together, these findings suggest that concomitant increases and decreases in the fluctuations of functionally diverse muscle interactions across scales characterize aging-induced changes in upper limb motor function.

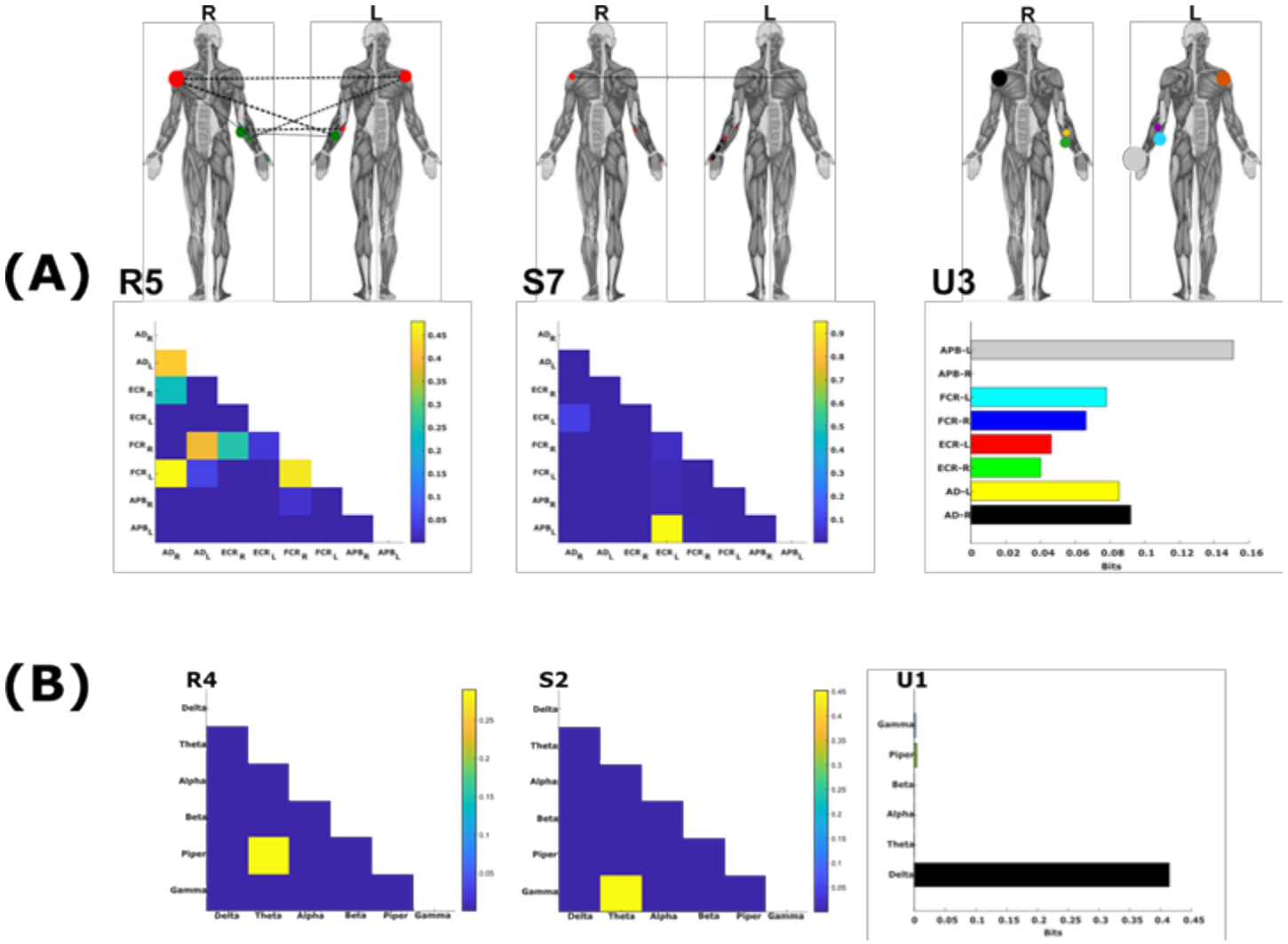

Fig.8: **(A)** The intermuscular components (R5, S7, U3) whose underlying recruitment variability ($\sum Error$) was significantly predictive of participants' age group. All three components formed part of a binary logistic regression model (R5: [β= -2.12±0.801, p<0.01], S7: [β= 1.36±0.704, p=0.053], U3: [β= 0.964±0.445, p<0.05]) and classified 75% of participants correctly. Above the adjacency matrices, human body models illustrate the network connectivity with relative edge width, node size and color representing the connection strength, muscle importance and sub-modularity [72, 79, 116]. **(B)** The intramuscular components (R4, S2, U1) whose underlying recruitment variability ($\sum Error$) was significantly predictive of participants' age group. All three components formed part of a binary logistic regression model (R4: [β= -0.557±0.313, p=0.075], S2: [β= -11.75±4.6, p=0.011], U1: [β= 1.94±0.982, p<0.05]) and classified 84.4% of participants correctly.

4.4 Discussion

In this study, we aimed to quantify and characterize the functional organization of hierarchical muscular interactions. To this end, we proposed a novel approach to muscle synergy analysis that separately and simultaneously quantifies the redundant, synergistic and unique contributions of muscle interactions to task performance at both intermuscular (i.e. pairs of muscle activations) and intramuscular (i.e. pairs of rhythmic activities) levels. This approach builds on a previously established pipeline for the extraction of task-relevant muscle interaction patterns whose basic premise is that muscle interactions should be directly mapped to task performance to understand their specific functional underpinnings. Our innovation here goes further by enabling the quantification of the independent contributions of muscles (or intramuscular oscillations) to task performance, thus integrating novel theoretical perspectives on motor modularity into muscle synergy analysis. In applying this framework to benchmark datasets, we firstly demonstrated how the decomposition of task-relevant muscle combinations reveals a complex functional architecture underlying everyday human movements. This functional architecture displayed a highly nested network structure of functionally similar and complementary information processing between muscles along with their independent functional contributions. We then investigated the functional interactions at the intramuscular level between frequency-specific oscillatory amplitudes, revealing that functional modularity is a scale-invariant characteristic fundamental to movement construction.

We found that the extracted inter- and intra-muscular components were consistently generalizable beyond any data subset and across disparate motor tasks such as whole-body reaching and balancing tasks. Finally, we showed that these motor components were differentially predictive of salient motor features including motor adaptation and age group, suggesting they offer complementary windows into movement control. Thus, we present the proposed framework as a powerful tool for fundamental mechanistic investigations with a novel lens into human action. As demonstrated here, this analytical tool can be used to a) characterize the functional outcomes of muscle interactions and compare them across populations or conditions and conversely b) identify physiological markers of motor performance, learning or impairment.

The proposed methodology aligns with recent theoretical innovations in the motor control research field that propose functional modularity both within- and between muscles as a mechanism for simplified and flexible movement control [37]. Within this theoretical framework, motoneurons affiliated with overlapping functional groups may innervate the same or different muscles (Fig.1.2), while individual muscles can also be independently controlled concomitantly. This proposition implies a diverse range of muscular interactions including muscles working together towards functionally similar, complementary and independent task-goals [50, 52, 134]. By posing the degrees-of-freedom problem of coordinated movement as the problem of information sharing across muscle networks [15, 130], our framework effectively reveals this hierarchical and diverse functional architecture. To elaborate, the extracted motor components captured multiple, co-occurring subnetworks of muscles (or intramuscular rhythms) forming overlapping functional groups. The functional nestedness unveiled here suggests that the motor system generates hierarchical task representations whose dimensions are folded into one another to simplify movement control. In effect this suggests that the motor system adaptively breaks down the problem of task execution into manageable sub-tasks addressed through hierarchical recursion, interestingly mirroring dynamic programming architectures [158]. Several of these patterns were shared across interaction types (e.g. Supp. Fig. 1-3), indicating diverse information processing indeed occurred concomitantly within the same muscle networks. Many of these motor components were centrally defined or were more widespread across the body. These networks of functional muscle connectivity across the body are underpinned by polysynaptic communication pathways involving feedforward and feedback processes. Among these communication pathways, both the centralized and peripheral routing of task information globally integrates muscle functionality across the body while diffusive processes prevail locally, promoting a segregation of functional roles [146, 108, 159, 160]. Moreover, the unique adherence of top-down and bottom-up motor processes to specific task features likely enhances the selectivity of sensorimotor representations and consequently the adaptability of movement control [161]. The further involvement of network communication models (e.g. network communicability used here for illustrative purposes only [140, 116]) in future applications of the proposed framework may prove useful for understanding how motor signals are broadcast throughout the muscle space [162].

The separate quantification of unique, redundant, and synergistic task information proposed here brought about interesting insights into human motor control. For instance, we were able to identify the functional underpinnings of increased motor variability in older adults. We found variability in functionally complementary intermuscular couplings increased with age but decreased intramuscularly with age also (Fig.8), suggesting ageing has differential effects on functionally integrative mechanisms across scales. Meanwhile, variability in functionally redundant and independent networks reduced and increased respectively across both scales in the older adults group. These findings firstly contest the notion of increased motor variability with aging being simply a manifestation of motor noise, but demonstrate in fact that this variability manifests in functionally relevant channels of muscle interaction. These insights also support empirical work highlighting functional integration as a compensatory mechanism in individuals with age-related neurodegeneration [163],going further in showing that this supplementary integration is not present across all scales but, in fact, may come at the expense of other scales. Finally, the fact that all three interaction types each had unique predictive information about ageing highlights the comprehensive characterization of motor control our approach can provide about multifaceted health conditions. Future work identifying the exact neural underpinnings of these distinct types of muscle interaction will further bolster the clinical insights of this approach. Continuing, we were also able to show that diverse types of task information are not isolated to specific muscle couplings or rhythms but are dynamically generated by various oscillatory signals to meet task demands. Among intramuscular R, gamma amplitudes were repeatedly associated with improved balance performance across participants when coupled in a functionally similar way with alpha- and beta-bands (Fig.7(B)). The alpha and beta-bands have been the subject of focus in several studies showing their crucial role in muscle synergy generation and monitoring [34, 164, 165]. Here we add to this line of research by uncovering a potentially crucial role of higher gamma oscillations in movement control, showing that gamma amplitudes alone can provide much of the functionally relevant information provided by these lower-frequency bands. In sum, the application of our approach brought about novel insights into human motor control. Nevertheless, the neural substrates underpinning these diverse interaction types remain a topic of future research that we aim to investigate through the incorporation of electroencephalographic and high-density EMG signals to quantify cortico-muscle interactions and motoneuron level modules respectively.

Despite the strong base of evidence demonstrating the capacity of the individual muscle to augment whole movement patterns [146, 33, 7], muscle synergy research has generally focused on muscle clustering. Our findings here support recent formal applications of the muscle synergy concept to the intramuscular level, where task-specific modules have been identified [149, 150, 151]. Of note, past research suggested that intramuscular modules represent spinal-level circuitry while the intermuscular

space primarily captures supraspinal mechanisms [151]. Indeed, this observation is supported by work from several research groups using different analytical techniques [166, 32, 167]. Here, we consistently found that the intramuscular level represented aspects of motor behavior indicative of superior task performance and proficiency (Fig.7-8), while the intermuscular level mainly represented decrements in performance and compensatory mechanisms (Fig.7-8). This opposing pattern intuitively aligns with this recent work, as erroneous performance requires more frequent intervention by supraspinal mechanisms while more effective movement can be coordinated automatously by spinal circuitry. An exception to this pattern however lies in the independent control of muscles quantified here as unique task information which demonstrated a correlation with better task performance inter-muscularly (Fig.7(A)) and of which increased fluctuations were consistently related to older age across both scales (Fig.8). This independent control mechanism is likely invoked where coarse-grained control mechanisms are insufficient, allowing for the necessary selectivity to maintain task performance. This suggests that variability in independent control mechanisms both between and within muscles plays a major role in the manifestation of (and/or compensation for) behavioral inconsistency among older adults. However, as other related work also proposed [51, 134, 164, 166], our findings here (Fig.7-8) suggest that there is not a clear distinction between the neural substrates underlying inter- and intra-muscular dynamics, and that they likely reflect the contributions of multiple neural substrates simultaneously, together holistically representing the motor system in a scale-invariant manner. Finally, our findings also highlight the crucial role of the individual muscle level in movement organization and promote further investigations on modular control at this scale. Indeed, an interesting avenue for future research would be to investigate the causal emergence of intramuscular dynamics from intermuscular constraints and vice versa, with the aim of mapping out the hierarchical interactions underlying coordinated movement.

In conclusion, we have developed and successfully applied a novel computational framework for the extraction of functionally diverse muscular interactions across multiple scales. Our approach provides a more detailed and precise account of the functional organization of the motor system which has direct benefits in the clinical setting and in engineering applications (e.g. predicting motor intention). We were able to comprehensively characterize the functional underpinnings of several distinct motor tasks while ensuring physiological relevance and generalizability. This principled method further widens the scope of the muscle synergy concept, showing how muscles can work together redundantly, synergistically, and independently towards task performance. In doing so, we align current approaches to muscle synergy analysis with the forefront of theoretical work on movement modularity. Overall, our framework offers improved flexibility and opportunities to future investigations through novel perspectives on movement control.

4.5 Materials and Methods

Quantifying functionally diverse muscular interactions

To decompose the information a pair of muscles $[m_x, m_y]$ (or frequencies-specific amplitudes $[f_x, f_y]$) carries about τ into redundant, synergistic and unique components, we implemented the PID framework [152, 168, 169]. PID stems from a related information-theoretic measure known as co-information (co-I) that, by contrasting the sum of shared task information in m_x and m_y each alone ($I(m_x;\tau) + I(m_y;\tau)$) against their joint task information ($I(m_x, m_y;\tau)$), quantifies their multivariate mutual information ($II(m_x; m_y;\ \tau)$) (Equation 1.1) [125]. co-I results in a single value representing either a net redundancy (negative co-I values) or net synergy (positive co-I values) across the system. PID builds on this by removing the conflation of redundancy and synergy evident in co-I through the decomposition of $I(m_x, m_y;\tau)$ (i.e. the JMI) into separate redundant ($R(m_x : m_y;\tau)$) and synergistic ($S(m_x : m_y;\tau)$) information atoms and the unique task information provided by m_x ($U(m_x : \tau|m_y)$) and m_y ($U(m_y : \tau|m_x)$) (Equation 1.2).

$$-II(m_x; m_y;\ \tau) = I(m_x;\tau) + I(m_y;\tau) - I(m_x, m_y;\tau) \quad \text{(Equation 1.1)}$$

$$I(m_x, m_y;\tau) = R(m_x : m_y;\tau) + U(m_x : \tau|m_y) \quad (4.1)$$
$$+ U(m_y : \tau|m_x) + S(m_x : m_y;\tau) \quad \text{(Equation 1.2)}$$

To perform PID here, we implemented a novel PID framework for Gaussian variables based on local information estimates that has proven useful in neuroscientific applications [152, 155, 59, 170, 99]. We generated a multiplexed view of the muscular interactions underlying human movement by applying this method to all unique $[m_x,\ m_y]$ (or $[f_x, f_y]$) and τ combinations for each participant. To make these separate computations directly comparable, we normalized each PID component by their collective sum total which is equal to the JMI [155]. The resulting redundancy, synergy and two unique information estimates collectively form four symmetric adjacency matrices (A) (i.e. $A^T A = I$) that represent the functionally similar, complementary or unique connectivities between muscles (frequencies) with respect to τ. When repeated across all available task variables τ

and participants, A is a multiplex network of dimension [No.of $[m_x, m_y]$ x [No.of τ x No.of participants]]. Thus, by applying network-theoretic statistical tools to A, we can identify functional modules carrying the same type of task information (i.e. redundant, synergistic, unique) (fig.1.2).

Identifying significant muscle interactions and their modular structure The percolation threshold (P_c) (i.e. a critical value specifying the probability of node connectivities occurring and at which large clusters and long-range connectivity begin to appear across a given network [171] has proven to be a fundamental constraint in nervous system organization [68, 66, 172]. To identify the network connections in our framework that align with P_c, we employed a modified percolation analysis [66]. We applied this method to each layer of A, sparsifying the network with respect to the P_c expected from equivalently sized random networks by thresholding connectivities iteratively until the largest cluster in the network (the '*giant component'*) begins to be affected (Fig.2(C)).

Following this, in previous applications of the NIF [145, 107], to determine the optimal number of clusters to extract with dimensionality reduction, we have implemented community detection protocols suitable for multiplexed networks [72, 71, 121]. In the current study however, due to the highly nested structure found in A, just a single cluster was identified using these established methods. Therefore, to determine the optimal modular structure within a multiplexed network of muscles with overlapping functional affiliations, we employed a link-based community detection protocol [153]. Specifically, we firstly normalize network edges within each layer of A ($A(i)$) with respect to their corresponding JMI [155], and then applied single-linkage hierarchical clustering. In doing so, we built dendrograms for each network layer describing the clustering of dependencies that is cut at a threshold determined by the maximum of the partition density (D) (Fig.2(D)), defined for a given partition of M links and N nodes into C subsets (Equation 2.1) [153]. Here, D is the average of the number of links in a subset (m_c) normalized by the possible maximum and minimum number of nodes with respect to the number of nodes those links touch (n_c). This computation essentially unravels the nested network structure of each layer in A, resulting in a set of binary adjacency matrices that represent whether a muscle belongs to an identified cluster or not.

$$D = \frac{2}{M} \sum_c m_c \frac{m_c - (n_c - 1)}{(n_c - 2)(n_c - 1)} \qquad \text{Equation 2.1}$$

We then sum across all of these computed matrices across all layers of A, resulting in a single aggregate graph. Finally, we then apply the conventional community detection method based on a modularity maximization cost-function known as the Q-statistic (Q) (Equation 2.2) [72, 79]. For a given partition of the network, the Q-statistic compares the number of edges between node i and j (A_{ij}) and what would be expected from an equivalent random network (P_{ij}). In letting $\delta(g_i, g_j)$=1 if nodes i and j belong to the same group (g) and 0 otherwise, thus this measure penalises partitions with a low ratio of within vs without cluster dependencies [72, 67]. The optimal cluster count to extract was defined as the partition that maximises this Q-statistic.

$$Q = \frac{1}{4m} \sum_{ij} \left(A_{ij} - P_{ij}\right) \delta(g_i, g_j) \qquad \text{Equation 2.2}$$

Extraction of low-dimensional motor components

Using the optimal cluster count derived a priori as the input parameter into dimensionality reduction, namely PNMF [63], we extracted low-dimensional components of motor behavior from muscle interactions of a specific type (i.e. redundant, synergistic or unique) across tasks and participants (Fig.2(E)). In the case of the intermuscular space, this input matrix (A) was of shape [No. of $[m_x, m_y]$ x [No. of τ x No. of Participants]], while for the intramuscular space, A had a dimensionality of [No. of $[f_x, f_y]$ x [No. of muscles x No. of τ x No. of Participants]]. As described in equation 3.1 for the *j*th module and single participant and task case, A is factorized into two components, $\mathbf{v}$ a vector of muscle weightings (m) of length equal to the number of unique muscle pairs (K) and corresponding activation coefficients (s). The extraction of the modules identified during model-rank specification is verifiable as shown in previous NIF applications [107]. We note here that for the aim of extracting motor components predictive of differences in the sampled population (see '*Hierarchies of functional muscle interactions capture distinct motor features'* in the results section), we input the normalized PID values into dimensionality reduction. However, for the aim of extracting generalizable motor components (see '*Generalizable components of functionally diverse muscular interactions'* and '*Functional modularity is scale-invariant across the human motor system'* of the results section), we input the non-normalized version of A into dimensionality reduction.

$$A = \begin{pmatrix} \mathbf{v}_j^{m^1} \\ \vdots \\ \mathbf{v}_j^{m^K} \end{pmatrix} . \begin{pmatrix} s_j & \dots & s_j \end{pmatrix} \qquad \text{Equation 3.1}$$

Examining the generalizability of extracted motor components

To determine the generalizability of the extracted motor components, using Pearson's correlation we determined the similarity between the extracted motor components and equivalent components extracted from a subset of the input data (i.e. when an individual participant or task was removed). We carried out this procedure for all tasks and participants and then focused our analysis on the correlation between functionally equivalent motor components (>0.5 correlation). To summarize this comparison, we converted the remaining coefficients into Fisher's Z values, computed averages and standard deviations, and then reverted these values back to correlation coefficients.

Salient features of motor performance

To probe how functionally diverse inter- and intra-muscular interactions represent motor performance, we quantified Error in specific ways for dataset 2 and 3 for use in separate statistical analyses.

For dataset 2, ΣError was defined as the absolute cumulative error of the balance board parameter ($|\sigma|$) across the *n*th trial (Equation 4.1). σ was any deviation from 0 degrees of the balance board along the horizontal plane. Using a repeated measures correlation [156], associations between ΣError and trial-specific activation coefficients from inter- and intra-muscular componenets were determined. For the intramuscular activation coefficients specifically, we averaged them across muscles to get a [No. of trials x No. of participants] size vector equivalent to the intermuscular coefficients.

For dataset 3, a binary variable representing participants' age group (Young=0 vs. Old=1) was used as the dependent variable in a binary logistic regression model. ΣError, a measure of motor variability, was used as the predictors in this model. ΣError was defined as the absolute cumulative sum across trials of an inter- or intra-muscular activation coefficient σ demeaned with respect to their condition-specific average (i.e. light vs heavy objects) (Equation 4.1).

$$\sum Error = \sum_{n} |\sigma| \qquad \text{Equation 4.1}$$

We calculated ΣError of all inter- and intra-muscular components and input these as predictors of age group in the logistic regression model. An optimally parsimonious model, including the minimal number of predictors, was determined using forward selection via the Wald's test criterion (inclusion: p<0.05, exclusion: p>0.1).

Subnetwork analysis

To illustrate the relative importance of individual muscles on the depicted human body models [81], we determined the total communicability ($C(i)$) of individual nodes (i) [116]. $C(i)$ is defined as the row-wise sum of all matrix exponentials (e) in the adjacency matrix (A) that consider the number of walks between each pair of nodes i and j (Equation 5.1) [140, 116].

$$C(i) = \sum_{j=1}^{N} [e^{A}]_{ij} \qquad \text{Equation 5.1}$$

To emphasize salient functional connectivities present in the motor components, we further sparsified all dependencies with a below average network communicability and illustrated the output on the accompanying human body models [140, 81]. To uncover salient subnetwork structures consisting of more closely functionally related muscles (indicated by node color on the human body model), we applied the community detection algorithm described in equation 2.3 to the extracted motor components [72, 79]. **Data acquisition and experimental conditions**

To illustrate our framework, we applied it to four datasets of EMG signals and corresponding continuous task parameters recorded while human participants performed different motor tasks. In dataset 1 (fig.3(a)) [82], 3 healthy, adult participants performed whole-body, unimanual point-to-point reaching movements in various directions and to varying heights while EMG from 30 muscles (tibialis anterior, soleus, peroneus, gastrocnemius, vastus lateralis, rectus femoris, biceps femoris, gluteus maximus, erector spinae, pectoralis major, trapezius, anterior deltoid, posterior deltoid, biceps and triceps brachii) across both hemibodies were captured (Fig.3(a)). Alongside these EMG recordings, 3D kinematic data from 18 body locations (elbow, wrist, mid-arm, index finger, shoulder, hip, knee, ankle and foot) across both hemibodies were captured along with additional kinematics from the head, right eye, left ear, and the center of pressure. Participants performed ~2160 pseudo randomized trials each in structured blocks across two days to avoid fatigue. Movement onsets and offsets were determined at the timepoints which the index finger kinematic was 5% above and below its peak velocity in the trial respectively.

In dataset 2 (fig.3(b)), 3 healthy participants performed 10 consecutive trials of balancing on a balance board (Model 16130 Stability Platform, Lafayette Instrument) while self-induced perturbations were experienced along the frontal plane. Each trial lasted 30 seconds in which participants were instructed to maintain a balance board position parallel to the floor as best they could while focusing ahead at eye-level on a dot on the wall (<5 meters distance). Between trials, participants had 1

minute to rest. EMG recordings (Delsys Trigno™ wireless EMG, sampling frequency: 2000Hz) were taken from the bilateral medial gastrocnemius (MGN), tibialis anterior (TA), rectus femoris (RF) and biceps femoris (BF) while the horizontal angular displacement of the balance board was simultaneously recorded. Ethical approval was given by the Faculty of Biological Sciences Ethical Review Committee, University of Leeds.

For dataset 3 (fig.3(c)) [154], 14 young adults (22.1±2.4 years old, two left-handed, two males) and 18 older adults (71.6±6.9 years old, two left-handed, 8 males) performed a bimanual grasp-lift-hold-replace task of both a light (0.2kg) and heavy (0.4kg) object (two manipulanda made from carbon-filled nylon) while in a seated position in front of a table. The objects were placed on the table 75% of shoulder width and 70% of maximum reach for each participant who were instructed to grasp the object and lift it to a target height in front of them (300mm height) and to hold the object as still as possible at this position for 10 seconds. Following this holding period, the participant was instructed to replace the object(s) back on the starting position markers. Participants performed 10 consecutive repetitions for each weight condition while EMG signals from the bilateral anterior deltoid (AD), extensor carpi radialis (ECR), flexor carpi radialis (FCR) and abductor pollicis brevis (APB) were recorded (Delsys Trigno™, sampling frequency: 2000Hz). Grip forces were recorded from 50N load cells (Omega, LCM201-50), acquired from a 16-bit data acquisition card (National Instruments, USB-6002) and processed in Labview (v.1.4). For load forces, six degree-of-freedom models were created in Qualisys for each object and were used to compute their 3D acceleration from which net load forces were calculated with respect to object mass. Trials commenced from 100ms prior to first contact until 100ms after last point of contact of either hand with the object, determined via recorded kinematic data of the objects position.

Data pre-processing

Intermuscular analyses

The processing of EMG signals from dataset 1 and 2 for the purpose of analyses in the intermuscular space included the application of a bidirectional low-pass Butterworth filter with zero-phase distortion (order: 4^{th}, cut-off: 20Hz) to the rectified signals. Extrapolation of the kinematic data for dataset 1 and 2 to align with the corresponding EMG signals was carried out using a cubic spline method. For dataset 3, the signals were processed as described in [154]. More specifically, the rectified EMG signals were low-pass filtered (filter: 4^{th} order Butterworth with zero-phase distortion, cut-off: 10Hz) and down-sampled to 200Hz to align with kinetic and kinematic datapoints. The filtered EMG signals were then normalized against their peak amplitudes across trials. The grip and load forces were smoothed using a low-pass filter (cut-off: 12Hz, filter: 4^{th} order Butterworth).

Intramuscular analyses

The processing of EMG signals for the purpose of intramuscular analyses in the intramuscular space were uniform across datasets 1-3. This processing firstly included the filtration of the raw, unrectified EMG signals into specific frequency bands (Delta [0.1-4 Hz], Theta [4-8 Hz], Alpha [8-12 Hz], Beta [12-30 Hz], Low-Gamma (Piper rhythm) [30-60 Hz], High Gamma (Gamma) [60-80 Hz]) using a low- and high-pass filter combination (bi-directional 4^{th} order Butterworth filters with zero-phase distortion). Then the absolute values from a Hilbert transform of the filtered signals representing their oscillatory amplitudes were extracted for further analysis. In the case of dataset 3, no down-sampling of the EMG signals occurred as carried out for intermuscular analyses. The task parameters for datasets 1-3 were all extrapolated using a cubic spline method to temporally align with the corresponding, processed EMGs and no further processing was carried out.

4.6 Author contribution

DOR: Methodological development, conceptual development, coding, testing, data curation (Dataset 2), processing and framework application, manuscript writing and editing. *WS*: Data curation (Dataset 3). *PH*: Data curation (Dataset 1), manuscript review. *RA*: Data curation (Dataset 2), Data pre-processing, manuscript review. *SA*: Data curation (Dataset 3), manuscript review. *ID*: Supervision, conceptual and methodological development, manuscript editing.

4.7 Acknowledgments

We would like to thank Daniel Chicharro for the helpful discussions on Partial Information Decompositions.

Chapter 5

Conclusions

5.1 Summary

In this work, I set out to firstly address important limitations among current approaches to muscle synergy analysis by directly including task parameters during muscle synergy extraction. To this end, in Chapter 2 I established a computational framework known as the Network-Information Framework (NIF). The NIF leverages information- and network-theoretic statistical tools along with machine-learning to extract networks of spatial, temporal, or spatiotemporal muscle interactions under relaxed model assumptions. I applied this novel framework to benchmark datasets of human movements, framing the results in terms of the key attributes of the muscle synergy (i.e. a sharing pattern, reciprocity and task dependence) [31, 105]. In doing so, I communicated the close alignment of this approach with previous conceptual intuitions on the muscle synergy. I also pointed towards several key differences in my proposed approach that uniquely place it in the literature in terms of research opportunities and novel insights. Furthermore, I demonstrated the utility of the NIF by proving the generalisability of extracted components across participants and tasks.

In Chapter 3, I addressed the second research objective of this project by building upon current approaches and the NIF pipeline I established to propose a novel perspective to the muscle synergy. This novel perspective describes how muscles can cooperate towards not only functionally similar task-goals but also complementary task-goals and objectives irrelevant towards overt task performance. In this work, I made this perspective implicit to an analytical approach by firstly establishing a way to quantify task-irrelevant muscle interactions using the NIF. This innovation revealed muscle couplings representative of gross motor functions present across tasks and secondary, physiological objectives such as the maintenance of internal joint mechanics and reciprocal inhibition. Having characterised the space of muscle interactions that do not contribute to task-specific motor behaviours, I then incorporated a higher-order information-theoretic measure known as Co-Information into the NIF to dissect the task-relevant space. This procedure enabled the principled characterisation of both functionally similar (i.e. redundant) and complementary (i.e. synergistic) muscle couplings. The task-redundant muscle networks were comprised of prime-mover muscles and several supporting muscles working together towards common task-goals. Meanwhile, the task-synergistic muscle networks consisted of complementary functional connections between modules identified in the task-redundant space. Across task-relevant and -irrelevant networks, submodular structures were consistently identified that comprised of muscles with a closer functional association than other muscles, suggesting functional modularity may be a scale invariant property of the human motor system. Accompanying the spatial networks, I concurrently identified temporal patterns representing the parallel control of muscles towards desired end-point states whilst continually controlling present movement trajectories. Again, I framed these results as building upon current methods, however demonstrating the superior functional and physiological relevance of my proposed approach when applied to both healthy and impaired populations.

Finally in Chapter 4, I completed the aims of this thesis by addressing the third research objectives, namely the development of a comprehensive analytical approach to quantifying diverse types of muscle interaction. More specifically, i developed a methodology for the extraction of functionally diverse muscle interaction types (i.e. functionally similar, complementary and independent). I introduced a novel information-theoretic framework to the motor control field, namely Partial Information Decomposition (PID) [152, 168]. I integrated the PID approach into the NIF and applied it to various human movement datasets with the aim of probing a recently proposed functional architecture of the motor system where functional modularity persists across both inter- and intra-muscular scales [37]. I uniquely revealed the multi-functionality of muscle interactions by concurrently extracting highly nested networks of functionally similar and complementary muscle couplings along with their functionally independent contributions. In doing so, I aligned current muscle synergy analysis with the forefront in theoretical understanding on human movement modularity [37]. Finally, to showcase the utility of this approach, I then probed the task representation of inter- and intra-muscular components, showing how they were differently predictive of motor adaptation and

of differences between age groups.

5.2 Implications for neurobiological mechanisms

The neural substrates that underpin these diverse types of functional muscle interaction is an open question emerging from this work and builds on many years of progressive research [39]. Since the establishment of the NIF, i have carried out preliminary applications of this approach on clinical populations which have begun to provide hints towards what these types of muscle interaction may represent. Briefly, from preliminary applications to data on stroke survivors, i have found that synergistic interactions are predictive of Mini mental state examination scores. Moreover, post-stroke rehabilitation had a normalising effect on the redundancy-synergy balance of these interactions, promoting greater synergy between muscles. Meanwhile, among human and rat subjects with a spinal cord injury, i have found an opposing effect, where rehabilitation reconfigured functionally redundant modules. Together, in the context of the location of these neurological impairments, my findings suggest that synergistic interactions may have a cortical origin whereas redundancy may be induced by spinal circuitry. Regarding the functional independence between muscles, quantified in my frameworks as unique information, i have yet to gather any preliminary findings on this type of interaction. However, i will conjecture here on possible sources. Briefly, it is a well recognised capacity of the human nervous system to be able to control individual muscles, an ability that can indeed improve with training [36]. Further, the information processing capacity of muscle spindles has garnered increasing attention in the research lately [146]. Thus, there are potentially both top-down and bottom-up mechanisms contributing to the unique information found here among individual muscles. The latter example is particularly interesting as the frameworks i have developed consider muscles as receivers of motor commands rather than an active contributor to movement construction. Modelling muscles as an information processing unit rather than a simple actuator may reveal novel details about the neurobiological mechanisms of human movement.

Future work applying these frameworks in this way and also incorporating other physiological signals such as HD-EMG and/or EEG will provide more concrete evidence for the neural origins of these distinct types of muscle interactions.

5.3 Future perspectives

The work I have presented here provides a significant contribution to muscle synergy research, both methodologically and conceptually. Looking into the future of the research field, there are several key areas where these proposed approaches can be applied and further developed to maintain its continued progression.

Effective physiological markers of motor impairment have been developed using traditional muscle synergy analysis [173, 117]. However, this approach has yet to fulfil its promise in this regard, encouraging the development of novel ways to tackling open research problems in motor control research [21]. For the contributions presented in this work to be realised as useful insights into movement control, it is important that the proposed approaches are applied to various healthy (e.g children, young and older adults, sedentary and trained individuals etc) and impaired (e.g. stroke, cerebral palsy etc) populations performing activities-of-daily-living. These applications should devise new ways to quantify healthy and impaired movement while linking reported findings with existing research in the field to ensure a consistent progression in understanding. Growing a common understanding of the novel perspectives, analytical approaches and nomenclature employed in this work across the scientific community will be aided by review and perspectives papers and close collaboration with other research groups.

Speaking to readers of the published work from this project, a particular point of interest has been the remarkable generalisability of the extracted components, consistently beyond any individual participant or task. Indeed, this innovation has important implications for the clinical setting, where normative references are frequently used to quantify impairment and treatment progress but are currently highly dataset dependent. The capability to extract such generalisable motor patterns can improve significantly upon the accuracy of these clinical tools. A current barrier to the uptake of muscle synergy approaches in the clinical setting however is the lack of training on the capture, analysis, and interpretation of EMG data [174]. The development of specialised software packages that incorporate many of these computational approaches in an accessible way may prove to be impactful in encouraging the transition of muscle synergy research to clinical practice.

From an engineering perspective, an important limitation in the practical application of current muscle synergy techniques is the lack of a direct mapping to task performance, resulting in poor performance in simulation studies [27, 19]. The functional mappings presented in this work should address this limitation while the network- and information-theoretic underpinning of the frameworks make them directly applicable to various applications (e.g. robotics, prosthetics) [19, 18]. As mentioned previously, my work here also presents the opportunity to incorporate other physiological signals into muscle synergy extraction [21]. For example, applying and or integrating high-dimensional EMG and/or electroencephalography signals into the NIF to extract muscle interactions whose neural origins are directly falsifiable will be a fruitful research avenue in the practical application of muscle synergies (e.g. brain-machine interfaces, predicting motor intention).

Finally, regarding methodological developments, traditional muscle synergy analysis has focused on extracting clusters of muscle activity at the group level whereas the NIF proposes to first extract pairwise dependencies and then cluster at the group level.

Although this innovation improves upon the possible insights gained from the outputs, there are several orders of interaction between the muscle pair and whole group that may provide useful insights into movement control. Indeed, exclusively focusing on pairwise interactions emphasises redundancies at the expense of higher-order, synergistic dependencies and results in non-specific and most likely incomplete representations of the system [175]. Developments of the NIF to quantify intermediate level interactions will benefit from recent efforts in the neurosciences to move functional connectivity estimation beyond the pairwise level [176]. This line of research may also benefit from the emerging field of explainable artificial intelligence (XAI) that seeks to draw mechanistically interpretable insights from the inner workings of machine-learning models. Dissecting the neural representations of task-relevant muscle activations derived from neural network models by leveraging these techniques may prove useful in furthering scientific insights.

References

[1] Matteo Colombo. "Moving forward (and beyond) the modularity debate: A network perspective". In: *Philosophy of Science* 80.3 (2013), pp. 356–377.

[2] Jerry A Fodor. *The modularity of mind*. MIT press, 1983.

[3] John A Bullinaria. "Understanding the emergence of modularity in neural systems". In: *Cognitive science* 31.4 (2007), pp. 673–695.

[4] Felipe S Abrahão and Hector Zenil. "Emergence and algorithmic information dynamics of systems and observers". In: *Philosophical Transactions of the Royal Society A* 380.2227 (2022), p. 20200429.

[5] Nadia Dominici et al. "Locomotor primitives in newborn babies and their development". In: *Science* 334.6058 (2011), pp. 997–999.

[6] Michael Levin. "The computational boundary of a "self": developmental bioelectricity drives multicellularity and scale-free cognition". In: *Frontiers in psychology* 10 (2019), p. 2688.

[7] Vincent CK Cheung et al. "Central and sensory contributions to the activation and organization of muscle synergies during natural motor behaviors". In: *Journal of Neuroscience* 25.27 (2005), pp. 6419–6434.

[8] Emilio Bizzi and Vincent CK Cheung. "The neural origin of muscle synergies". In: *Frontiers in computational neuroscience* 7 (2013), p. 51.

[9] Elodie Hinnekens et al. "Generating variability from motor primitives during infant locomotor development". In: *eLife* 12 (2023), e87463.

[10] Vincent CK Cheung et al. "Plasticity of muscle synergies through fractionation and merging during development and training of human runners". In: *Nature communications* 11.1 (2020), p. 4356.

[11] John W Krakauer et al. "Neuroscience needs behavior: correcting a reductionist bias". In: *Neuron* 93.3 (2017), pp. 480–490.

[12] Jennifer N Kerkman et al. "Network structure of the human musculoskeletal system shapes neural interactions on multiple time scales". In: *Science advances* 4.6 (2018), eaat0497.

[13] Mark L Latash. "The bliss (not the problem) of motor abundance (not redundancy)". In: *Experimental brain research* 217 (2012), pp. 1–5.

[14] Noor Sajid et al. "Degeneracy and redundancy in active inference". In: *Cerebral Cortex* 30.11 (2020), pp. 5750–5766.

[15] Nicholas Bernstein. "The coordination and regulation of movements". In: *(No Title)* (1967).

[16] Bastien Berret et al. "Optimality and modularity in human movement: from optimal control to muscle synergies". In: *Biomechanics of anthropomorphic systems* (2019), pp. 105–133.

[17] Tetsuro Funato et al. "Muscle synergy analysis yields an efficient and physiologically relevant method of assessing stroke". In: *Brain Communications* 4.4 (2022), fcac200.

[18] Marco Santello et al. "Towards a synergy framework across neuroscience and robotics: Lessons learned and open questions. Reply to comments on:"Hand synergies: Integration of robotics and neuroscience for understanding the control of biological and artificial hands"". In: *Physics of life reviews* 17 (2016), pp. 54–60.

[19] Cristiano Alessandro et al. "Muscle synergies in neuroscience and robotics: from input-space to task-space perspectives". In: *Frontiers in computational neuroscience* 7 (2013), p. 43.

[20] Mohammad Fazle Rabbi et al. "Non-negative matrix factorisation is the most appropriate method for extraction of muscle synergies in walking and running". In: *Scientific reports* 10.1 (2020), p. 8266.

[21] Vincent CK Cheung and Kazuhiko Seki. "Approaches to revealing the neural basis of muscle synergies: a review and a critique". In: *Journal of neurophysiology* 125.5 (2021), pp. 1580–1597.

[22] Yuri P Ivanenko, Richard E Poppele, and Francesco Lacquaniti. "Five basic muscle activation patterns account for muscle activity during human locomotion". In: *The Journal of physiology* 556.1 (2004), pp. 267–282.

[23] Ioannis Delis et al. "A unifying model of concurrent spatial and temporal modularity in muscle activity". In: *Journal of neurophysiology* 111.3 (2014), pp. 675–693.

[24] Andrea d'Avella, Philippe Saltiel, and Emilio Bizzi. "Combinations of muscle synergies in the construction of a natural motor behavior". In: *Nature neuroscience* 6.3 (2003), pp. 300–308.

[25] Jason J Kutch and Francisco J Valero-Cuevas. "Challenges and new approaches to proving the existence of muscle synergies of neural origin". In: *PLoS computational biology* 8.5 (2012), e1002434.

[26] Matthew C Tresch and Anthony Jarc. "The case for and against muscle synergies". In: *Current opinion in neurobiology* 19.6 (2009), pp. 601–607.

[27] Aymar de Rugy, Gerald E Loeb, and Timothy J Carroll. "Are muscle synergies useful for neural control?" In: *Frontiers in computational neuroscience* 7 (2013), p. 19.

[28] Ioannis Delis et al. "Quantitative evaluation of muscle synergy models: a single-trial task decoding approach". In: *Frontiers in computational neuroscience* 7 (2013), p. 8.

[29] Ioannis Delis et al. "Task-discriminative space-by-time factorization of muscle activity". In: *Frontiers in human neuroscience* 9 (2015), p. 399.

[30] Alessandro Scano, Robert Mihai Mira, and Andrea d'Avella. "Mixed matrix factorization: A novel algorithm for the extraction of kinematic-muscular synergies". In: *Journal of Neurophysiology* 127.2 (2022), pp. 529–547.

[31] Mark L Latash. *Synergy*. Oxford University Press, 2008.

[32] Simon A Overduin et al. "Representation of muscle synergies in the primate brain". In: *Journal of Neuroscience* 35.37 (2015), pp. 12615–12624.

[33] William J Kargo and Simon F Giszter. "Individual premotor drive pulses, not time-varying synergies, are the units of adjustment for limb trajectories constructed in spinal cord". In: *Journal of Neuroscience* 28.10 (2008), pp. 2409–2425.

[34] Coen S Zandvoort et al. "The human sensorimotor cortex fosters muscle synergies through cortico-synergy coherence". In: *Neuroimage* 199 (2019), pp. 30–37.

[35] Sergi Valverde. "Breakdown of modularity in complex networks". In: *Frontiers in physiology* 8 (2017), p. 497.

[36] John V Basmajian. "Control and training of individual motor units". In: *Science* 141.3579 (1963), pp. 440–441.

[37] François Hug et al. "Common synaptic input, synergies and size principle: Control of spinal motor neurons for movement generation". In: *The Journal of Physiology* 601.1 (2023), pp. 11–20.

[38] Simon F Giszter and Corey B Hart. "Motor primitives and synergies in the spinal cord and after injury—the current state of play". In: *Annals of the New York Academy of Sciences* 1279.1 (2013), pp. 114–126.

[39] Ioannis Delis, Enrico Chiovetto, and Bastien Berret. “On the origins of modularity in motor control”. In: *Journal of Neuroscience* 30.22 (2010), pp. 7451–7452.

[40] Simon A Overduin et al. “Microstimulation activates a handful of muscle synergies”. In: *Neuron* 76.6 (2012), pp. 1071–1077.

[41] William J Kargo and Simon F Giszter. “Rapid correction of aimed movements by summation of force-field primitives”. In: *Journal of Neuroscience* 20.1 (2000), pp. 409–426.

[42] Matthew C Tresch, Philippe Saltiel, and Emilio Bizzi. “The construction of movement by the spinal cord”. In: *Nature neuroscience* 2.2 (1999), pp. 162–167.

[43] Andrea d’Avella and Francesco Lacquaniti. “Control of reaching movements by muscle synergy combinations”. In: *Frontiers in computational neuroscience* 7 (2013), p. 42.

[44] Mohammad Moein Nazifi et al. “Shared and task-specific muscle synergies during normal walking and slipping”. In: *Frontiers in human neuroscience* 11 (2017), p. 40.

[45] David J Clark et al. “Merging of healthy motor modules predicts reduced locomotor performance and muscle coordination complexity post-stroke”. In: *Journal of neurophysiology* 103.2 (2010), pp. 844–857.

[46] Ken Takiyama et al. “Speed-dependent and mode-dependent modulations of spatiotemporal modules in human locomotion extracted via tensor decomposition”. In: *Scientific reports* 10.1 (2020), p. 680.

[47] Lena H Ting and Jane M Macpherson. “A limited set of muscle synergies for force control during a postural task”. In: *Journal of neurophysiology* 93.1 (2005), pp. 609–613.

[48] Stacie A Chvatal and Lena H Ting. “Common muscle synergies for balance and walking”. In: *Frontiers in computational neuroscience* 7 (2013), p. 48.

[49] Teresa E Flaxman et al. “Functional muscle synergies to support the knee against moment specific loads while weight bearing”. In: *Journal of Electromyography and Kinesiology* 56 (2021), p. 102506.

[50] François Hug et al. “Muscles from the same muscle group do not necessarily share common drive: evidence from the human triceps surae”. In: *Journal of applied physiology* 130.2 (2021), pp. 342–354.

[51] Cristiano Alessandro et al. “Coordination amongst quadriceps muscles suggests neural regulation of internal joint stresses, not simplification of task performance”. In: *Proceedings of the National Academy of Sciences* 117.14 (2020), pp. 8135–8142.

[52] François Hug et al. “Correlation networks of spinal motor neurons that innervate lower limb muscles during a multijoint isometric task”. In: *The Journal of Physiology* 601.15 (2023), pp. 3201–3219.

[53] Jennifer N Kerkman et al. “Muscle synergies and coherence networks reflect different modes of coordination during walking”. In: *Frontiers in physiology* 11 (2020), p. 751.

[54] Tjeerd W Boonstra et al. “Information decomposition of multichannel EMG to map functional interactions in the distributed motor system”. In: *NeuroImage* 202 (2019), p. 116093.

[55] Claude Elwood Shannon. “A mathematical theory of communication”. In: *The Bell system technical journal* 27.3 (1948), pp. 379–423.

[56] Karl J Friston. “Functional and effective connectivity: a review”. In: *Brain connectivity* 1.1 (2011), pp. 13–36.

[57] Ioannis Delis et al. “Information-theoretic characterization of the neural mechanisms of active multisensory decision making”. In: *International Conference on NeuroRehabilitation*. Springer. 2018, pp. 584–588.

[58] Corey B Hart and Simon F Giszter. “A neural basis for motor primitives in the spinal cord”. In: *Journal of Neuroscience* 30.4 (2010), pp. 1322–1336.

[59] Robin AA Ince et al. “A statistical framework for neuroimaging data analysis based on mutual information estimated via a gaussian copula”. In: *Human brain mapping* 38.3 (2017), pp. 1541–1573.

[60] M Sklar. “Fonctions de répartition à n dimensions et leurs marges”. In: *Annales de l’ISUP*. Vol. 8. 3. 1959, pp. 229–231.

[61] Roger B Nelsen. *An introduction to copulas*. Springer, 2006.

[62] Jian Ma and Zengqi Sun. “Mutual information is copula entropy”. In: *Tsinghua Science & Technology* 16.1 (2011), pp. 51–54.

[63] Zhijian Yuan, Zhirong Yang, and Erkki Oja. “Projective nonnegative matrix factorization: Sparseness, orthogonality, and clustering”. In: *Neural Process. Lett* (2009), pp. 11–13.

[64] Zhirong Yang and Erkki Oja. “Linear and nonlinear projective nonnegative matrix factorization”. In: *IEEE Transactions on Neural Networks* 21.5 (2010), pp. 734–749.

[65] Christos Boutsidis and Efstratios Gallopoulos. “SVD based initialization: A head start for nonnegative matrix factorization”. In: *Pattern recognition* 41.4 (2008), pp. 1350–1362.

[66] Lazaros K Gallos, Hernán A Makse, and Mariano Sigman. “A small world of weak ties provides optimal global integration of self-similar modules in functional brain networks”. In: *Proceedings of the National Academy of Sciences* 109.8 (2012), pp. 2825–2830.

[67] Mark EJ Newman and Michelle Girvan. “Finding and evaluating community structure in networks”. In: *Physical review E* 69.2 (2004), p. 026113.

[68] Lazaros K Gallos, Mariano Sigman, and Hernán A Makse. “The conundrum of functional brain networks: small-world efficiency or fractal modularity”. In: *Frontiers in physiology* 3 (2012), p. 123.

[69] Cécile Bordier, Carlo Nicolini, and Angelo Bifone. “Graph analysis and modularity of brain functional connectivity networks: searching for the optimal threshold”. In: *Frontiers in neuroscience* 11 (2017), p. 441.

[70] Nicolas A Turpin, Stéphane Uriac, and Georges Dalleau. “How to improve the muscle synergy analysis methodology?” In: *European journal of applied physiology* 121.4 (2021), pp. 1009–1025.

[71] Peter J Mucha et al. “Community structure in time-dependent, multiscale, and multiplex networks”. In: *science* 328.5980 (2010), pp. 876–878.

[72] Vincent D Blondel et al. “Fast unfolding of communities in large networks”. In: *Journal of statistical mechanics: theory and experiment* 2008.10 (2008), P10008.

[73] Francesco De Pasquale et al. “A dynamic core network and global efficiency in the resting human brain”. In: *Cerebral Cortex* 26.10 (2016), pp. 4015–4033.

[74] David Meunier, Renaud Lambiotte, and Edward T Bullmore. “Modular and hierarchically modular organization of brain networks”. In: *Frontiers in neuroscience* 4 (2010), p. 200.

[75] Danielle S Bassett et al. “Dynamic reconfiguration of human brain networks during learning”. In: *Proceedings of the National Academy of Sciences* 108.18 (2011), pp. 7641–7646.

[76] Matthew L Stanley et al. “Changes in brain network efficiency and working memory performance in aging”. In: *PLoS One* 10.4 (2015), e0123950.

[77] Christopher J Hasson, Olga Gelina, and Garrett Woo. “Neural control adaptation to motor noise manipulation”. In: *Frontiers in human neuroscience* 10 (2016), p. 59.

[78] Grégoire Vergotte et al. “Concurrent changes of brain functional connectivity and motor variability when adapting to task constraints”. In: *Frontiers in physiology* 9 (2018), p. 909.

[79] Mikail Rubinov and Olaf Sporns. “Complex network measures of brain connectivity: uses and interpretations”. In: *Neuroimage* 52.3 (2010), pp. 1059–1069.

[80] Ioannis Delis et al. “A methodology for assessing the effect of correlations among muscle synergy activations on task-discriminating information”. In: *Frontiers in computational neuroscience* 7 (2013), p. 54.

[81] Sergey N Makarov, Gregory M Noetscher, and Ara Nazarian. *Low-frequency electromagnetic modeling for electrical and biological systems using MATLAB*. John Wiley & Sons, 2015.

[82] Pauline M Hilt et al. “Space-by-time modular decomposition effectively describes whole-body muscle activity during upright reaching in various directions”. In: *Frontiers in computational neuroscience* 12 (2018), p. 20.

[83] Ioannis Delis et al. “Deciphering the functional role of spatial and temporal muscle synergies in whole-body movements”. In: *Scientific reports* 8.1 (2018), p. 8391.

[84] Andrea d’Avella et al. “Control of fast-reaching movements by muscle synergy combinations”. In: *Journal of Neuroscience* 26.30 (2006), pp. 7791–7810.

[85] Andrea d’Avella et al. “Modulation of phasic and tonic muscle synergies with reaching direction and speed”. In: *Journal of neurophysiology* 100.3 (2008), pp. 1433–1454.

[86] Martha Flanders. “Temporal patterns of muscle activation for arm movements in three-dimensional space”. In: *Journal of Neuroscience* 11.9 (1991), pp. 2680–2693.

[87] Scott T Albert et al. “Postural control of arm and fingers through integration of movement commands”. In: *Elife* 9 (2020), e52507.

[88] Alex H Williams. “Combining tensor decomposition and time warping models for multi-neuronal spike train analysis”. In: *bioRxiv* (2020), pp. 2020–03.

[89] James M Shine et al. “The modulation of neural gain facilitates a transition between functional segregation and integration in the brain”. In: *Elife* 7 (2018), e31130.

[90] Raz Leib et al. “A bang-bang control model predicts the triphasic muscles activity during hand reaching”. In: *Journal of Neurophysiology* 124.1 (2020), pp. 295–304.

[91] Joachim Groß et al. “The neural basis of intermittent motor control in humans”. In: *Proceedings of the National Academy of Sciences* 99.4 (2002), pp. 2299–2302.

[92] Amir Karniel. “The minimum transition hypothesis for intermittent hierarchical motor control”. In: *Frontiers in computational neuroscience* 7 (2013), p. 12.

[93] Stefano Panzeri et al. “Sensory neural codes using multiplexed temporal scales”. In: *Trends in neurosciences* 33.3 (2010), pp. 111–120.

[94] Hamidreza Abbaspourazad et al. “Multiscale low-dimensional motor cortical state dynamics predict naturalistic reach-and-grasp behavior”. In: *Nature communications* 12.1 (2021), p. 607.

[95] Maxwell JD Ramstead et al. “Multiscale integration: beyond internalism and externalism”. In: *Synthese* 198 (2021), pp. 41–70.

[96] Karl Friston. “The free-energy principle: a unified brain theory?” In: *Nature reviews neuroscience* 11.2 (2010), pp. 127–138.

[97] Enrico Chiovetto et al. “Investigating reduction of dimensionality during single-joint elbow movements: a case study on muscle synergies”. In: *Frontiers in computational neuroscience* 7 (2013), p. 11.

[98] Marilyn Gatica et al. “High-order interdependencies in the aging brain”. In: *Brain connectivity* 11.9 (2021), pp. 734–744.

[99] Hyojin Park et al. “Representational interactions during audiovisual speech entrainment: Redundancy in left posterior superior temporal gyrus and synergy in left motor cortex”. In: *PLoS biology* 16.8 (2018), e2006558.

[100] Fernando E Rosas et al. “Reconciling emergences: An information-theoretic approach to identify causal emergence in multivariate data”. In: *PLoS computational biology* 16.12 (2020), e1008289.

[101] John P Scholz and Gregor Schöner. “The uncontrolled manifold concept: identifying control variables for a functional task”. In: *Experimental brain research* 126 (1999), pp. 289–306.

[102] Emanuel Todorov and Michael Jordan. “A minimal intervention principle for coordinated movement”. In: *Advances in neural information processing systems* 15 (2002).

[103] Tom Macpherson et al. “Parallel and hierarchical neural mechanisms for adaptive and predictive behavioral control”. In: *Neural Networks* 144 (2021), pp. 507–521.

[104] Harris S Kaplan et al. “Nested neuronal dynamics orchestrate a behavioral hierarchy across timescales”. In: *Neuron* 105.3 (2020), pp. 562–576.

[105] Michaela Bruton and Nicholas O’Dwyer. “Synergies in coordination: A comprehensive overview of neural, computational, and behavioral approaches”. In: *Journal of neurophysiology* 120.6 (2018), pp. 2761–2774.

[106] Naama Brenner et al. “Synergy in a neural code”. In: *Neural computation* 12.7 (2000), pp. 1531–1552.

[107] David Ó’Reilly and Ioannis Delis. “A network information theoretic framework to characterise muscle synergies in space and time”. In: *Journal of Neural Engineering* 19.1 (2022), p. 016031.

[108] Remi Ronzano et al. “Proximal and distal spinal neurons innervating multiple synergist and antagonist motor pools”. In: *Elife* 10 (2021), e70858.

[109] Francisco J Valero-Cuevas, Madhusudhan Venkadesan, and Emanuel Todorov. “Structured variability of muscle activations supports the minimal intervention principle of motor control”. In: *Journal of neurophysiology* 102.1 (2009), pp. 59–68.

[110] Kianoush Nazarpour, Amy Barnard, and Andrew Jackson. “Flexible cortical control of task-specific muscle synergies”. In: *Journal of Neuroscience* 32.36 (2012), pp. 12349–12360.

[111] Andrea d’Avella and Emilio Bizzi. “Shared and specific muscle synergies in natural motor behaviors”. In: *Proceedings of the national academy of sciences* 102.8 (2005), pp. 3076–3081.

[112] Andrea Lancichinetti and Santo Fortunato. “Consensus clustering in complex networks”. In: *Scientific reports* 2.1 (2012), p. 336.

[113] Jonathan Camargo et al. “A comprehensive, open-source dataset of lower limb biomechanics in multiple conditions of stairs, ramps, and level-ground ambulation and transitions”. In: *Journal of Biomechanics* 119 (2021), p. 110320.

[114] Giuseppe Averta et al. “U-Limb: A multi-modal, multi-center database on arm motion control in healthy and post-stroke conditions”. In: *GigaScience* 10.6 (2021), giab043.

[115] Domenico Buongiorno et al. “Task-oriented muscle synergy extraction using an autoencoder-based neural model”. In: *Information* 11.4 (2020), p. 219.

[116] Michele Benzi and Christine Klymko. “Total communicability as a centrality measure”. In: *Journal of Complex Networks* 1.2 (2013), pp. 124–149.

[117] Michael H Schwartz, Adam Rozumalski, and Katherine M Steele. “Dynamic motor control is associated with treatment outcomes for children with cerebral palsy”. In: *Developmental Medicine & Child Neurology* 58.11 (2016), pp. 1139–1145.

[118] Katherine M Steele, Adam Rozumalski, and Michael H Schwartz. “Muscle synergies and complexity of neuromuscular control during gait in cerebral palsy”. In: *Developmental Medicine & Child Neurology* 57.12 (2015), pp. 1176–1182.

[119] Armin Bunde and Shlomo Havlin. *Fractals and disordered systems*. Springer Science & Business Media, 2012.

[120] Per Bak, Chao Tang, and Kurt Wiesenfeld. "Self-organized criticality: An explanation of the 1/f noise". In: *Physical review letters* 59.4 (1987), p. 381.

[121] Gilles Didier, Alberto Valdeolivas, and Anaıs Baudot. "Identifying communities from multiplex biological networks by randomized optimization of modularity". In: *F1000Research* 7 (2018).

[122] Matteo Magnani et al. "Community detection in multiplex networks". In: *ACM Computing Surveys (CSUR)* 54.3 (2021), pp. 1–35.

[123] Russell L Hardesty et al. "Computational evidence for nonlinear feedforward modulation of fusimotor drive to antagonistic co-contracting muscles". In: *Scientific Reports* 10.1 (2020), p. 10625.

[124] M Cincotta and U Ziemann. "Neurophysiology of unimanual motor control and mirror movements". In: *Clinical Neurophysiology* 119.4 (2008), pp. 744–762.

[125] William McGill. "Multivariate information transmission". In: *Transactions of the IRE Professional Group on Information Theory* 4.4 (1954), pp. 93–111.

[126] Philippe G Schyns et al. "Revealing the information contents of memory within the stimulus information representation framework". In: *Philosophical Transactions of the Royal Society B* 375.1799 (2020), p. 20190705.

[127] Nathaniel T Pickle et al. "The functional roles of muscles during sloped walking". In: *Journal of biomechanics* 49.14 (2016), pp. 3244–3251.

[128] Cristina Brambilla et al. "Spatial and temporal muscle synergies provide a dual characterization of low-dimensional and intermittent control of upper-limb movements". In: *Neuroscience* 514 (2023), pp. 100–122.

[129] Alex H Williams et al. "Unsupervised discovery of demixed, low-dimensional neural dynamics across multiple timescales through tensor component analysis". In: *Neuron* 98.6 (2018), pp. 1099–1115.

[130] Elad Schneidman, William Bialek, and Michael J Berry. "Synergy, redundancy, and independence in population codes". In: *Journal of Neuroscience* 23.37 (2003), pp. 11539–11553.

[131] Sunny Nigam, Sorin Pojoga, and Valentin Dragoi. "Synergistic coding of visual information in columnar networks". In: *Neuron* 104.2 (2019), pp. 402–411.

[132] Andrea I Luppi et al. "A synergistic core for human brain evolution and cognition". In: *Nature Neuroscience* 25.6 (2022), pp. 771–782.

[133] Anne E Urai et al. "Large-scale neural recordings call for new insights to link brain and behavior". In: *Nature neuroscience* 25.1 (2022), pp. 11–19.

[134] Alessandro Del Vecchio et al. "Common synaptic inputs are not distributed homogeneously among the motor neurons that innervate synergistic muscles". In: *BioRxiv* (2022), pp. 2022–01.

[135] Daniele Borzelli et al. "Independent synaptic inputs to motor neurons driving antagonist muscles". In: *bioRxiv* (2022), pp. 2022–08.

[136] Luisa Sartori, Elisa Straulino, and Umberto Castiello. "How objects are grasped: the interplay between affordances and end-goals". In: *PloS one* 6.9 (2011), e25203.

[137] Natalia Dounskaia et al. "A simple joint control pattern dominates performance of unconstrained arm movements of daily living tasks". In: *PloS one* 15.7 (2020), e0235813.

[138] Giulia Dominijanni et al. "The neural resource allocation problem when enhancing human bodies with extra robotic limbs". In: *Nature Machine Intelligence* 3.10 (2021), pp. 850–860.

[139] Rick A Adams, Stewart Shipp, and Karl J Friston. “Predictions not commands: active inference in the motor system”. In: *Brain Structure and Function* 218 (2013), pp. 611–643.

[140] Ernesto Estrada and Naomichi Hatano. “Communicability in complex networks”. In: *Physical Review E* 77.3 (2008), p. 036111.

[141] Michael Levin. “Collective intelligence of morphogenesis as a teleonomic process”. In: (2022).

[142] Virgil Griffith and Christof Koch. “Quantifying synergistic mutual information”. In: *Guided self-organization: inception*. Springer, 2014, pp. 159–190.

[143] Paolo Perrone and Nihat Ay. “Hierarchical quantification of synergy in channels”. In: *Frontiers in Robotics and AI* 2 (2016), p. 35.

[144] Paola Salmas and Vincent CK Cheung. “Gradient descent decomposition of force-field motor primitives optogenetically elicited for motor mapping of the murine lumbosacral spinal cord”. In: *Zoological Research* 44.3 (2023), p. 604.

[145] David Ó’ Reilly and Ioannis Delis. “Dissecting muscle synergies in the task space”. In: *bioRxiv* (2023), pp. 2023–03.

[146] Michael Dimitriou. “Human muscle spindles are wired to function as controllable signal-processing devices”. In: *Elife* 11 (2022), e78091.

[147] Emanuele Formento, Paul Botros, and Jose M Carmena. “Skilled independent control of individual motor units via a non-invasive neuromuscular–machine interface”. In: *Journal of Neural Engineering* 18.6 (2021), p. 066019.

[148] Jeroen Aeles et al. “Revealing the unique features of each individual’s muscle activation signatures”. In: *Journal of the Royal Society Interface* 18.174 (2021), p. 20200770.

[149] Shirin Madarshahian, John Letizi, and Mark L Latash. “Synergic control of a single muscle: The example of flexor digitorum superficialis”. In: *The Journal of Physiology* 599.4 (2021), pp. 1261–1279.

[150] Shirin Madarshahian and Mark L Latash. “Synergies at the level of motor units in single-finger and multi-finger tasks”. In: *Experimental Brain Research* 239 (2021), pp. 2905–2923.

[151] Shirin Madarshahian and Mark L Latash. “Effects of hand muscle function and dominance on intra-muscle synergies”. In: *Human Movement Science* 82 (2022), p. 102936.

[152] Robin AA Ince. “Measuring multivariate redundant information with pointwise common change in surprisal”. In: *Entropy* 19.7 (2017), p. 318.

[153] Yong-Yeol Ahn, James P Bagrow, and Sune Lehmann. “Link communities reveal multiscale complexity in networks”. In: *nature* 466.7307 (2010), pp. 761–764.

[154] Chang Ye et al. “A Tensor Decomposition Uncovers the Effect of Ageing on Muscle and Grip-Load Force Couplings During Grasping”. In: *bioRxiv* (2022), pp. 2022–02.

[155] Christoph Daube, Robin AA Ince, and Joachim Gross. “Simple acoustic features can explain phoneme-based predictions of cortical responses to speech”. In: *Current Biology* 29.12 (2019), pp. 1924–1937.

[156] Jonathan Z Bakdash and Laura R Marusich. “Repeated measures correlation”. In: *Frontiers in psychology* 8 (2017), p. 456.

[157] Sandra K Hunter, Hugo M Pereira, and Kevin G Keenan. “The aging neuromuscular system and motor performance”. In: *Journal of applied physiology* (2016).

[158] Aswin Paul et al. “On efficient computation in active inference”. In: *arXiv preprint arXiv:2307.00504* (2023).

[159] Martijn P Van Den Heuvel et al. “High-cost, high-capacity backbone for global brain communication”. In: *Proceedings of the National Academy of Sciences* 109.28 (2012), pp. 11372–11377.

[160] Andrea Avena-Koenigsberger, Bratislav Misic, and Olaf Sporns. “Communication dynamics in complex brain networks”. In: *Nature reviews neuroscience* 19.1 (2018), pp. 17–33.

[161] Roland S Johansson and J Randall Flanagan. “Coding and use of tactile signals from the fingertips in object manipulation tasks”. In: *Nature Reviews Neuroscience* 10.5 (2009), pp. 345–359.

[162] Caio Seguin et al. “Network communication models narrow the gap between the modular organization of structural and functional brain networks”. In: *NeuroImage* 257 (2022), p. 119323.

[163] Anagh Pathak et al. “Biophysical mechanism underlying compensatory preservation of neural synchrony over the adult lifespan”. In: *Communications Biology* 5.1 (2022), p. 567.

[164] Freschta Zipser-Mohammadzada et al. “Intramuscular coherence during challenging walking in incomplete spinal cord injury: Reduced high-frequency coherence reflects impaired supra-spinal control”. In: *Frontiers in human neuroscience* 16 (2022), p. 927704.

[165] Christopher M Laine, Brian A Cohn, and Francisco J Valero-Cuevas. “Temporal control of muscle synergies is linked with alpha-band neural drive”. In: *The Journal of physiology* 599.13 (2021), pp. 3385–3402.

[166] Coen S Zandvoort, Andreas Daffertshofer, and Nadia Dominici. “Cortical contributions to locomotor primitives in toddlers and adults”. In: *Iscience* 25.10 (2022), p. 105229.

[167] Jens Schouenborg. “Action-based sensory encoding in spinal sensorimotor circuits”. In: *Brain research reviews* 57.1 (2008), pp. 111–117.

[168] Paul L Williams and Randall D Beer. “Nonnegative decomposition of multivariate information”. In: *arXiv preprint arXiv:1004.2515* (2010).

[169] Nicholas Timme et al. “Synergy, redundancy, and multivariate information measures: an experimentalist’s perspective”. In: *Journal of computational neuroscience* 36 (2014), pp. 119–140.

[170] Ioannis Delis et al. “Neural encoding of active multi-sensing enhances perceptual decision-making via a synergistic cross-modal interaction”. In: *Journal of Neuroscience* 42.11 (2022), pp. 2344–2355.

[171] Ming Li et al. “Percolation on complex networks: Theory and application”. In: *Physics Reports* 907 (2021), pp. 1–68.

[172] Rostam M Razban et al. “Early path dominance as a principle for neurodevelopment”. In: *Proceedings of the National Academy of Sciences* 120.16 (2023), e2218007120.

[173] Vincent CK Cheung et al. “Muscle synergy patterns as physiological markers of motor cortical damage”. In: *Proceedings of the national academy of sciences* 109.36 (2012), pp. 14652–14656.

[174] Lara McManus, Giuseppe De Vito, and Madeleine M Lowery. “Analysis and biophysics of surface EMG for physiotherapists and kinesiologists: Toward a common language with rehabilitation engineers”. In: *Frontiers in neurology* 11 (2020), p. 576729.

[175] Thomas F Varley et al. “Partial entropy decomposition reveals higher-order information structures in human brain activity”. In: *Proceedings of the National Academy of Sciences* 120.30 (2023), e2300888120.

[176] Federico Battiston et al. “Networks beyond pairwise interactions: Structure and dynamics”. In: *Physics Reports* 874 (2020), pp. 1–92.

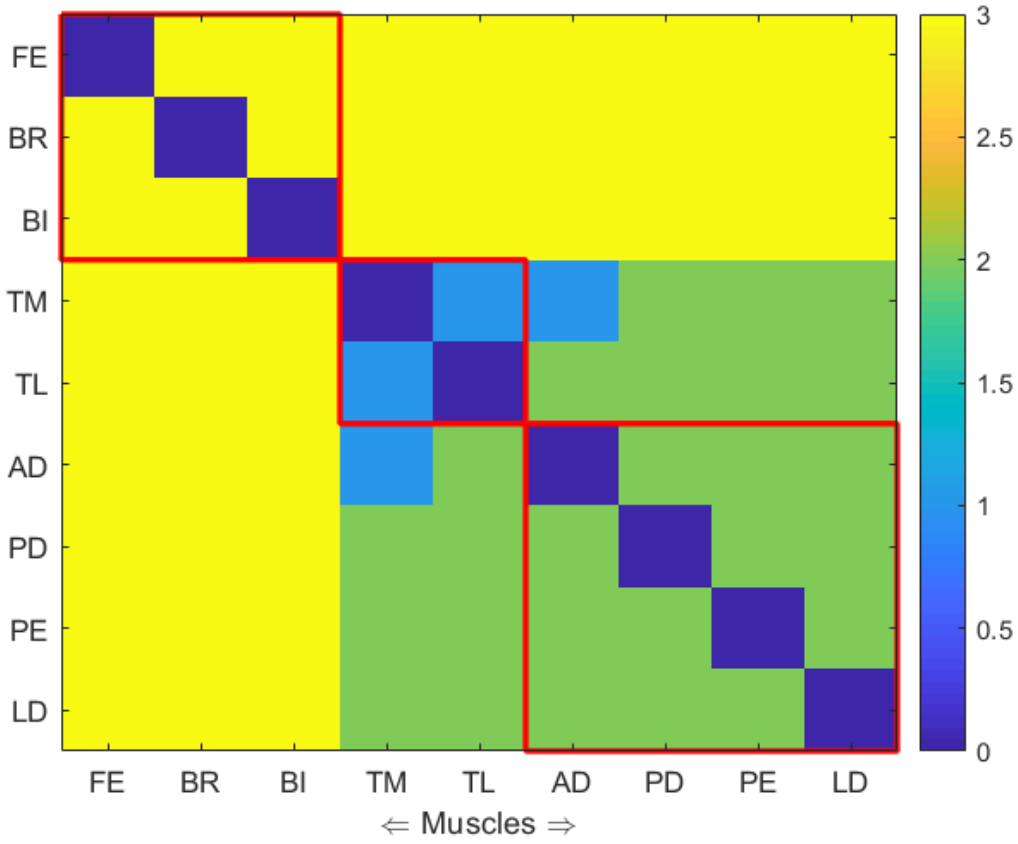

Fig.1: An example of the cluster assignment verification procedure described in the Materials and methods section applied to dataset 1. The red grid lines represent the hard-clustering assignment provided by the generalised Louvain algorithm while the colours in the adjacency matrix indicate the cluster assignment produced by PNMF.

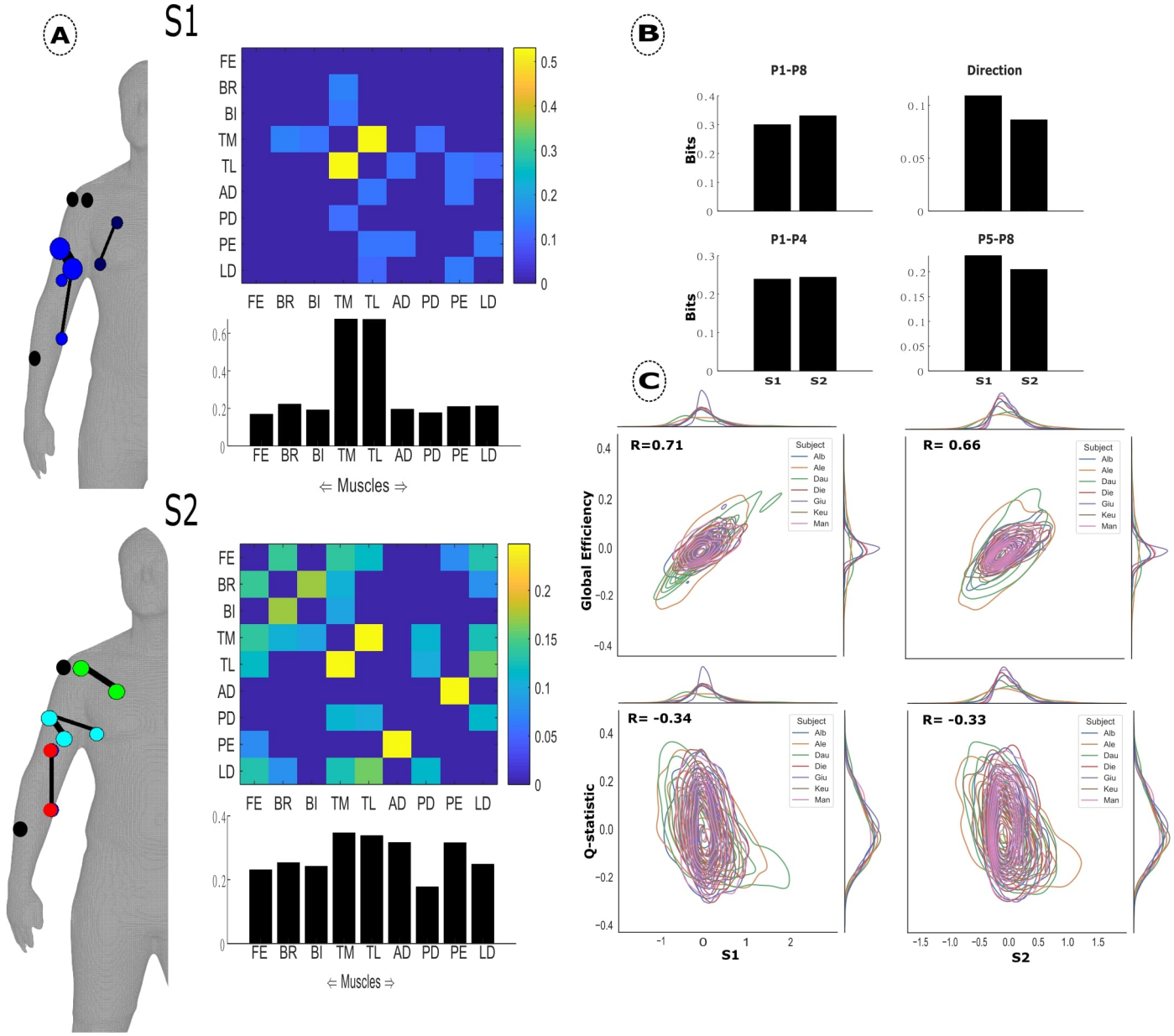

Fig.2: **(A)** The average spatial synergies across participants. The bar graph below represents the average values in each column of the adjacency matrix. The human body models illustrates the values in the adjacency matrix with the width of the edges and colour and size of the nodes providing insight into connection strengths, modular structure and involvement respectively [81]. Submodular structure was identified using the conventional Louvain algorithm on the synergy matrices [72]. Unconnected nodes are in black. **(B)** The average task encoded information for two spatial synergies found to be representative of dataset 1 participants. The task attributes analysed included: P1-P8, P1-P4, P5-P8 and Direction. **(C)** Average correlation between trial-to-trial fluctuations in Global Efficiency/Q-statistic for modularity and noise in the spatial activation coefficients across participants. The curves along the axes of each plot are kernel density estimates for each participants' x- and y-variables.

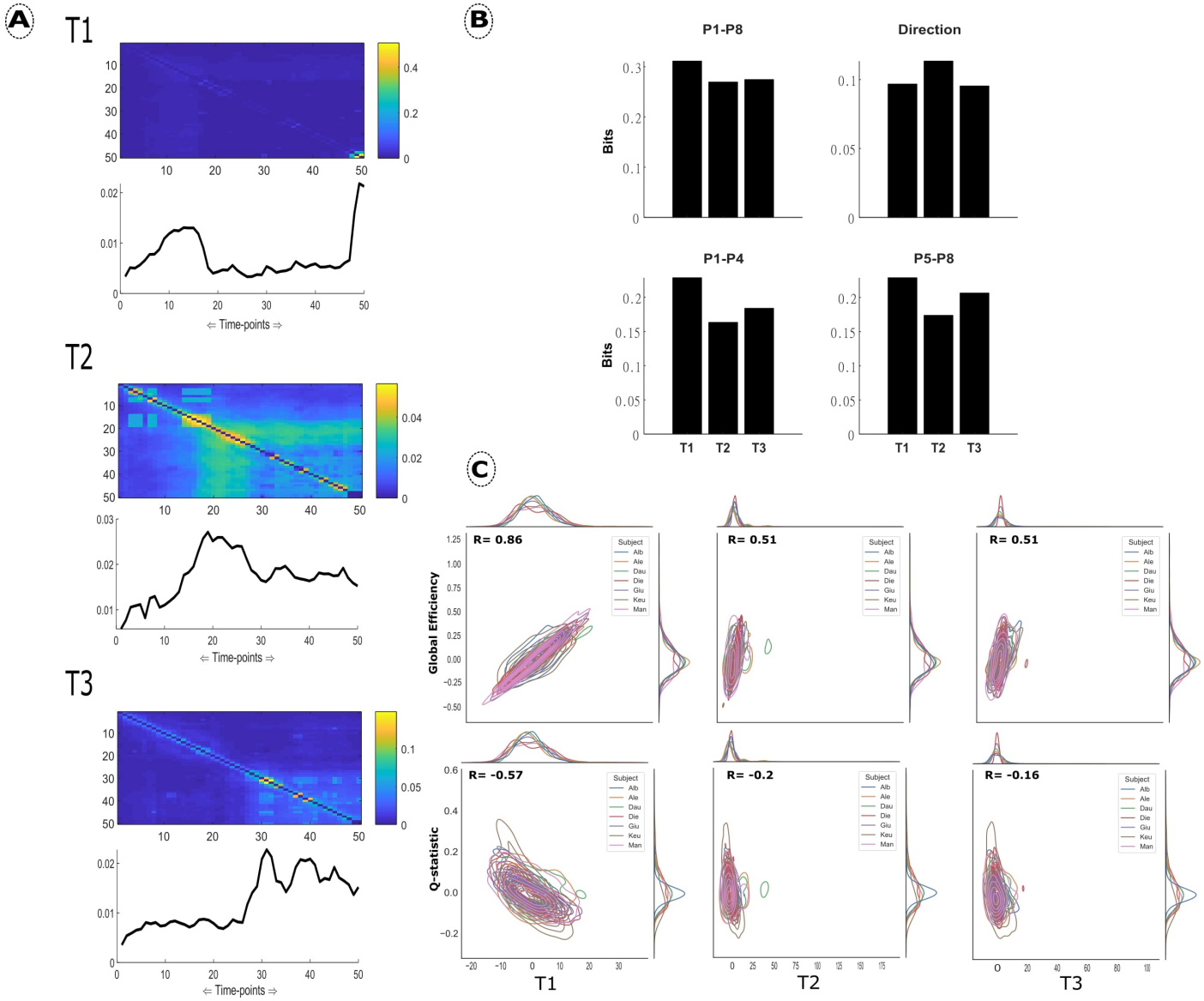

Fig.3: **(A)** The average temporal synergies across participants in Dataset 1. The line plots represent the average of each column in the adjacency matrix above. **(B)** The average task encoded information for three temporal synergies found to be representative of dataset 1 participants. The task attributes analysed included: P1-P8, P1-P4, P5-P8 and Direction. **(C)** The average noise correlation between temporal synergy activations and Global Efficiency/Q-statistic across participants. The curves along the axes of each plot are kernel density estimates for each participants' x- and y-variables.

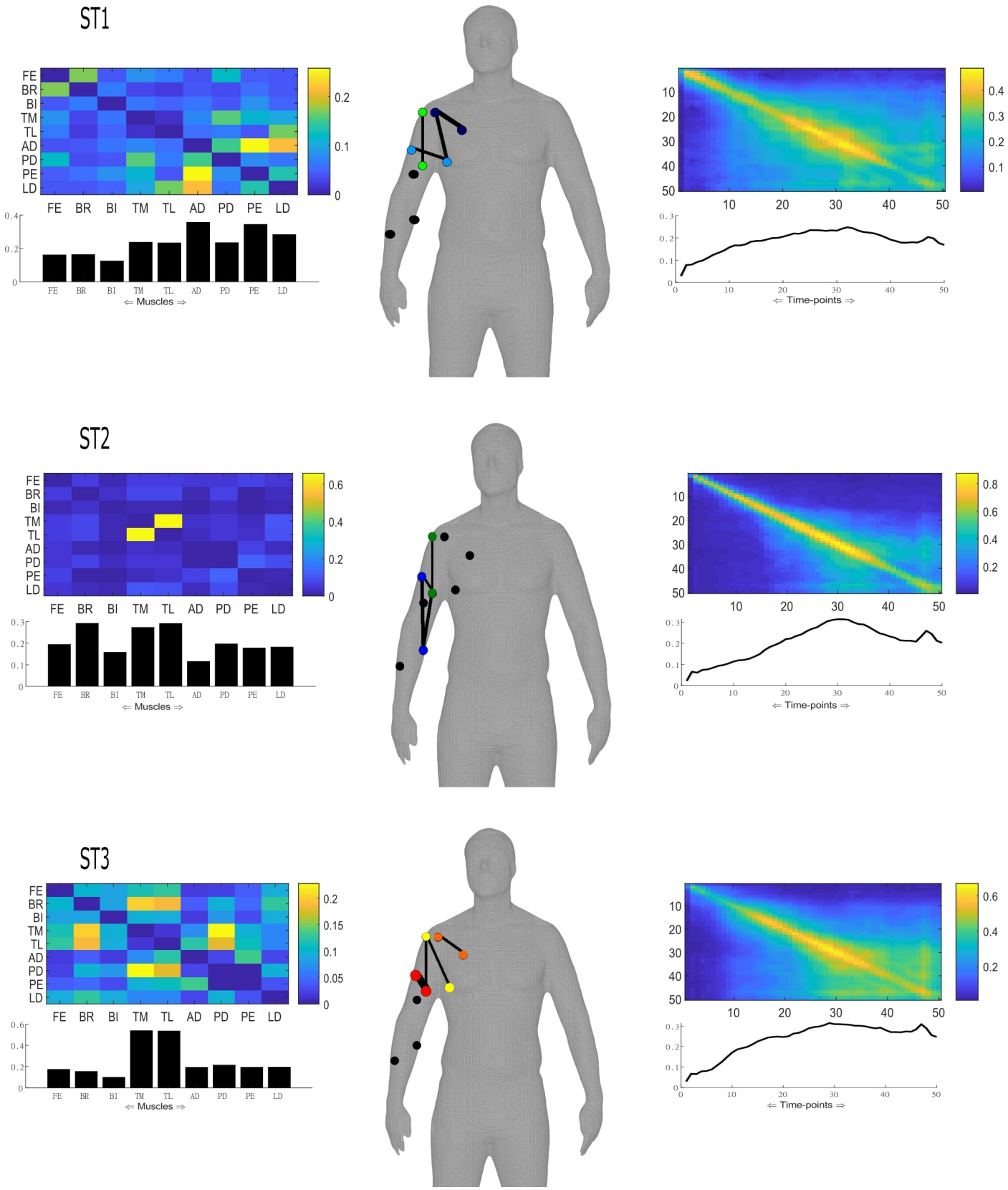

Fig.4: The average space-time synergies across participants in dataset 1. Spatial and temporal synergies correspond on a 1:1 basis as shown across rows. The bar/line plots represent the average of each column in the adjacency matrix above. The human body model illustrates the values in the adjacency matrix with the width of the edges and colour and size of the nodes providing insight into connection strengths, submodular structure and involvement respectively [81]. Submodular structure was identified using the conventional Louvain algorithm on the muscle synergy matrices [72]. Unconnected nodes are in black.

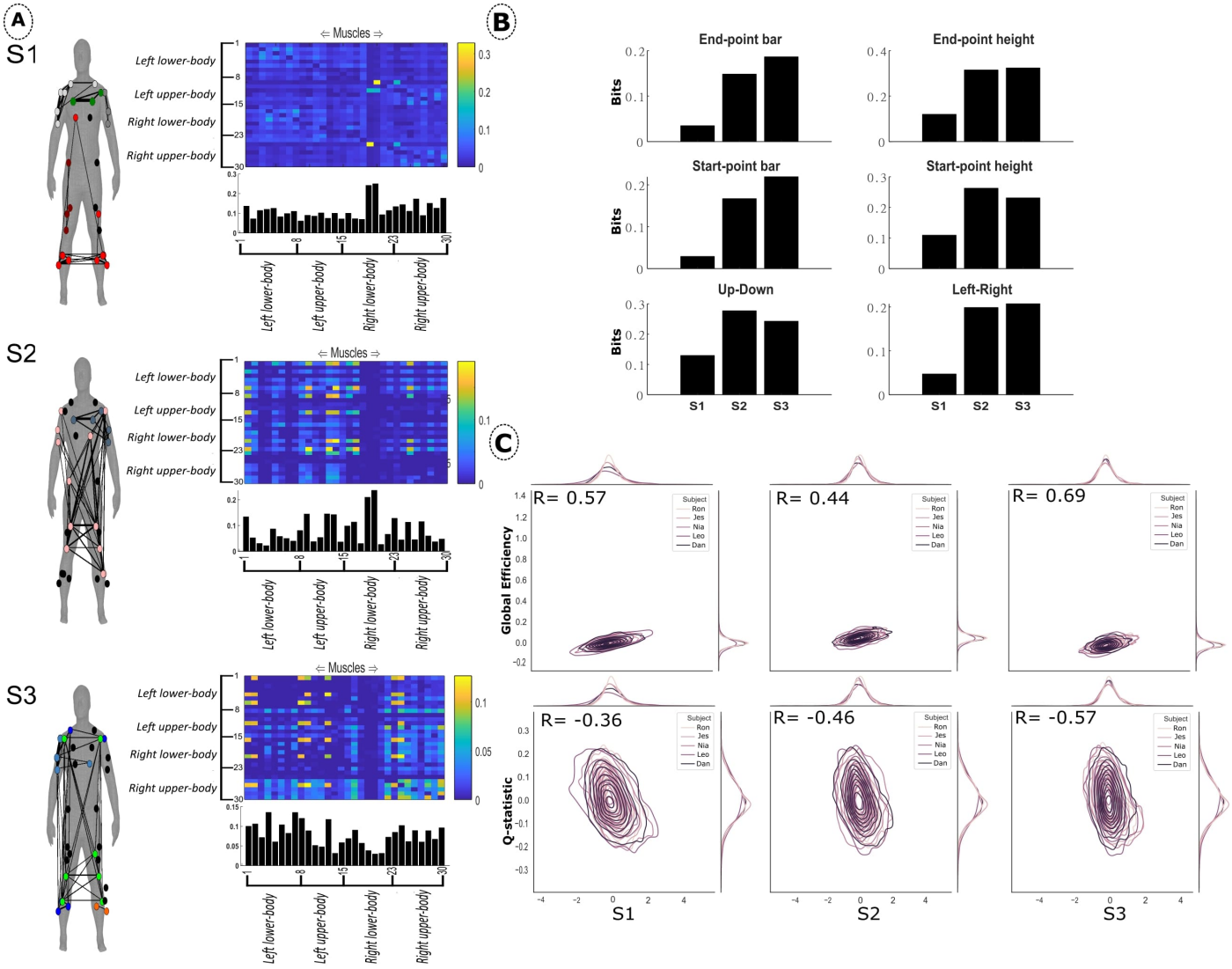

Fig.5: **(A)** The average spatial synergies across participants in dataset 2. The adjacency matrices are organised so that rows 1-8: left lower-limb, rows 9-15: left upper-body, rows 16-23: right lower-limbs and rows 24-30: right upper-body. The width of the edges on the human body model and the size and colour of the nodes indicate the connection strength, node involvement and submodular structure respectively [81]. Submodular structure was identified using the conventional Louvain algorithm on the synergy matrices [72]. Unconnected nodes are in black. **(B)** The average information encoded for six task attributes is presented in bits. **(C)** The average noise correlations between spatial synergy activations and Global Efficiency/Q-statistic across participants. The curves along the axes of each plot are kernel density estimates for each participants' x- and y-variables.

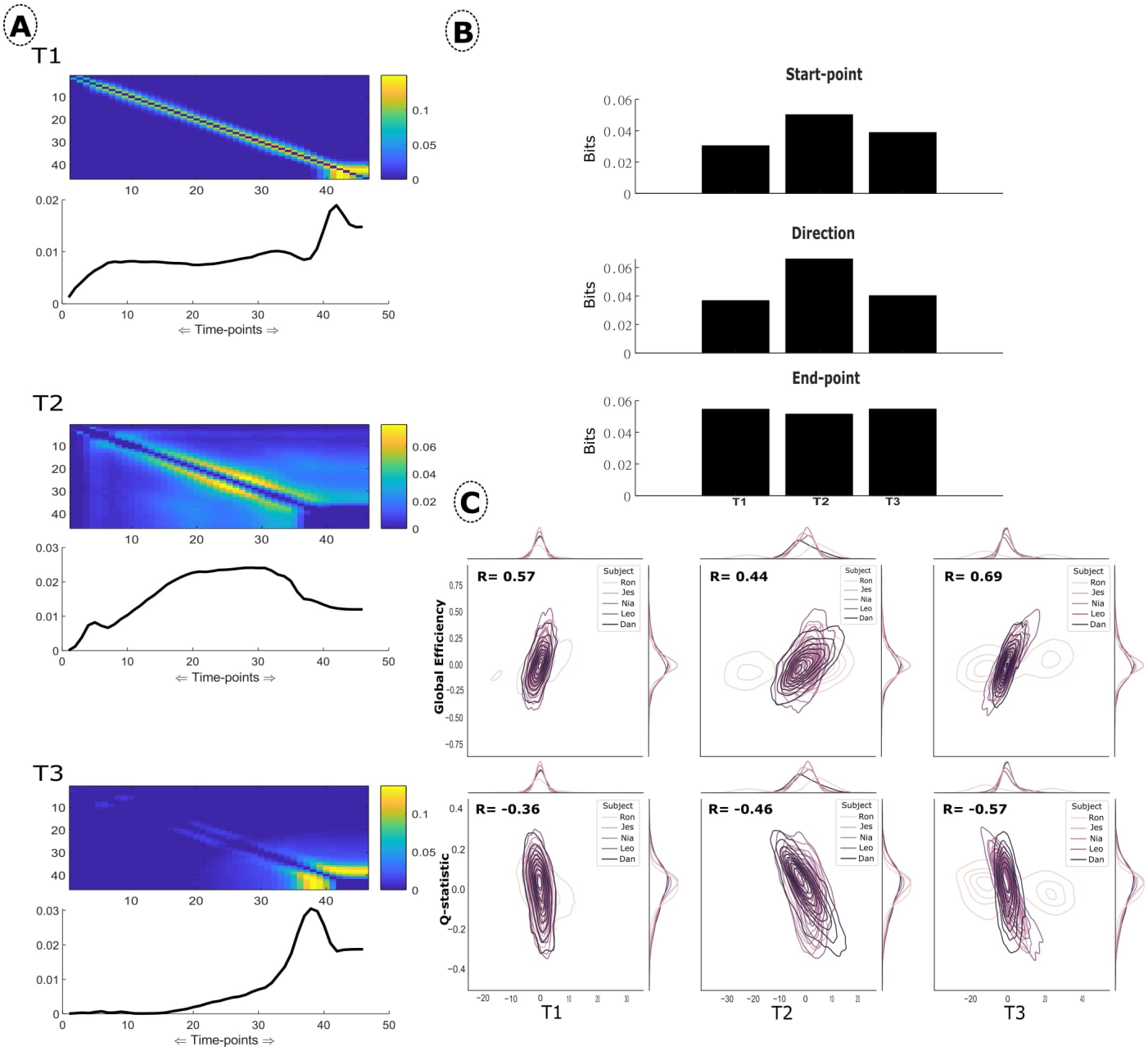

Fig.6:**(A)** The average temporal synergies extracted from dataset 2. The line plots represent the average of each column in the adjacency matrix above. **(B)** The mean task-encoded information for start- and end-points and direction. **(C)** The average noise correlations between temporal synergy activations and Global Efficiency/Q-statistic across participants. The curves along the axes of each plot are kernel density estimates for each participants' x- and y-variables.

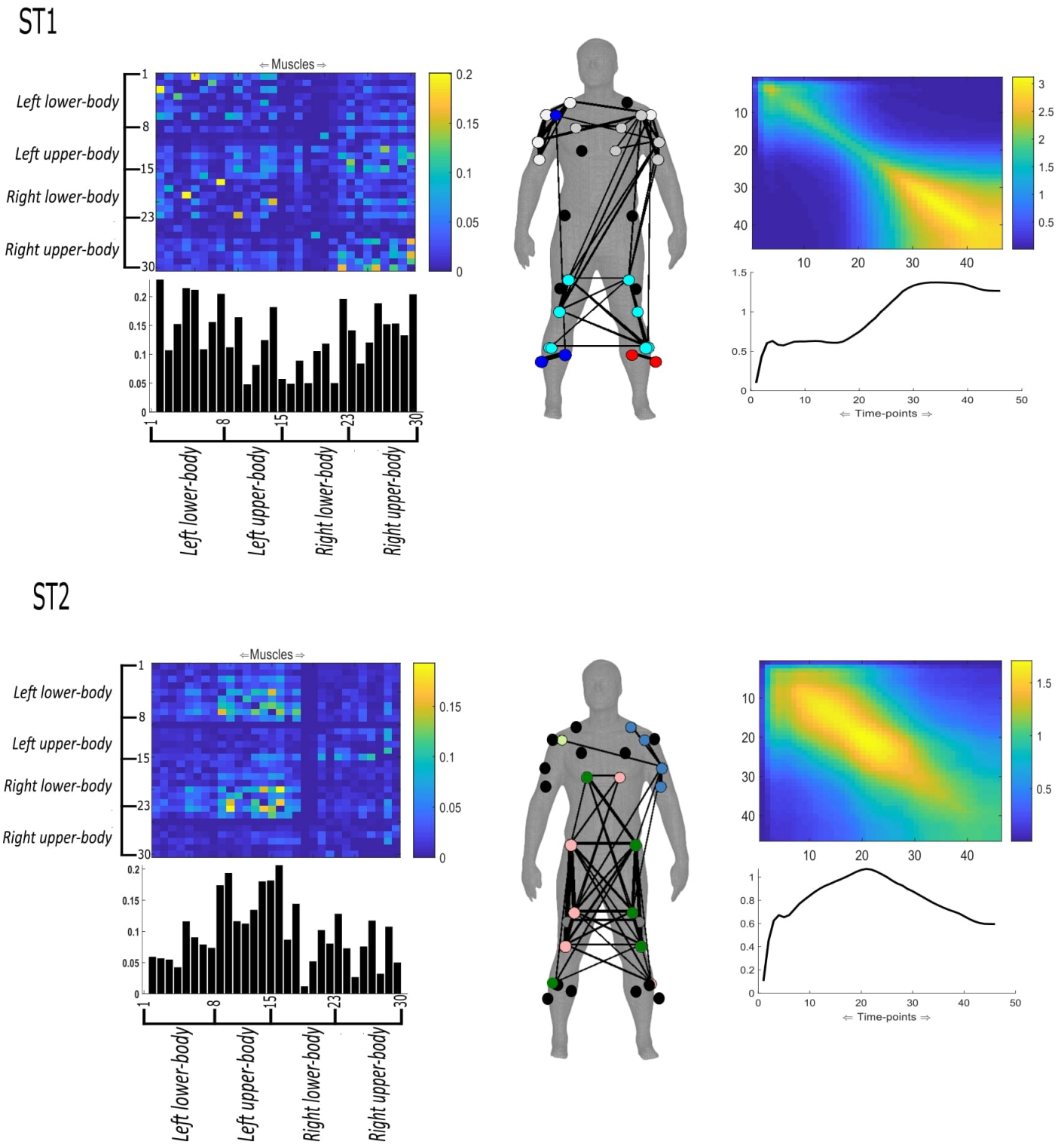

Fig.7: The average Space-Time synergies from dataset 2. Spatial and temporal synergies correspond on a 1:1 basis here as presented across rows. The spatial synergies are organised so that rows 1-8: left lower-limb, rows 9-15: left upper-body , rows 16-23: right lower-limbs and rows 24-30: right upper-body. The bar/line plots represent the average of each column in the adjacency matrix above. The connection strengths, submodular structure and involvement of nodes are indicated by the human body model via the edge widths, node colour and size respectively [81]. Submodular structure was identified using the conventional Louvain algorithm on the synergy matrices [72]. Unconnected nodes are in black.

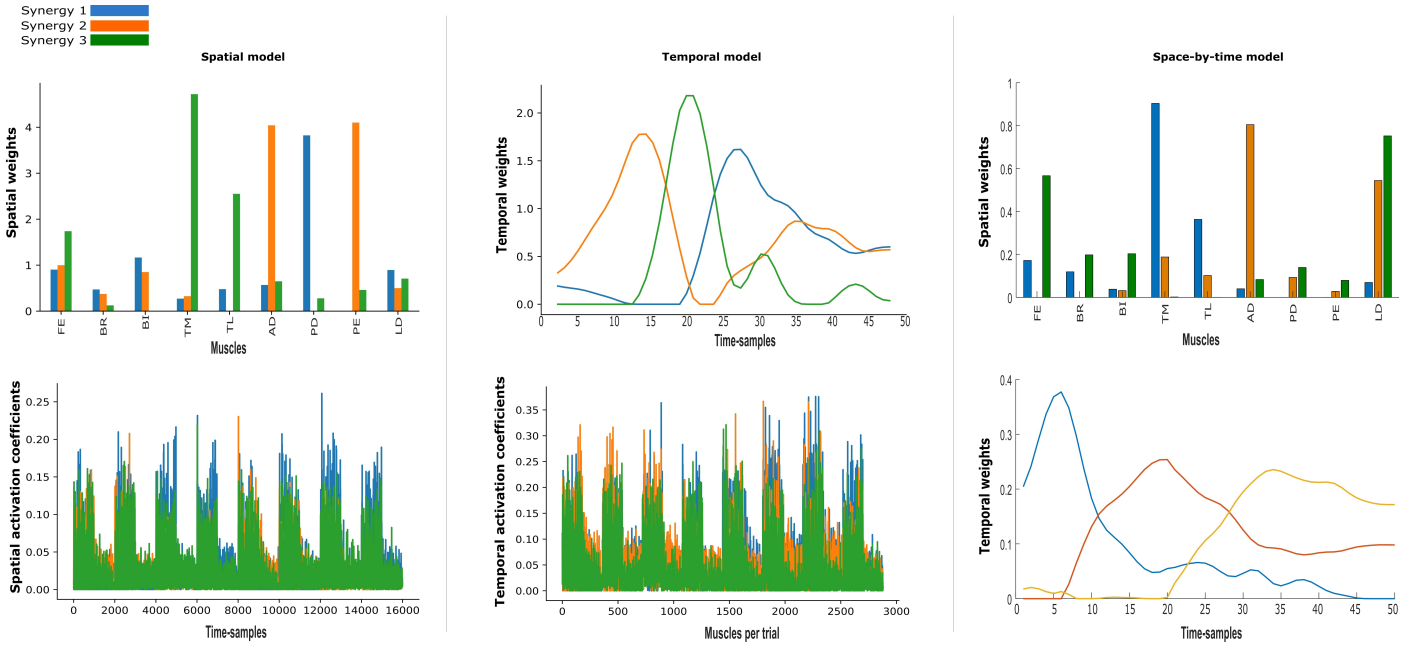

Fig.8: The application of current muscle synergy models to the example participant in dataset 1. A model rank of three was selected for all to assist in comparability with the GCMI frameworks output. Both the spatial and temporal models' synergies were extracted using non-negative matrix factorisation. The synergies presented for the space-by-time model were extracted using a non-negative matrix tri-factorisation method [23].

Comparison of proposed framework with existing approaches

An aim of this study was to develop a framework for the extraction of muscle synergies that would alleviate limitations in the current models including linearity and a lack of flexibility and generalisability. Here, we wish to further highlight some of the commonalities of proposed GCMI framework with existing models and outline the advantages of the proposed framework. In Fig.8 of this document, we present the output from an application of the spatial, temporal and space-by-time models to the nine muscle EMG data of the same example participant (Dataset 1) presented in the main text. This dataset consisted of 320 trials of fast reaching movements in various targets and in forward and backward directions.

Starting with the spatial synergy model, the medial- and lateral triceps (TM,TL) are predominant in the third synergy while more proximal musculature surrounding the shoulder joint (anterior deltoid (AD) and pectoralis major (PE)) are emphasised in the second synergy (Fig. 8). This grouping of muscles with respect to anatomical proximity is also captured in the GCMI spatial synergy model (Fig.5 of main text). However, the coupling between the finger extensors (FE), brachioradialis (BR) and biceps brachii (BI) is uniquely captured in S3 of Fig.5 (main text) while the only feature these muscles share in the spatial model of Fig. 8 is a shared relatively low-weighting across all three synergies. This example demonstrates how the current spatial synergy model, due to its reliance on variance explained, may put an emphasis on muscles with a predominant role in the movement and which explain most of the variance in the dataset. This inevitably comes at the expense of more subtle couplings such as in the forearm musculature here.

The temporal synergies produced by the GCMI temporal model are highly consistent with what is produced by the current temporal and space-by-time models. In contrast, the output of the space-time model we introduced here differs significantly from any other model, with a co-activation synergy and two tonic waveforms. This is probably a result of the current formulation of the space-time model, which simultaneously extracts spatial and temporal modules that are consistent across trials. This trial-by-trial consistency is a unique feature of the space-time model that can be used to reveal couplings that are shared across tasks or experimental conditions. For instance, ST3 is unique to the GCMI output with no such shared weighting among the triceps with the posterior deltoid (PD) found in the space-by-time model output.

Another notable advantage of the GCMI formulation is that the specific timing of movement onset and cessation is more interpretable due to the orthogonality introduced during cluster extraction. For example, T2 of Fig.6 (main text) illustrates a phasic burst of activation at time-sample 15-23 approximately that share information with the remaining time-samples in the movement, an attribute not present in the current muscle synergy models.

More importantly, the interaction between individual muscle, time-sample or muscle - time-sample pairings is a novel characteristic of the GCMI framework. As recent evidence has shown [50, 51, 52], a single muscle may belong simultaneously to a number of functional groups, pertaining to the various functional roles a muscle can take on for a given task (e.g. internal

joint stiffness, acceleration-deceleration, postural stabilisation etc.). These pairwise interactions are uniquely present across all three GCMI models, revealing submodular structures that may represent these complex interactions and cannot be inferred by the traditional synergy extraction approaches. The reliance of the current models on dimensionality reduction furthers the significance of this point as the more subtle interactions are potentially not captured at all.

Moreover, the model-rank procedures implemented by the existing approaches seek to optimise the variance accounted for. Although many important findings have been produced, this approach may limit the generalisability and task relevancy of the synergy output [19]. Within the GCMI framework, we implement a data-driven approach for model-rank selection that relies purely on the data structure and the number of identifiable clusters a priori, thus alleviating this limitation.

Finally, the activation coefficients, which are inferred to be the neural commands driving the muscle patterns, are captured across time-samples and across muscles per trial for the spatial and temporal models respectively (supplementary materials Fig.8). This output is difficult to contrast against any specific trial or task, a difficulty overcome by the space-by-time model. In contrast, the GCMI formulation of the spatial and temporal models produces trial-specific modulations which can be easily assessed against other variables of interest, offering greater flexibility in analysis but also a unique within-trial view into the underlying spatial or temporal dynamics.

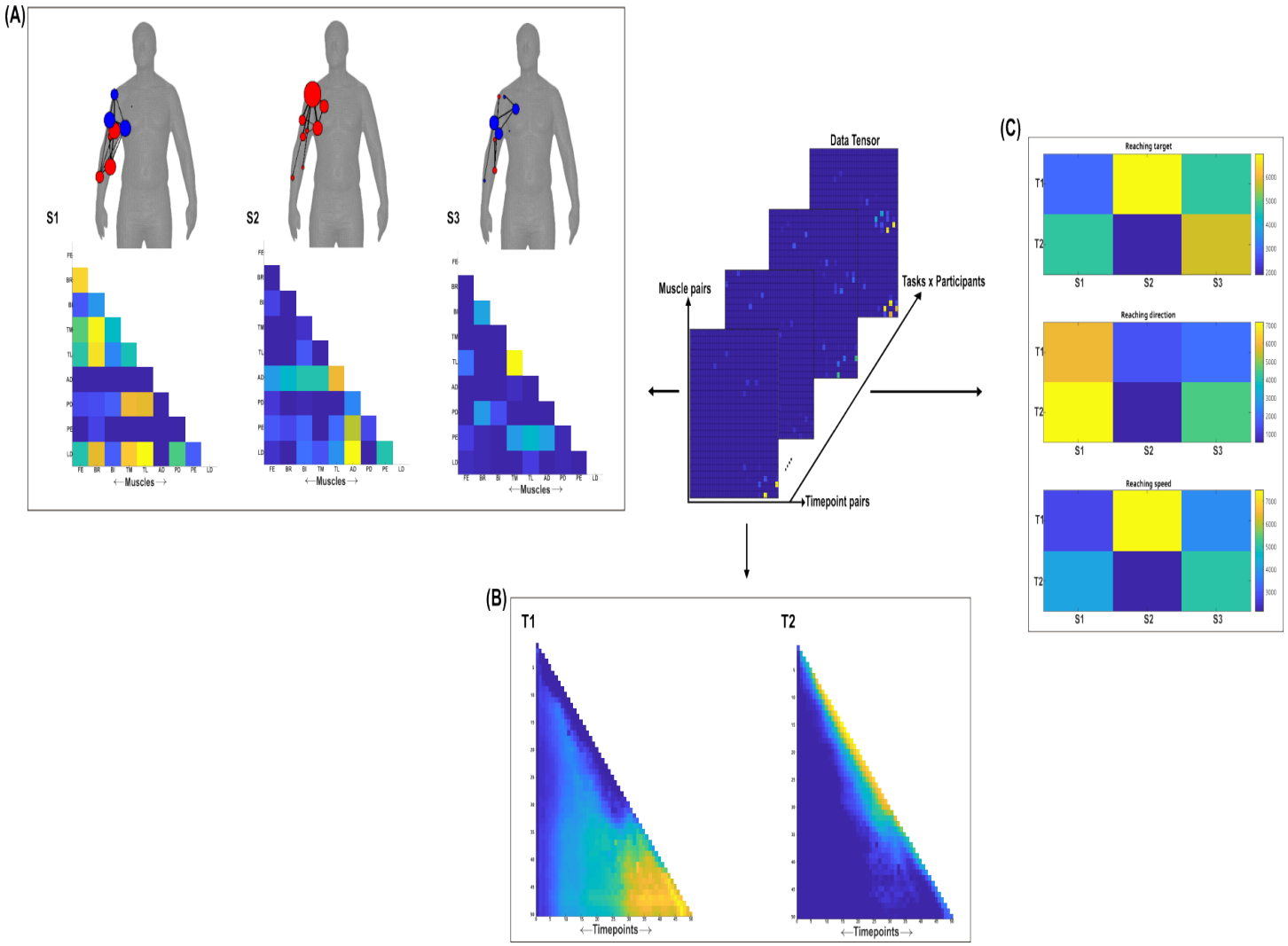

Fig.7-supplementary materials 1: Three spatial (S1-S3) and two temporal task-irrelevant muscle networks (T1-T2) were empirically identified and extracted across participants and task parameters from dataset 1 using the NIF pipeline (Panel **A**-**B**) [107, 23]. Human body models accompanying each spatial network illustrate their respective submodular structure with node colour and size and edge width indicating community affiliation [72], network centrality and connection strength respectively [81, 116]. (Panel **C**) Activation coefficients are presented to the right of the networks, indicating their task parameter-specific scaling averaged across participants.

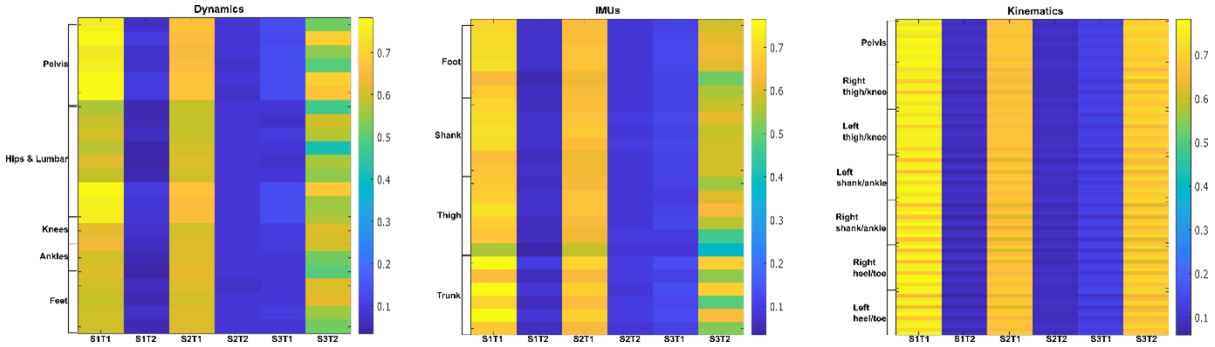

Fig.8-supplementary materials 1: Task-irrelevant activation coefficients (Dataset 3) [113]. Dynamic, inertial motion unit (IMU) and kinematic data were captured from the bilateral lower-limbs while 17 participants performed various locomotion modes (i.e. stair ascents/descents, ramp inclines/declines and level-ground walking). Activation coefficients are averaged across participants.

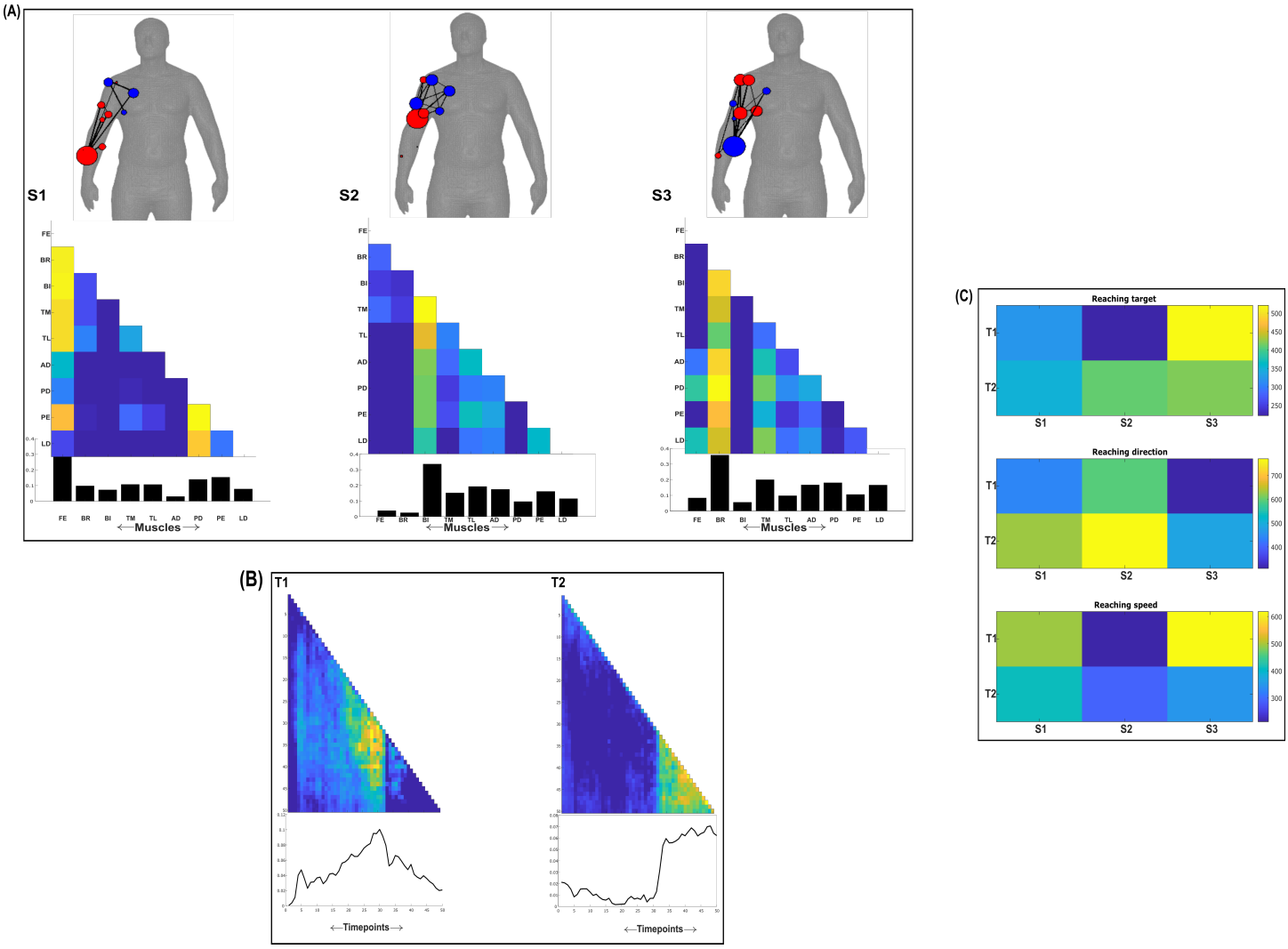

Fig.9-supplementary materials 1: Three spatial (S1-S3) and two temporal task-redundant muscle networks (T1-T2) were empirically identified and extracted across participants and task parameters from dataset 1 using the NIF pipeline (Panel **A**-**B**) [107, 23]. Human body models accompanying each spatial network illustrate their respective submodular structure with node colour and size and edge width indicating community affiliation [72], network centrality and connection strength respectively [81, 116]. (Panel **C**) Activation coefficients are presented to the right of the networks, indicating their task parameter-specific scaling averaged across participants.

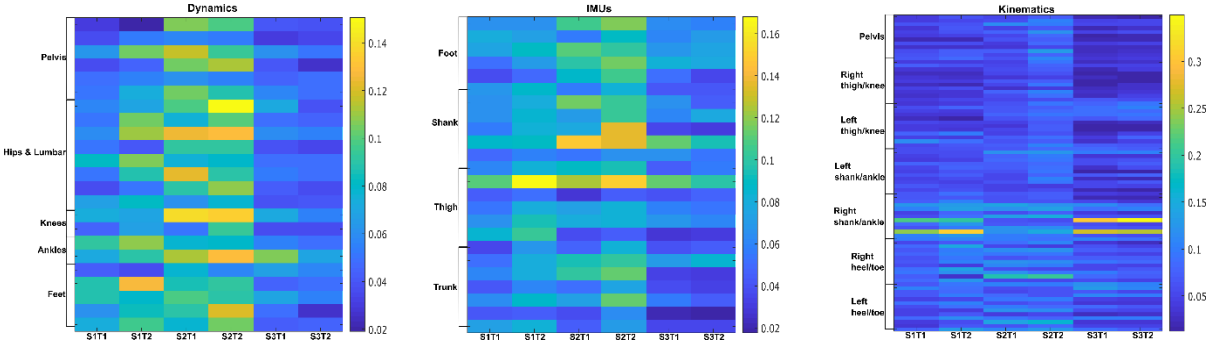

Fig.10-supplementary materials 1: Task-redundant activation coefficients (Dataset 3) [113]. Dynamic, inertial motion unit (IMU) and kinematic data were captured from the bilateral lower-limbs while 17 participants performed various locomotion modes (i.e. stair ascents/descents, ramp inclines/declines and level-ground walking). Activation coefficients are averaged across participants.

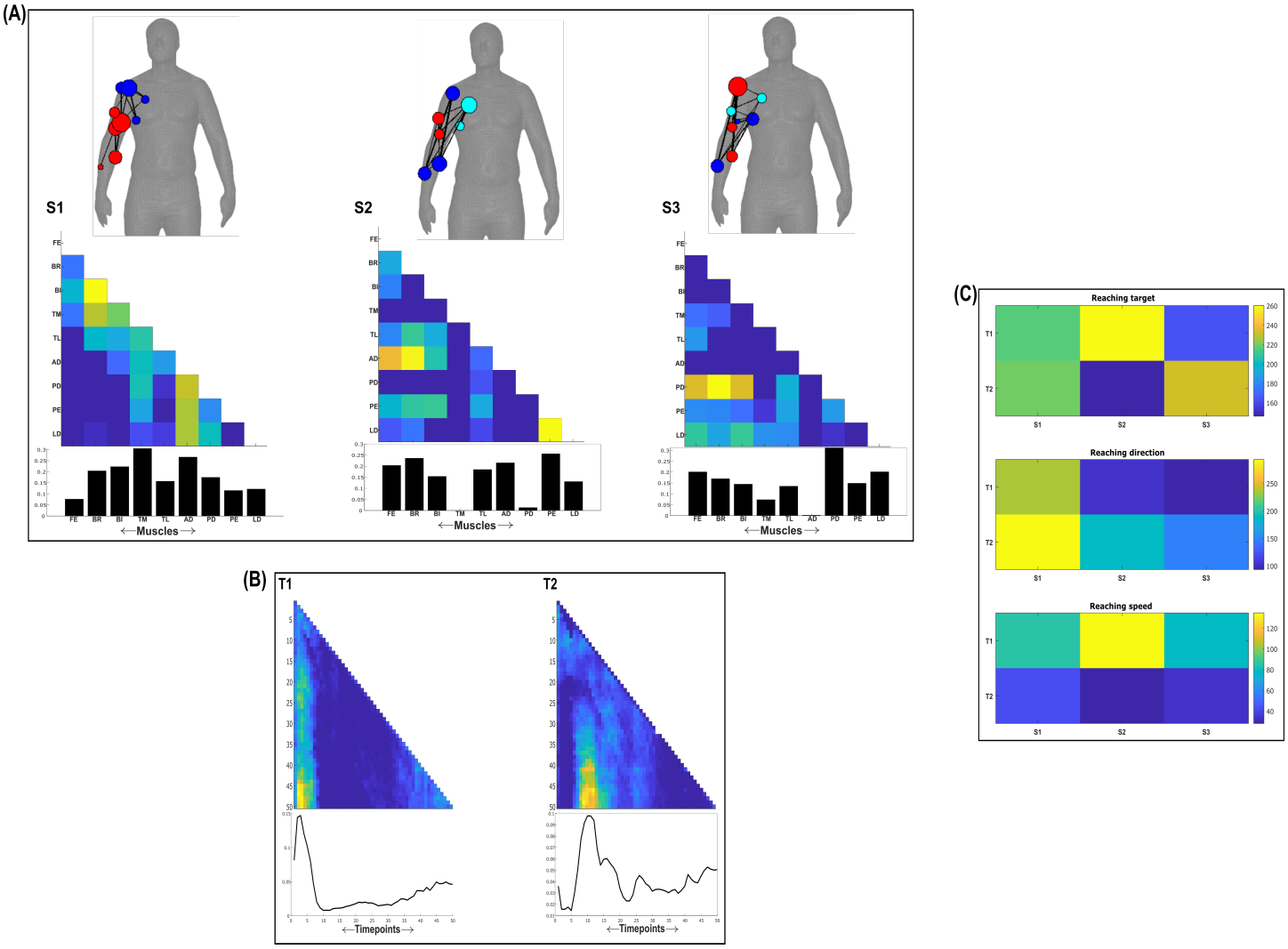

Fig.11-supplementary materials 1: Three spatial (S1-S3) and two temporal task-synergistic muscle networks (T1-T2) were empirically identified and extracted across participants and task parameters from dataset 1 using the NIF pipeline (Panel **A**-**B**) [107, 23]. Human body models accompanying each spatial network illustrate their respective submodular structure with node colour and size and edge width indicating community affiliation [72], network centrality and connection strength respectively [81, 116]. (Panel **C**) Activation coefficients are presented to the right of the networks, indicating their task parameter-specific scaling averaged across participants.

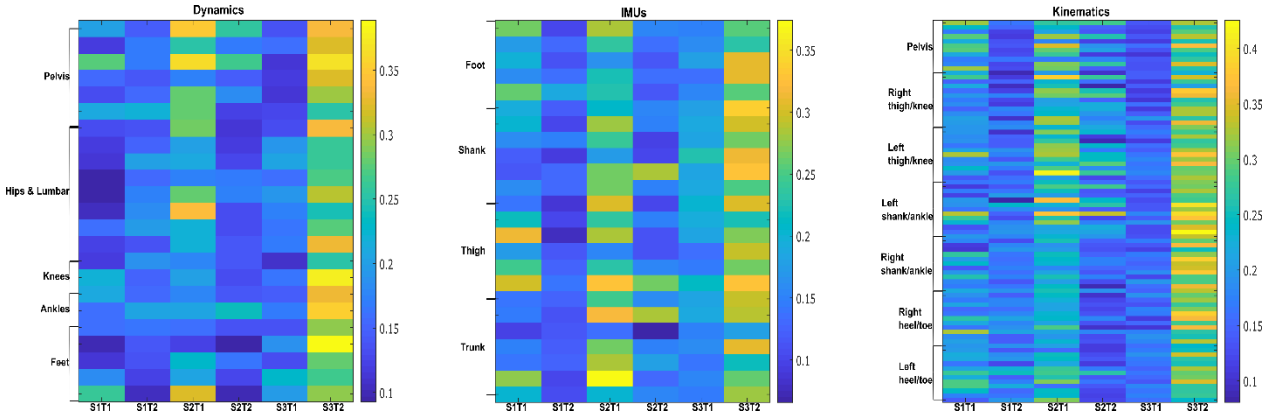

Fig.12-supplementary materials 1: Task-synergistic activation coefficients (Dataset 3) [113]. Dynamic, inertial motion unit (IMU) and kinematic data were captured from the bilateral lower-limbs while 17 participants performed various locomotion modes (i.e. stair ascents/descents, ramp inclines/declines and level-ground walking). Activation coefficients are averaged across participants.

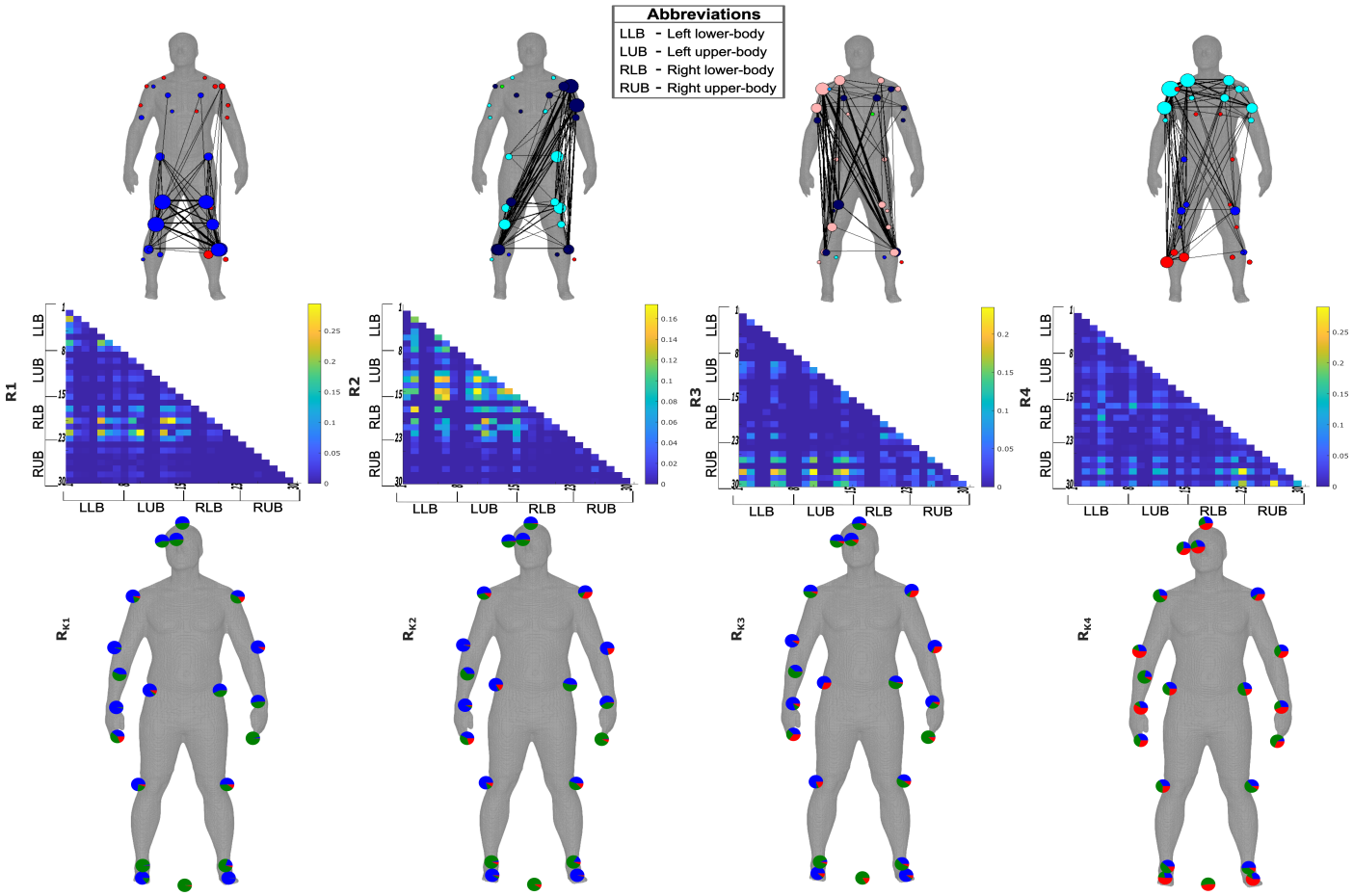

Supp. Fig.1: The R muscle networks (**R1**-**R4**) extracted from the three participants of dataset 1 who performed a variety of whole-body reaching movements. Above R1-R4, their accompanying human body models with muscle networks overlaid illustrating the strongest connectivities (edge-width) [81], the subnetwork community structure (node color) and network centrality (relative node size) [72, 79, 116]. Below the adjacency matrices, the proportional encoding of XYZ kinematics in the activation coefficients averaged across participants ($\mathbf{R_{K1}}$-$\mathbf{R_{K4}}$) are depicted as pie charts (anteroposterior (red), mediolateral (green) and vertical (blue) directions) on corresponding bodily locations of a human body model.

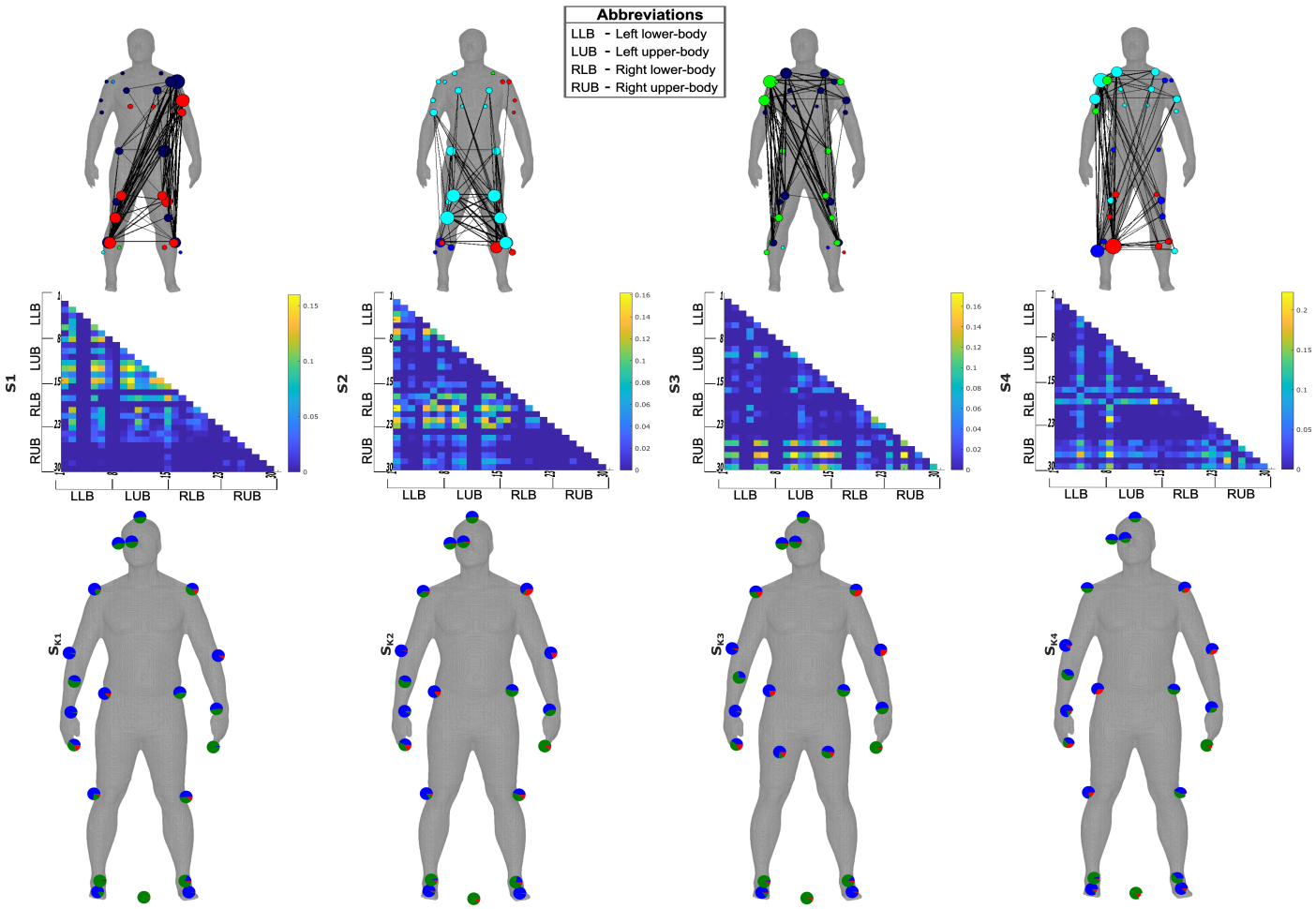

Supp.Fig.2: The S muscle networks (**S1**-**S4**) extracted from the three participants of dataset 1 who performed a variety of whole-body reaching movements. Above S1-S4, their accompanying human body models with muscle networks overlaid illustrating the strongest connectivities (edge-width) [81], the subnetwork community structure (node color) and network centrality (relative node size) [72, 79, 116]. Below, the proportional encoding of XYZ kinematics in the activation coefficients averaged across participants ($\mathbf{S_{K1}}$-$\mathbf{S_{K4}}$) are depicted as pie charts (anteroposterior (red), mediolateral (green) and vertical (blue) directions) on corresponding bodily locations of a human body model.

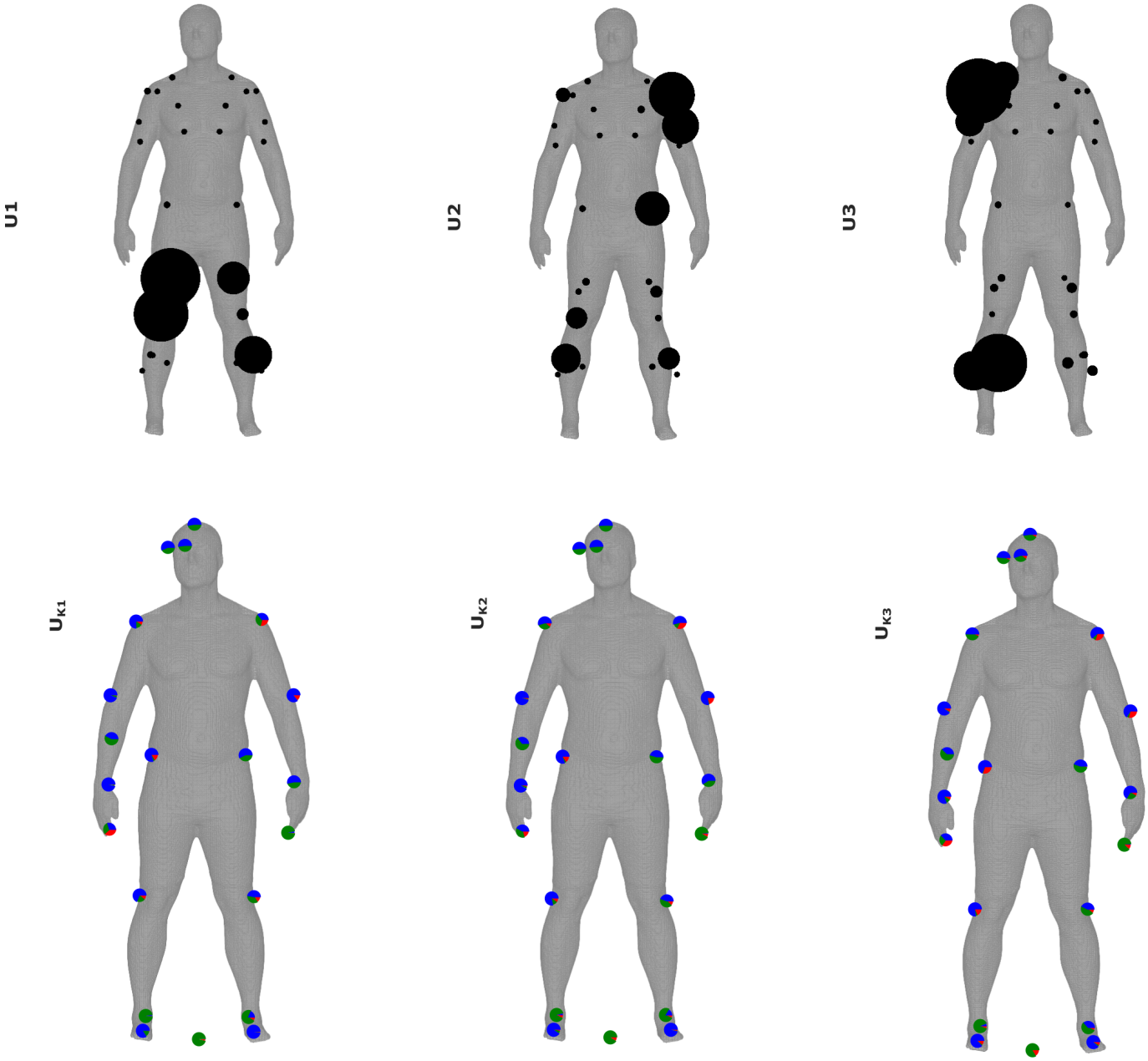

Supp. Fig.3: The U_{xy} modules (**U1-U3**) extracted from the three participants of dataset 1 who performed a variety of whole-body reaching movements. The U_x and U_y terms are not considered as a muscle coupling, as they encode the task information present in one muscle that is not present in another and vice versa, and so instead the average unique information (U_{xy}) for each muscle is presented as the relative side of black nodes on a human body model. Below, the proportional encoding of XYZ kinematics in the activation coefficients averaged across participants ($\mathbf{U_{K1}}$-$\mathbf{U_{K3}}$) are depicted as pie charts (anteroposterior (red), mediolateral (green) and vertical (blue) directions) on corresponding bodily locations of a human body model.

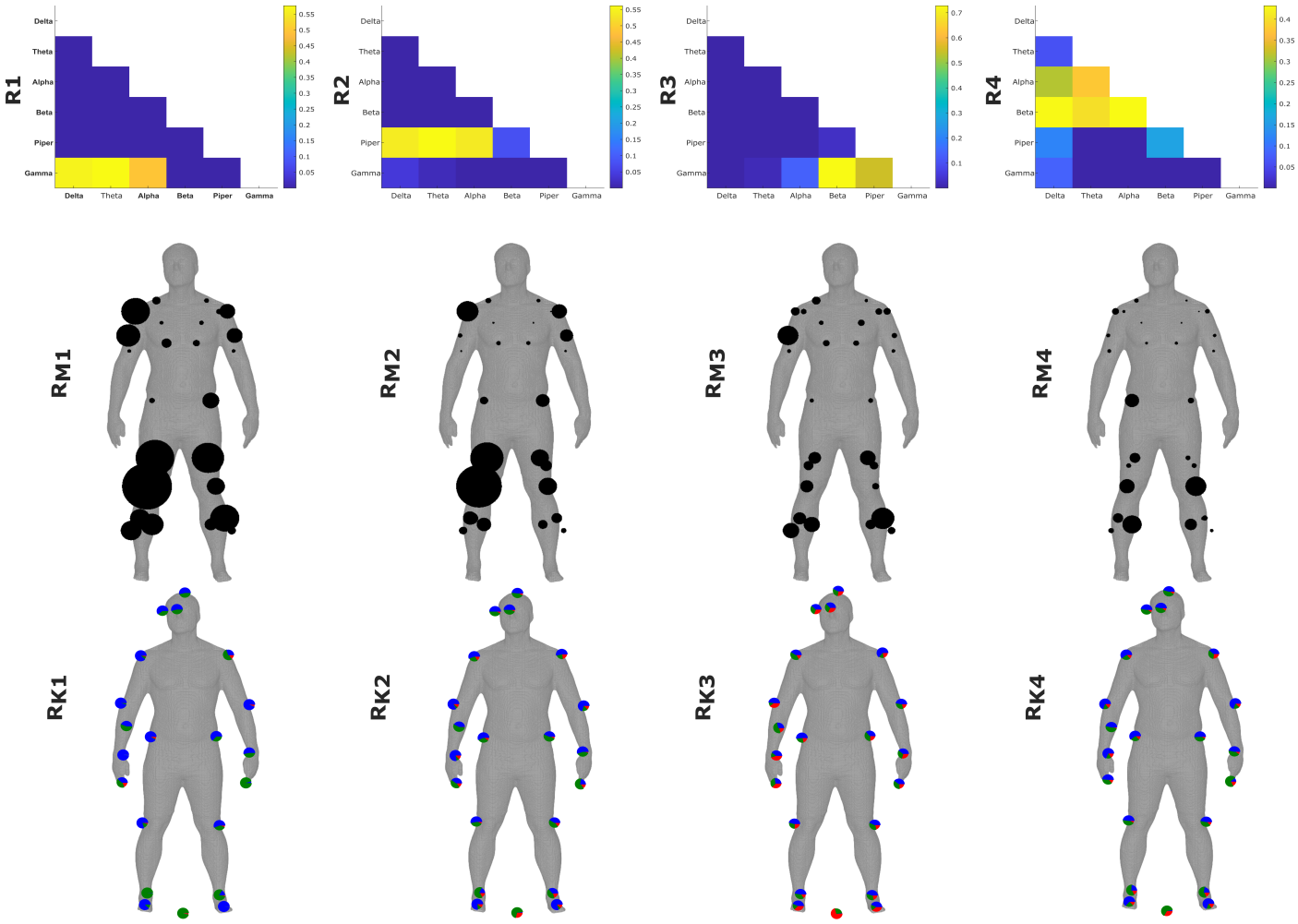

Supp. Fig.4: The R intramuscular networks (**R1**-**R4**) extracted from the three participants of dataset 1 who performed a variety of whole-body reaching movements. Muscle- ($\mathbf{R_{M1}}$-$\mathbf{R_{M4}}$) and kinematic- ($\mathbf{R_{K1}}$-$\mathbf{R_{K4}}$) specific activation coefficients averaged across participants and each other are illustrated below their corresponding representations. For $\mathbf{R_{M1}}$-$\mathbf{R_{M4}}$, the relative size of the black nodes represents the activation of corresponding individual muscles. For $\mathbf{R_{K1}}$-$\mathbf{R_{K4}}$, intramuscular redundancy was determined with respect to 63 XYZ kinematic coordinates whose proportional task encodings are depicted as pie charts (anteroposterior (red), mediolateral (green) and vertical (blue) directions) on corresponding bodily locations of human body models.

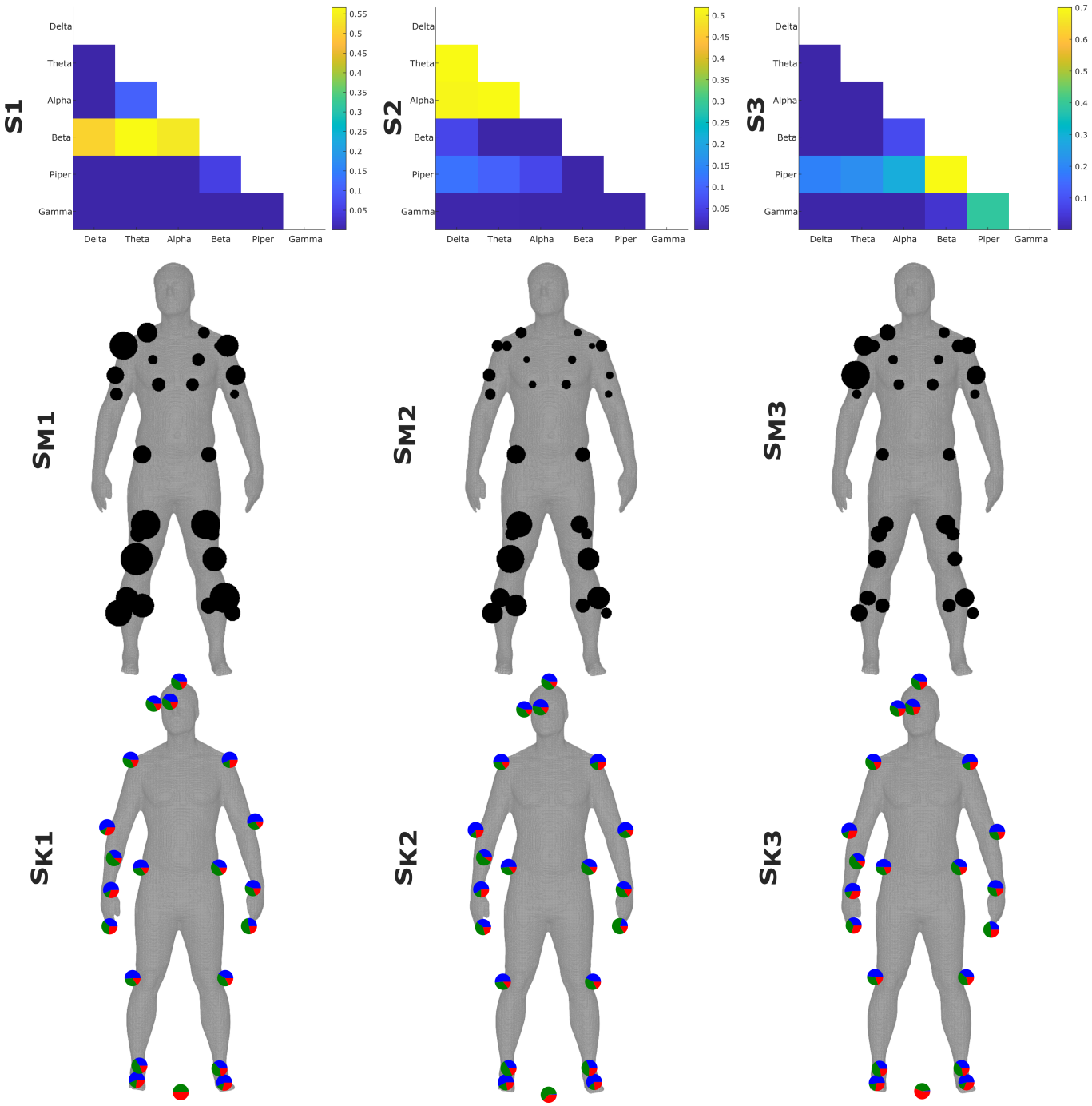

Supp. Fig.5: The S intramuscular networks (**S1**-**S3**) extracted from the three participants of dataset 1 who performed a variety of whole-body reaching movements. Muscle- ($\mathbf{S_{M1}}$-$\mathbf{S_{M3}}$) and kinematic- ($\mathbf{S_{K1}}$-$\mathbf{S_{K3}}$) specific activation coefficients averaged across participants and each other are illustrated below their corresponding representations. For $\mathbf{S_{M1}}$-$\mathbf{S_{M3}}$, the relative size of the black nodes represents the activation of corresponding individual muscles. For $\mathbf{S_{K1}}$-$\mathbf{S_{K3}}$, intramuscular functional complementarity was determined with respect to 63 XYZ kinematic coordinates whose proportional task encodings are depicted as pie charts (anteroposterior (red), mediolateral (green) and vertical (blue) directions) on corresponding bodily locations of human body models.

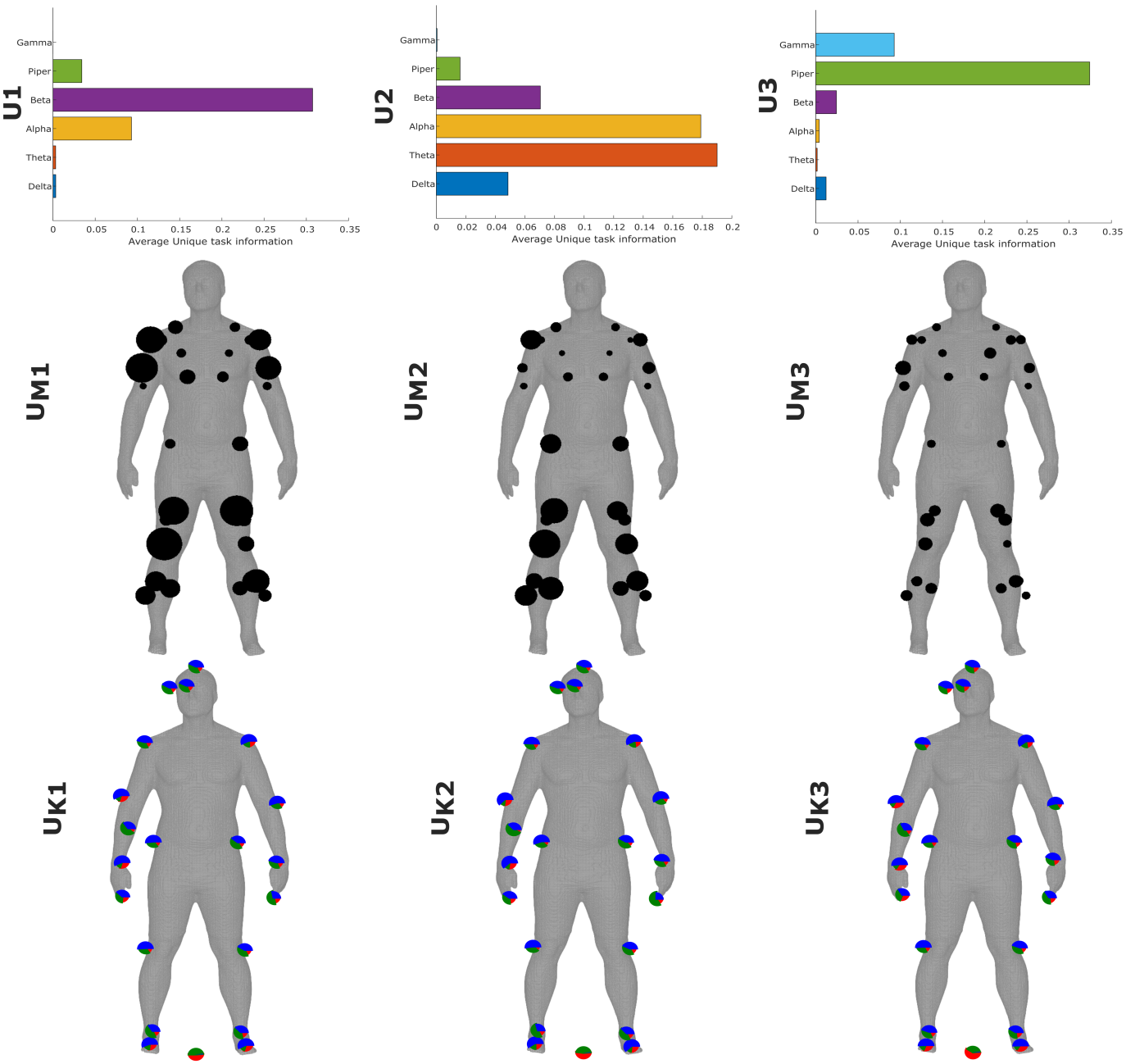

Supp. Fig.6: The U_{xy} intramuscular networks (**U1**-**U3**) extracted from the three participants of dataset 1 who performed a variety of whole-body reaching movements. Muscle- ($\mathbf{U_{M1}}$-$\mathbf{U_{M3}}$) and kinematic- ($\mathbf{U_{K1}}$-$\mathbf{U_{K3}}$) specific activation coefficients averaged across participants and each other are illustrated below their corresponding representations. For $\mathbf{U_{M1}}$-$\mathbf{U_{M3}}$, the relative size of the black nodes represents the activation of corresponding individual muscles. For $\mathbf{U_{K1}}$-$\mathbf{U_{K3}}$, intramuscular functional independence was determined with respect to 63 XYZ kinematic coordinates whose proportional task encodings are depicted as pie charts (anteroposterior (red), mediolateral (green) and vertical (blue) directions) on corresponding bodily locations of human body models.